

Universidade de Lisboa

Faculdade de Farmácia



**MODELLING GRANULES SIZE DISTRIBUTION PRODUCED ON A CONTINUOUS
MANUFACTURING LINE WITH NON-LINEAR AUTOREGRESSIVE ARTIFICIAL
NEURAL NETWORKS**

Diana Catherina Manaig Nunes

Dissertation supervised by Professor João Almeida Lopes.

Pharmaceutical Engineering

2018

Abstract

Particle size is a critical quality parameter in several pharmaceutical unit operations. An adequate particle size distribution is essential to ensure optimal manufacturability which, in turn, has an important impact on the safety, efficacy and quality of the end product. Thus, the monitoring and control of the particle size via in-process size measurements is crucial to the pharmaceutical industry. Currently, a wide range of techniques are available for the determination of particle size distribution, however a technique that enables relevant real-time process data is highly preferable, as a better understanding and control over the process is offered.

The pharmaceutical industry follows the “technology-push model” as it depends on scientific and technological advances. Hence, optimization of product monitoring technologies for drug products have been receiving more attention as it helps to increase profitability. An increasing interest in the usage of virtual instruments as an alternative to physical instruments has arisen in recent years. A software sensor utilizes information collected from a process operation to estimate values of some property of interest, typically difficult to measure experimentally. One of the most significant benefits of the computational approach is the possibility to adapt the measuring system through several optimization solutions.

The present thesis focuses on the development of a mathematical dynamic model capable of predicting particle size distribution in-real time. For this purpose, multivariate data coming from univariate sensors placed in multiple locations of the continuous production line, ConsiGma™-25, was utilized to determine the size distribution (d50) of granules evaluated at a specific site within the line. The ConsiGma™-25 system is a continuous granulation line developed by GEA Pharma. It consists of three modules: a continuous twin-screw granulation module, a six-segmented cell fluid bed dryer and a product control unit. In the continuous granulation module, granules are produced inside the twin-screw granulator via mixing of the powder and the granulation liquid (water) fed into the granulation barrel. Once finalized the granulation operation, the produced granules are then pneumatically transferred to the fluid bed dryer module. In the dryer module, the granules are relocated to one specific dryer cell, where drying is performed for a pre-defined period of time. The dry granules are formerly transported to the product control hopper with an integrated mill situated in the product control unit. The granules are milled, and the resulting product is gravitationally discharged and can undergo further processing steps, such as blending, tableting and coating. The size distribution (d50) of the granules to be determined in this work were assessed inside dryer cell no.4, located at the dryer module. The size distribution was measured every ten seconds by a focused beam reflectance measurement technique.

A non-linear autoregressive with exogenous inputs network was developed to achieve accurate predictions of granules size distribution values. The development of the predictive model consisted of the implementation of an optimization strategy in terms of topology, inputs, delays and training methodology. The network was trained against the d50 obtained from particle size distribution collected in-situ by the focused beam reflectance measurement technique mentioned above.

The model presented the ability to predict the d50 value from the beginning to the end of the several drying cycles. The accuracy of the artificial neural network was determined by a root mean squared error of prediction of 6.9%, which demonstrated the capability to produce close results to the experimental data of the cycles/runs included on the testing set. The predictive ability of the neural network, however, could not be extended to drying cycle that presented irregular fluctuations.

Due to the importance of the precise monitoring of the size distribution within pharmaceutical operations, a future adjustment of the optimization strategy is of great interest. In the future, a higher number of experimental runs/cycles can be used during the training process to enable the network to identify and predict more easily atypical cases. In addition, a more realistic optimization strategy could be performed for all process parameters in simultaneous through the implementation of a genetic algorithm, for example. Changes in terms of network topology can also be considered.

Keywords: Particle size distribution; Granules; Drying; Monitoring; Artificial neural network.

Resumo

O tamanho de partícula é um parâmetro crítico de qualidade em diversas operações unitárias da indústria farmacêutica. Uma distribuição de tamanho de partícula adequada é essencial para garantir condições ideais de fabrico, o que por sua vez, possui um impacto significativo na segurança, eficácia e qualidade do produto final. Deste modo, a monitorização e controlo do tamanho de partícula através de medições efetuadas durante o processo são consideradas cruciais para a indústria. Atualmente, uma ampla gama de técnicas encontra-se disponível para a determinação da distribuição de tamanho de partícula. Contudo, uma técnica que permita a obtenção de dados relevantes em tempo real é altamente preferível, visto que um melhor entendimento e controlo sobre o processo é obtido.

A indústria farmacêutica encontra-se altamente dependente de avanços científicos e tecnológicos. Nos últimos anos, um interesse crescente no uso de instrumentos virtuais como alternativa à instrumentalização física na monitorização de produto é evidente. Um sensor virtual faz uso da informação contida num determinado conjunto de dados para efetuar medições adequadas de uma propriedade de interesse. Uma das vantagens mais importantes desta abordagem computacional corresponde à possibilidade de adaptação do sistema de medição, recorrendo a variados métodos de otimização.

A presente tese encontra-se focada no desenvolvimento de um modelo matemático dinâmico capaz de prever a distribuição de tamanho de partícula em tempo real. Para o efeito, dados multivariados gerados, a cada segundo, por sensores localizados em múltiplos locais da linha de produção contínua, ConsiGmaTM-25, foram utilizados para determinar a distribuição de tamanho (d50) de grânulos avaliada num ponto específico da linha. O sistema ConsiGmaTM-25 trata-se de uma linha contínua de produção de grânulos, que pode ser dividida, essencialmente, em três módulos principais: granulador contínuo, secador de leito fluido e unidade de acondicionamento de produto. No módulo de granulação, ocorre a produção de grânulos através da mistura de pó e água (líquido de granulação). Uma vez finalizada a operação unitária, os grânulos produzidos são pneumáticamente transferidos para o secador de leito fluido. Neste local, os grânulos são introduzidos numa das seis células de secagem, onde ocorre o processo de secagem durante um período de tempo pré-definido. Os grânulos secos resultantes são, de seguida, transferidos para a unidade de acondicionamento de produto, integrado por um moinho, responsável pela operação de moagem. O material moído é gravitacionalmente descarregado e pode ser novamente processado através de operações como a mistura, compressão ou revestimento. A distribuição de tamanho (d50) dos grânulos a ser determinada neste trabalho foi medida, a cada dez segundos, através da técnica de reflectância por um feixe de luz focalizado. Um total de dezasseis corridas realizadas no mês de agosto foram utilizadas neste trabalho. Para cada corrida, dados relativos a parâmetros de

processo tais como, pressões, temperaturas, fluxos de ar, entre outros, bem como, a distribuição do tamanho (d50) dos grânulos foram disponibilizados. Com base na discrepância temporal verificada entre os dados de processo e os valores de distribuição de tamanho (d50) dos grânulos, diversas etapas de processamento foi executadas. O processamento de dados foi realizado, essencialmente, em três fases distintas: alinhamento, filtragem e organização/fragmentação. Uma vez finalizado o processamento, os dados foram utilizados no desenvolvimento do modelo preditivo (rede neural).

Uma rede neuronal não-linear autorregressiva com três entradas exógenas foi desenvolvida para realizar previsões da distribuição de tamanho (d50) dos grânulos. O desenvolvimento do modelo preditivo consistiu na implementação de uma estratégia de otimização em termos de topologia, atrasos, dados de entrada, seleção de corridas e metodologia de treino. Para cada variável de processo (entrada), um atraso foi assinalado com base em pressupostos fundamentados por estudos relativos ao tempo de residência dos três módulos da linha contínua. Os dados de entrada foram definidos com base no resultado de um modelo matemático desenvolvido para designar o conjunto de variáveis para o qual se observava um menor erro médio quadrático de previsão da propriedade de interesse, d50. De forma a possibilitar o treino da rede, os dados fragmentados foram divididos em dois principais conjuntos: treino e teste. A rede foi treinada e validada com dados de treino, sendo os dados de teste seguidamente utilizados para avaliar a capacidade preditiva do modelo otimizado.

O modelo apresentou a capacidade de prever o valor de d50 ao longo dos vários ciclos de secagem. A precisão da rede neural foi determinada por um valor de erro médio quadrático de previsão de 6,9%, demonstrando sua capacidade de produzir resultados próximos aos dados experimentais incluídos no conjunto de teste. A capacidade preditiva da rede neural, no entanto, não foi capaz de abranger casos atípicos.

Considerando a importância de uma monitorização precisa da distribuição de tamanho nas operações farmacêuticas, uma futura alteração na estratégia de otimização implementada é altamente aconselhável. No futuro, o uso de um número mais elevado de ciclos/corridas de secagem durante o processo de treino da rede poderá permitir que esta seja capaz de identificar e prever com maior facilidade casos atípicos. Adicionalmente, uma abordagem mais realista da estratégia de otimização poderá ser executada para todas os parâmetros de processo em simultâneo através da implementação de um algoritmo genético. Ainda, alterações na topologia da rede poderão ser também consideradas.

Palavras-chave: Distribuição de tamanho de partícula; Grânulos; Secagem; Monitorização; Rede neuronal artificial.

Acknowledgements

First, I would like to express my sincere gratitude to my supervisor, Prof. João Pedro Martins de Almeida Lopes, for his guidance, support and for sharing his expertise. I am extremely grateful for giving me the opportunity to present my work in the ninth pan-European Conference on PAT and QbD Sciences, it was truly life-changing.

I would like to thank Dr. Mafalda Sarraguça for the warmth shown in Manchester and for the constant availability to clarify my doubts.

I would like to express my gratitude to Niels Nicolaï for the willingness to meet with me and to provide me a depth insight on the ConsiGma system.

A big thank you to engineer Nuno Costa for all the support given throughout the whole semester.

To my colleagues, Ana, Cláudia and Inês, I thank them for their companionship and for the friendly working environment.

To my closer friends, I thank them for unconditional friendship and support.

I would like to thank Catarina. We are truly the proof that everything is achievable if you put your mind into it.

Thank you, Pablo, for your words of encouragement and support, especially in those moments where no time ever seemed to be enough to finalize this thesis. Thank you for the extra patience on the most stressful times.

A big thank you to my family, specially to my parents and my brother. Thank you for the unconditional support, encouragement and love, without which I would not have come this far.

I would like to thank everyone else who has contributed somehow to the realization of this thesis.

Contents

Abstract.....	i
Resumo.....	iii
Acknowledgements	v
Contents.....	vii
List of Figures.....	xi
List of Tables.....	xv
List of Abbreviations	xvii
1. Introduction	19
1.1. Pharmaceutical manufacturing: from batch to continuous.....	19
1.2. Drying process	22
1.3. Particle size characterization.....	23
1.3.1. Particle size characterization methods.....	25
1.3.1.1. Off-line methods	26
1.3.1.1.1. Laser diffraction	26
1.3.1.1.2. Sieve analysis.....	28
1.3.1.1.3. Image analysis.....	29
1.3.1.2. In-line methods.....	31
1.3.1.2.1. Acoustic emission.....	31
1.3.1.2.2. Methods based on chord length measurements.....	32
1.3.1.2.2.1. Spatial filtering velocimetry	33
1.3.1.2.2.2. Focused beam reflectance measurements	34
1.4. ConsiGma™-25 continuous manufacturing system	36
1.4.1. Continuous twin-screw granulator.....	37
1.4.2. Six-segmented cell fluid bed dryer.....	39
1.4.3. Product control unit.....	40
1.5. Artificial neural networks	41
1.5.1. Multilayer artificial neural networks	43
1.5.1.1. Single-layer feedforward artificial neural network.....	43

1.5.1.2. Multilayer feedforward artificial neural network	44
1.5.2. Recurrent artificial neural network.....	44
1.5.2.1. Non-linear autoregressive network with exogenous inputs.....	44
1.5.3. Training process	45
1.5.3.1. Supervised training	47
1.5.3.2. Unsupervised training	47
1.6. Objectives	47
2. Materials and methods	49
2.1. Pharmaceutical formulation	49
2.2. Manufacturing process	49
2.3. In-process measurements	50
2.3.1. In-line particle size analysis	50
2.4. Continuous manufacturing runs.....	50
2.5. Data collection.....	52
2.6. Data processing	54
2.6.1. Data alignment	54
2.6.2. Data filtering	55
2.7. Data organization	55
2.8. Supplementary data processing	56
2.9. Modelling strategy	56
2.9.1. Input delay.....	57
2.9.2. Input selection	57
2.9.3. Run selection.....	58
2.9.4. Training methodology	60
3. Results and Discussion	61
3.1. Data filtering	61
3.2. Data organization	62
3.3. Supplementary data processing	65
3.4. Modelling strategy	68

3.4.1. Input delay.....	68
3.4.2. Input selection	71
3.4.2.1. Manual input selection	71
3.4.2.2. Empirical input selection	73
3.4.3. Runs selection	78
3.5. Modelling strategy	80
3.6. ANN model calibration.....	80
4. Conclusions	89
5. References.....	91
6. Supplementary material	97

List of Figures

Figure 1: Usual particle size descriptors and its definitions (adapted from [34]).	24
Figure 2: Particle size distribution. (a) Symmetric distribution where mean, median and mode present the same value; (b) Non-symmetric distribution where mean, median and mode present different values.(adapted from [35])	24
Figure 3: D10, D50 and D90. (adapted from [35])	25
Figure 4: Particle size techniques according to the size range. (adapted from	26
Figure 5: Schematic illustration of particle measurement through AE sensing. [59]	32
Figure 6: Examples of the measurement of chord length (bold red line) when a laser beam crosses (1) a spherical particle and (2a and 2b) non-spherical particle in two distinct positions. Illustration of the influence of particle orientation on chord length. [38]	32
Figure 7: Illustration of three types of measurements with the probe systems. [63]	34
Figure 8: (a) The FBRM probe technique; (b) Measurement of a particle chord length using the FBRM technique. [68]	35
Figure 9: ConsiGma™-25 continuous manufacturing line. (1) Continuous twin-screw granulation module; (2) Six-segmented cell fluid bed dryer; (3) Product control unit. [4]	36
Figure 10: ConsiGma™-25 continuous line: 1. Twin-screw granulator; 2. Six-cell segmented fluid bed dryer; 3. Product control unit; 4. Blender (external phase); 5. Tablet press; 6. Tablet coater (Courtesy of GEA Pharma Systems). [4]	37
Figure 11: Continuous granulation module. [4]	37
Figure 12: Screw configuration with 12 kneading elements (two mixing blocks, each containing six kneading elements) indicating the geometry of the screws used in a TSG. [72]	38
Figure 13: The feed segment (a), work segment (b) and discharge segment (c) of a TSG during operation. [72]	39
Figure 14: Six-segmented cell fluid bed dryer. [4]	40
Figure 15: Inside view of the six-segmented cell fluid bed dryer. [4]	40
Figure 16: Product control unit. [4]	41
Figure 17: Structure of an artificial neuron. [79]	42
Figure 18: Example of neural networks. (a) single-layer feedforward network; (b) multilayer feedforward network; (c) recurrent network. (adapted from [76])	43
Figure 19: NARX neural network. (a) Series-Parallel Architecture. (b) Parallel Architecture. [82]	45
Figure 20: Types of training. [86]	47
Figure 21: Schematic representation of time lengths of cell filling, drying process and cell inactivity time.	49

Figure 22: Disturbances imposed on Runs 1, 2,5, 6, 7 and 16.....	52
Figure 23:d50 profile (Run 1).....	56
Figure 24: Generic representation of the NARX network.	57
Figure 25: Final arrangement of each two-dimensional array (a) reference runs; (b) runs with an imposed disturbance.	59
Figure 26: Example of the iterative steps occurring during the training of the neural network.	60
Figure 27: d50 profile of each drying cycle of every run.....	64
Figure 28: d50 profile of each drying cycle of every run after the removal of drying cycle no. 5 of Run 7 and drying cycle no. 7 of Run 14.....	67
Figure 29: d50 profile of each drying cycle of every run after the supplementary data processing.....	67
Figure 30: Normalized RTD (right) profile with a shaded region denoting the standard deviation at different screw speed (500, 900 rpm) during various experiments (ID) using twin screw granulation [SA: stagger angle ($^{\circ}$), NK: number of kneading discs (-), MFR: material throughput (kg/h), LSR: liquid-solid ratio (%). T1: mean residence time at 500 rpm (s), T2: mean residence time at 900 rpm (s)]. [89]	69
Figure 31: Schematic representation of the logical procedure behind the data alignment upon the delay implementation.....	70
Figure 32: User-set variables for Run 8. V4: Flow air inlet wet granule transfer; V6: Relative humidity dryer air inlet; V19: Speed granulator drive; V23: Temperature granulator barrel; V32: Temperature dryer air inlet; V37: Mass flow powder dosing 1; V46: Mass flow granulation liquid; V47: Flow dryer air inlet.	72
Figure 33: V1, V5, V18 and V22 for Run 8. V1: Liquid pumps speed; V5: Humidity air handling unit control; V18: Actual status opening control valve pressure dryer air inlet; V22: Temperature filter dryer air handling unit.....	73
Figure 34: V15 and V35 for Run 8. V15: Pressure atmospheric pressure; V35: Weight granulation liquid tank.	73
Figure 35: d_{50} RMSEP in each round of the empirical input selection. X-axis represents the variable removed at each round.	74
Figure 36: Differential pressure over the wet granule transfer line (V44) during Run 8.	75
Figure 37: Initial seventy-two sampling points for V4 and V44 during Run 8.	75
Figure 38: Temperature of dryer cells no. 1, 2, 3, 4, 5 and 6 during Run 8.	76
Figure 39: Temperature of dryer cell no. 4 and d_{50} profile during Run 8.	77
Figure 40: Temperature of the dryer air inlet outlet (V32) during Run 8.	77
Figure 41: PCA score plot from the first two principal components of the reference runs.....	78

Figure 42: PCA score plot from the first two principal components of the reference with an imposed disturbance.	79
Figure 43: Final topology of the optimized NARX neural network.	80
Figure 44: Drying cycles selected for training and testing.	82
Figure 45: Distribution of RMSE for the calibration and testing set.	82
Figure 46: RMSEP for runs 1-4, 7-16.	84
Figure 47: d50 prediction for drying cycle no.3 of Run 15 (training run) and drying cycle no.2 of Run 16 (testing run).....	85
Figure 48: d50 predictions for the drying cycles of runs 1-4,7-16.	86

List of Tables

Table 1: Sixteen continuous manufacturing runs.	51
Table 2: Starting and ending time of the fifty in-process measurements performed within the three modules of the ConsiGmaTM-25 system.	53
Table 3: Starting and ending time of the d50 measurements performed by the FBRM probe inserted inside the dryer cell no.4.	54
Table 4: Total number of rows for each two-dimensional array.	59
Table 5: Total number of sampling points removed after the two stages of data filtering.	61
Table 6: Total duration of both Xn and Yn arrays within each run.	62
Table 7: Number of drying cycles and number of sampling points of each cycle.	63
Table 8: Number of sampling points of each drying cycle after the outliers' removal.	66
Table 9: Total number of sampling points after the removal of drying cycles no.5 (Run 7) and 7 (Run 14).	66
Table 10: Total number of sampling points after the delay implementation.	71
Table 11: Runs chosen to integrate the training and test subset.	79
Table 12: Median RMSEP for each drying cycle of runs 5 and 6. Average RMSEP and standard deviation of runs 5 and 6.	81
Table 13: Median RMSE and standard deviation of the calibration and testing set.	82
Table 14: Median RMSEP (μm) for each drying cycle of runs 1-4,7-16.	83
Table 15: Average RMSEP for runs 1-4,7-16.	84
Table 16: Average d50 value (μm) for the testing runs.	87
Table 17: Average RMSEP (%) for the testing runs.	87

List of Abbreviations

AE	Acoustic Emission
ANN	Artificial Neural Network
API	Active Pharmaceutical Ingredient
ATM	Physical Atmosphere
FBD	Fluid Bed Drying
FBG	Fluid Bed Granulation
FBRM	Focused Beam Reflectance Measurement
FDA	Food and Drug Administration
CCD	Charged Coupled Device
CLD	Chord Length Distribution
HEPA	High Efficiency Particulate Arrestance
HIV	Human Immunodeficiency Virus
ICH	International Conference on Harmonization
ISO	International Organization for Standardization
LD	Laser Diffraction
LSR	Liquid-Solid Ratio
MBAR	Millibar
MFR	Material Throughput
NaN	Not a Number
NARX	Non-linear Autoregressive Network with Exogenous Inputs
NIR-CI	Near Infra-red Chemical Imaging
NK	Number of Kneading Discs
NOC	Normal Operating Conditions
PA	Pascal
PAT	Process Analytical Technology
PCA	Principal Component Analysis
PID	Proportional-Integral-Derivate
PSD	Particle Size Distribution
PSI	Photometric Stereo Imaging
RMSE	Root Mean Squared Error

RMSEC	Root Mean Squared Error of Calibration
RMSEP	Root Mean Squared Error of Prediction
RTD	Residence Time Distribution
R&D	Research and Development
SA	Stagger Angle
SFV	Spatial Filtering Velocimetry
QbD	Quality by Design
TCU	Temperature Control Unit
TSG	Twin-screw Granulator

1. Introduction

1.1. Pharmaceutical manufacturing: from batch to continuous

The modern pharmaceutical industry is showing a growing interest in transitioning from the more traditional batch manufacturing to continuous manufacturing, a movement that FDA is seeking to encourage among more pharmaceutical manufacturers. [1], [2]

Nowadays, pharmaceutical production is dominated by batch manufacturing processes. [3] However, continuous manufacturing has gained an increasingly amount of attention in recent years. Producing a pharmaceutical product continuously has been considered an innovative approach that has a great deal of potential to improve agility, flexibility, and robustness in the manufacture of pharmaceuticals, providing opportunities for product quality improvement, process enhanced cost-efficiency and reduced environmental effect. [4]–[6]

Batch manufacturing plants operate through multiple discrete steps and often a few or even all process units are shut down and started up. [7] Raw materials are fed and removed from the process at different times, i.e., all materials are charged before the process begins and the final product is discharged at the end of the corresponding process unit operation. [1] In contrast to batch processing, in continuous manufacturing, material is simultaneously charged and discharged from the process throughout its duration. [5], [8] In this case, the raw materials undergo an assembly line of fully integrated components until the final product is obtained. [9], [10] A continuous production plant is designed to run twenty-four hours a day, seven days a week for more than fifty weeks per year. [7] The fact that the manufacturing line can run for a longer period of time reduces the likelihood of drug shortages and avoids scale-up issues. [9], [11] The continuous approach is considered to be more efficient, safer and faster as it eliminates ‘hold times’ between unit operations which are characteristic from batch manufacturing. The elimination of these ‘hold times’ decreases human intervention, hence decreasing the risk of human error. Additionally, ‘hold times’ can easily affect the integrity of product being manufactured considering that for some active pharmaceutical ingredients (APIs), there is the risk of degradation due to their sensitivity to the surrounding environment. [9], [10]

In batch manufacturing, a batch size increase involves dramatic changes in equipment. [12] Oppositely, in continuous manufacturing scale-up can be achieved in several ways including operating the process for longer periods of time, using parallel processing units or increasing the flow rate. [5] This eliminates the need to carry out the time-expensive scale-up studies as the production rate is increased by numbering up alternatively to scaling up. [3]

In batch manufacturing, a great demand for a certain drug requires an increase on production and consequently, a scale-up in terms of equipment. As more physical space is needed, a bigger plant footprint becomes mandatory requiring more time and additional investment. [10]

In continuous manufacturing, the operating system and the simplicity of the scale-up procedure greatly reduces the plant footprint resulting in significant savings in capital investment and operational costs. [8] Fundamentally, a small continuous plant capable of operating as long as necessary to manufacture the desired amount of product is more likely to be cheaper than constructing a large batch plant. [11] Additionally, a smaller footprint is associated to a more efficient use of energy, reduced waste and a smaller ecological impact. [3]

In a batch manufacturing process, materials are normally tested off-line and stored before being sent to the following processing step. If the in-process material does not meet the well-defined quality expectations, it can be discarded, or, on exceptional cases, it may be reprocessed to achieve the quality target prior further processing. [5] Thus, batch manufacturing offers the advantage of a simpler quality control procedure as a batch can be accepted or rejected. In a continuous process, the material is continuously sent to the next processing step. [4] However, it is possible for a continuous process to generate batches considering that the definition of batch is defined by the quantity of manufactured drug and not by the mode of manufacture (batch or continuous). According to the FDA, a batch is 'a specific quantity of a drug or other material that is intended to have uniform character and quality, within specified limits, and is produced according to a single manufacturing order during the same cycle of manufacture'. [8] From a regulatory point of view, this definition does not interfere with the adoption of a continuous manufacturing process as a batch in a continuous setting can be considered 'a specific identified amount produced in a unit of time or quantity in a manner that assures its having uniform character and quality with specified limits'. [6]

Batch processing can adopt both an off-line and real time quality control strategy by measuring or sampling at different spatial locations within the equipment. [11] In contrast with batch manufacturing, in continuous manufacturing, apart from local control, also the entire process flow must be mandatorily equipped with second-level control systems responsible for monitoring and aligning the performance of the individual unit operations. [13] For this reason, continuous processing is compatible with FDA's process analytical technology (PAT) initiative launched in 2003 that promotes the use of PAT tools to provide a more thorough understanding of pharmaceutical manufacturing processes. [14], [15] In a fully integrated continuous line, PAT tools are used to gather real-time data for process monitoring and control, and ultimately, to mitigate the impact of in-process material and process variability on the finished product's quality. This comes in line with FDA's Quality-by-Design (QbD) initiative for pharmaceutical development framed by the International Conference on Harmonization (ICH) Q8 guideline which promotes continuous improvement based on scientific understanding of critical process and product attributes. [16] A QbD/PAT-strategy will enable quality to be built into the pharmaceutical product, ensuring an acceptable and reproducible product quality and performance throughout its lifecycle. [5], [15]

Despite the various advantages of continuous manufacturing, batch operations might be, in some instances, preferable to continuous manufacturing as there are still a few challenges related to its implementation. For several years, the strict regulatory environment was responsible for the pharmaceutical industry's reluctance on engaging on continuous manufacturing. Regardless on the FDA's support on the adoption of continuous processing, manufacturing continuously may not be approvable by other global regulators. [7] Another challenge is changing the mindset of the industry that pharmaceutical products should be produced used traditionally out-of-date methodologies. Many companies prefer to maintain their current manufacturing procedure due to their deep comfort on methodologies that have been followed for years. [17] Implementing an integrated continuous manufacturing line would require the implementation of QbD/PAT principles, new product development processes and improvements in the technical skills of the professionals allowing them to analyze and understand process data. [15] During the 80s and 90s, a heavy capital investment was made on batch manufacturing for process improvement, throughput time reduction and operational efficiency enhance. [7], [15] A transition from batch to continuous manufacturing would imply an additional investment that companies with an established batch asset-base were not willing to make. The investment in continuous operations is easier for new products or specific processes where an investment would be required either way. [11] For that reason, it is expected for most pharmaceutical companies to convert or integrate several of their current batch operations into a continuous plant prior to investing in a fully continuous-based manufacturing operation. [7] Additionally, switching the manufacturing approach may require new equipment, process control parameters, control strategies and process operational models in order to stablish product equivalency. [18]

The transition from batch to continuous manufacturing is clearly not simple procedure. However, a growing number of manufacturers are working towards implementing continuous manufacturing into their processes as they have recognized that the challenges of transitioning can easily be compensated by the advantages offered by manufacturing continuously. [19] Several years ago, GlaxoSmithKline invested 60 U.S. dollars to set up a facility in Singapore to continuously process APIs for its respiratory drugs. [20] AstraZeneca has also recently invested in a continuous wet granulation unit for solid dosage forms (tablets) processing. The company selected GEA Pharma Systems equipment (ConsiGma™25) for use in developing novel drugs and to produce clinical trials materials, allowing cost, time and material saving throughout the product life-cycle. [21], [22] In 2016, Eli Lilly announced a 40 million U.S. dollars investment to build a continuous API manufacturing facility at its 37-year-old manufacturing site in Cork Country, Ireland. The continuous processing facility will be used for development and commercialization of late-stage drug pipeline. [9] Vertex has been using a continuous manufacturing process for a cystic fibrosis drug, Orkambi, since its approval in July 2015.

Orkambi was the first ever oral solid dosage drug to be continuously produced. [23] Recently, FDA approved Vertex's third medicine to treat the underlying cause of cystic fibrosis, Symdeko, which is Vertex's second approved drug produced by a continuous manufacturing process. [24] In 2016, the FDA allowed for the first time in history a manufacturer to switch from batch to continuous manufacturing. The manufacturing change is for Janssen's HIV-1 infection medication, Prezista (darunavir), a direct compression product. Janssen Supply Chain can now produce tablets on a continuous manufacturing production line at its facility in Gurabo, Puerto Rico. The incorporation of one of the industry's first full continuous direct compression solid oral dosage manufacturing facilities will decrease the timeline from a two-week to a one-day production and allow continuous monitoring of product quality. Janssen and Johnson and Johnson aim to "manufacture 70% of its highest-volume products using continuous manufacturing" within 6 years. [2], [25] The trend of transition from batch to continuous manufacturing will continue, and it is expected more companies to invest in continuous manufacturing technologies. The increasingly demand for higher-quality pharmaceutical products to be produced in a faster and more cost-efficient way, will offer early adopters of continuous manufacturing a substantial competitive advantage over other companies. [26]

1.2. Drying process

Drying is defined as the operation used to remove liquid from a moist material by converting the liquid into its gaseous state, which can be achieved by heat application. Usually, water is the liquid aimed to be removed and air is the medium used to promote the heat transfer to the water. Drying is a unitary process extensively utilized in various applications within the pharmaceutical industry. It is an essential unit operation to produce granules, in the context of wet granulation, which may be dispensed in that same form or used in tablets or capsules. Drying is also known for its ability to reduce size and weight of the material and for facilitating milling as it turns the dried substance much more friable. A great variety of dryers is available to perform the operation described above, reason why it is impossible to describe every existing equipment. Given this, more attention must be provided to dryers that have a direct application in the manufacturing of drug products, such as fluid bed dryers. [27]

1.2.1. Fluid bed dryer

Nowadays, fluid bed drying (FBD) is the most common and best-known method to prepare granules for compression or to simply dry wet granules. [27] This is due to the numerous benefits that it offers over other drying methods, such as drying time reduction. [28] It also enables drying of a large amount of material, and a relatively low capital cost. [29]

A fluid bed dryer works on the principle of fluidization, a process in which hot gas or air passes vertically through a bed of solid particles. The gas is expected to be introduced at a higher rate than the settling rate of the particles, in order to allow the particles to fluctuate and be partially suspended in the gas stream. A state of fluidization exists as the particles continuously fall into a random motion similar to the appearance of a boiling liquid. The fluidization technique is efficient and offers a uniform drying process since each particle is entirely surrounded by the drying gas. Furthermore, the intense mixing between the solid particles and the gas causes uniform conditions of temperature, composition and dispersion of particle size in the bed. [27] The air stream for fluidization is produced by a fan mounted at the top of the equipment. The air is heated to the required temperature and moves vertically through the wet material, placed at the bottom of the drying chamber. [30], [31] The flow is adjusted, and the filters situated at the top of the drying chamber prevent the release of fine particles to the outer environment. Both flow rate and operating temperature are regulated by a control panel. [32] The temperature of the inlet air should be monitored to ensure that only a determined amount of moisture evaporates. A high inlet air temperature can lead to the formation of a crust on the surface of the material or even inhibit the moisture to be transferred from the interior of the granulate to its surface, which will consequently delay the drying process. [33]

1.3. Particle size characterization

Particle size distribution (PSD) are one of the most important quality attributes of solid dosage forms, such as granulated products. An inadequate PSD can influence granule properties, which might cause problems in the performance, processability, stability and appearance of the end product. Particle size analysis has become a routine measurement during granulation as it can be indicative of batch development and quality. Thus, it is significantly important to monitor granule growth and understand its effects on the end product. Nevertheless, a discussion about size is not possible without first taking into mind the diameter of the particle, which in turn is influenced by shape and morphology. [4] The concept of diameter is more easily applicable to spherical particles as its size is determined exclusively by the diameter. In contrast, for non-spherical particles defining other parameters is required. The most broadly used particle size parameters are projected area diameter, length and width, and two other related particle size descriptors, Feret's diameter and Martin's diameter (Figure 1). These parameters are extremely useful upon the measurement of particle size through microscopy since the measuring sample is composed by static particles. [34] Many other techniques used to determine particle size assume that every single particle corresponds to a sphere design and therefore will present the same volume of one of equivalent diameter. In this case, length and weight descriptors must be derived either into its spherical equivalent. For example, the

volume diameter will be referred as the diameter of a sphere whose volume is the same as of the non-spherical particle. [35]

Particle size determination is performed to provide information about the size attributes of an ensemble of particles whose size is typically not the same, reason why particle size is usually described as a distribution. Ideally, the central values of the distribution (mean, median and mode) and distribution width descriptors should be taken into account. For a bell-shaped normal distribution (Figure 2a), mean, median and mode present the same value, and therefore is fully described by distribution width descriptors, the mean particle size and the standard deviation. Oppositely, for a non-symmetric distribution (Figure 2b) the central values of the distribution will differ.

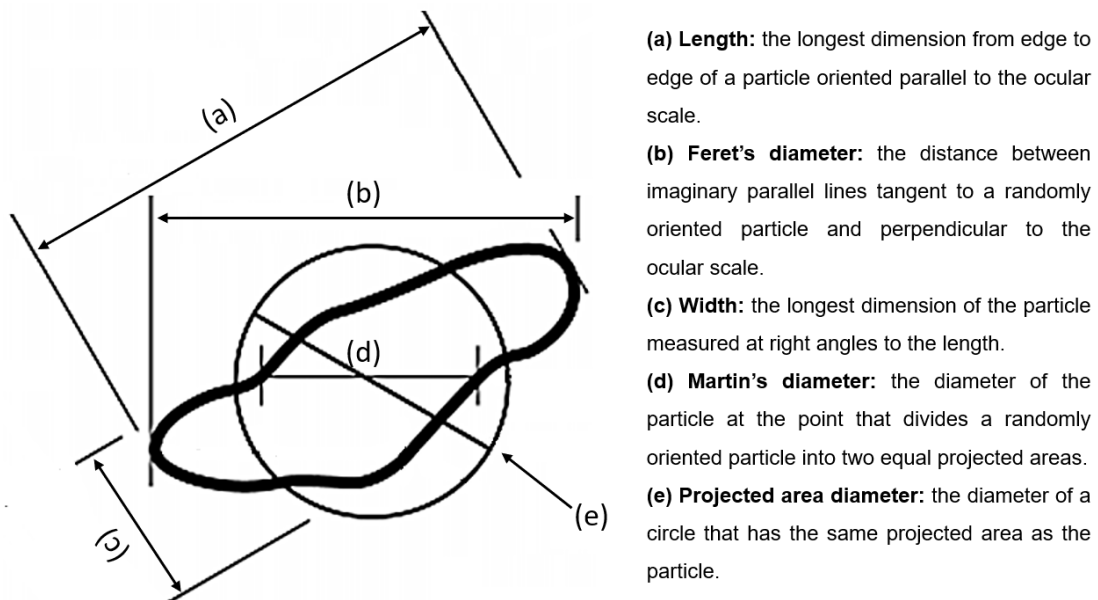


Figure 1: Usual particle size descriptors and its definitions (adapted from [34]).

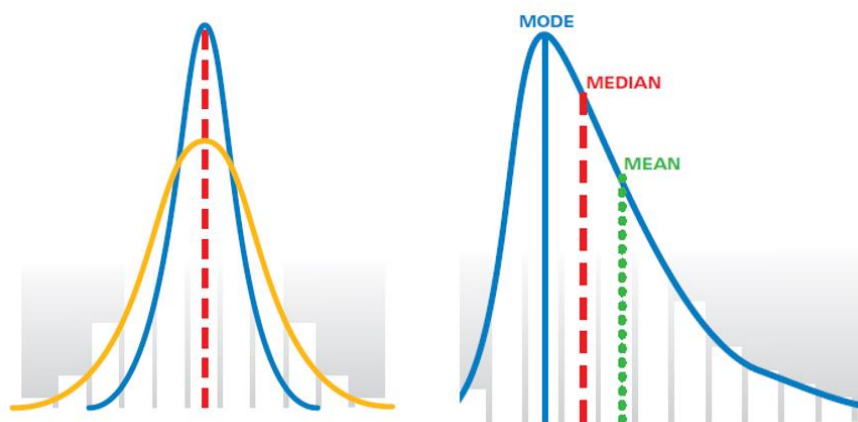


Figure 2: Particle size distribution. (a) Symmetric distribution where mean, median and mode present the same value; (b) Non-symmetric distribution where mean, median and mode present different values. (adapted from [35])

The mode corresponds to the value at which the frequency presents its maximum value and is characterized by the highest peak in the distribution. Moreover, it denotes which particle size is more usual to be found in the distribution. The median will provide the value at which the frequency curve is divided into two equal parts, where half of the population lies below this value and the other half above. For PSDs the median is usually referred as the D50. In regard to the mean, it corresponds to the average particle size of a sample within a given distribution. An alternative common approach to characterize a distribution is the usage of D-values, D10, D50 and D90, as shown in (Figure 3). To better understand the D-value concept, particles arranged by ascending mass must be considered. In this sense, the Dx will describe the diameter where x% of the particles in the sample have a smaller particle size and (100-x) % a larger particle size. As previously mentioned, the D50 value corresponds to the median. Accordingly, 90 and 10 percent of the distribution lies below the D90 and D10 value, respectively. [35], [36]

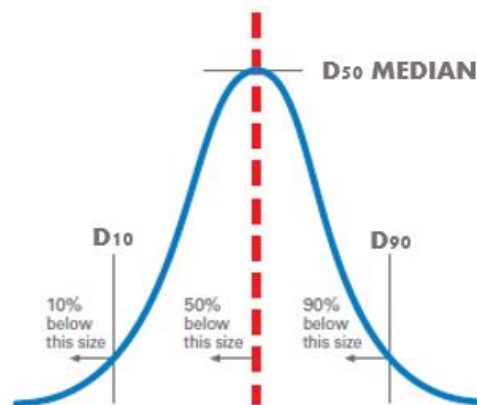


Figure 3: D10, D50 and D90. (adapted from [35])

1.3.1. Particle size characterization methods

A wide range of techniques are available for PSD determination (Figure 4). Currently, the most broadly utilized technique is laser diffraction. However, alternative approaches can include the use of other techniques such as image and sieve analysis, spatial filter velocimetry (SFV), focused beam reflectance measurement (FBRM), and acoustic emission (AE). [4], [37] Prior to the decision of which technique to use, the purpose of the analysis itself must be considered. Therefore, the choice of a suitable analyzer must acknowledge different aspects as the theoretical assumption behind the measurement mechanism, applicability (e.g. size range), ease and speed with which the analysis can be performed, the cost of the apparatus and known advantages and drawbacks. Once the different criterions are reviewed, particle size can be appropriately measured generating reproducible data in a form that is relevant to the process. An in-line technique may be preferable as enables more relevant real-time process

data and thus offers a better understanding and control over the process. However, due to the challenges associated to the sensitivity of an in-line technique within the process stream, an at-line, on-line and off-line approach might also be applicable. [38], [39] In fact, it is possible nowadays for an off-line instrument to be adapted to an on-line operation by integrating a simple accessory to the original instrument. [34]

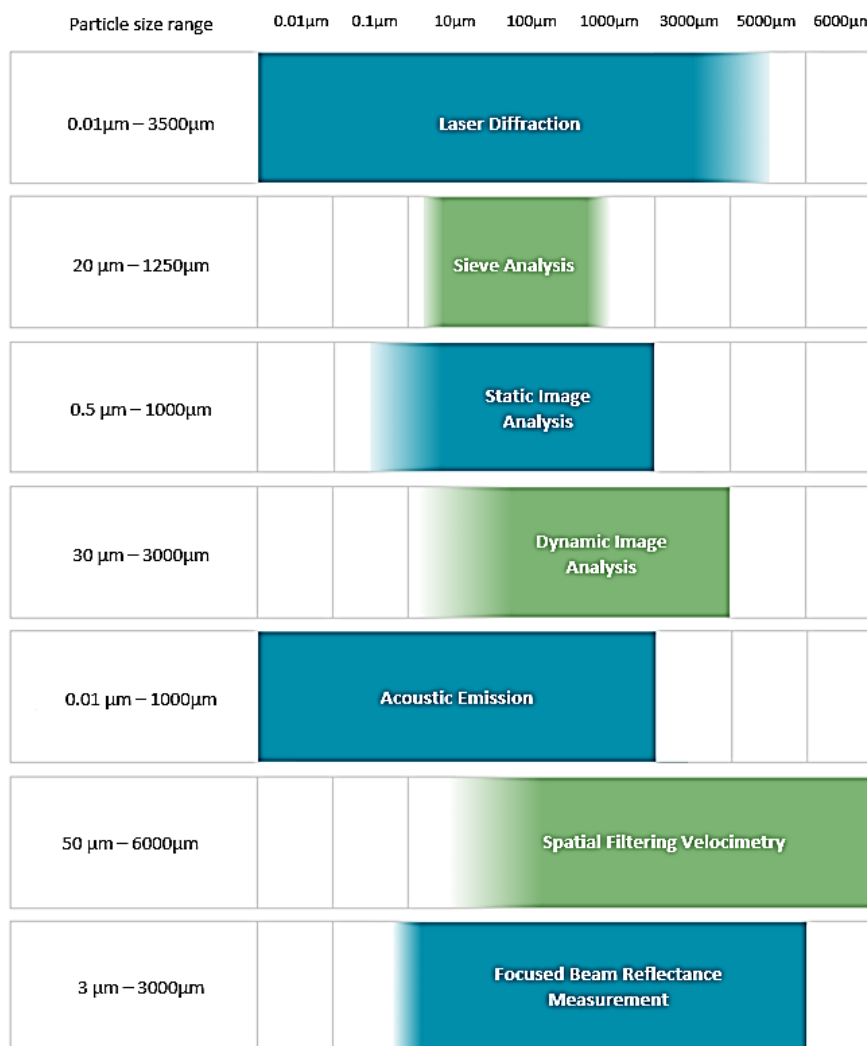


Figure 4: Particle size techniques according to the size range. (adapted from [40]).

1.3.1.1. Off-line methods

1.3.1.1.1. Laser diffraction

Laser diffraction (LD) is a well-established technique for particle size determination of pharmaceutical powders and granules. The method has been used for several years as it allows the sizing of a wide range of particles from hundreds of nanometers up to numerous millimeters in size. It can be used as both an in-process and an off-line method.

A sample, dispersed at a suitable concentration, is passed through the beam of monochromatic light causing light scattering, which produces a diffraction pattern with different light intensities at various angles. The diffraction pattern is captured by laser diffraction analyzers and an optical model is used to generate particle size information. In general, large particles scatter light at narrow angles and small particles at wide angles. [41], [42]

The early LD particle size analyzers relied on the Fraunhofer approximation by using exclusively scattering at small angles. In addition to the Fraunhofer approximation, recent LD instruments use the Mie theory to calculate PSD based on light scattered in a wider angular range. The Fraunhofer approximation is a simplified approach that does not assume the optical properties of the measured material, and therefore, can be used for to measure mixtures consisting of different materials. Furthermore, it assumes that the particles are opaque disks, that the scattering phenomena presents the same efficiency for all particle sizes and that light is scattered exclusively at narrow angles. Taking into consideration that large particles scatter light at narrow angles, the Fraunhofer approximation can provide accurate results when measuring large particles. Distinctly, the Mie theory predicts the scattering intensity induced by particles, regardless of the fact of them being opaque or transparent. It uses the assumption of spherical particles in its optical model, making it not possible to distinguish between scattering by single particles and scattering by clusters of primary particles. The particles are considered homogeneous, i.e., they are uniform in terms of composition, and the suspension diluted, so the light is scattered by one single particle and is detected prior interaction with other particles. This theory requires knowledge of the optical properties (refractive index) of the particles and the dispersant as the light intensity distribution pattern will be slightly altered depending on the value of the refractive index. [34], [38], [43] Nowadays, both the Fraunhofer approximation and the Mie theory are utilized, but the ISO13310 acknowledges the superiority of the Mie theory. The use of Fraunhofer is limited to the measurement of particles with a minimum of 50 μm in size while Mie theory enables the analysis of particles between 0.1 μm up to 3 mm. [44] In most cases, the LD technique results are presented as a volume-weighted PSD. Therefore, if the median value (D_{50}) of a volume-weighted PSD is 200 μm , it means that particles whose size goes up to 200 μm account for 50% of the sample volume. Depending on the software of the analyzer, the results might be extracted as a number-weight distribution. [38]

Nowadays, a variety of instruments are available (e.g. Malvern, Coulter, Fritsch, Retsch and Horiba instruments) which vary in terms of complexity and sensitivity. This will determine which range of particle size can be analyzed, how easy the data can be processed and summarized, and the quality of the information obtained. [45]

1.3.1.1.2. Sieve analysis

Sieve analysis is one of the oldest and most applied techniques to characterize granules through PSD. The sieve size is described in the American Pharmacopoeia as 'the length of the side of the minimum square aperture through which the particle will pass'. [46] This can be used to serve two main purposes, (1) powder separation or deagglomeration into different fractions of sizes and (2) determination of particle size, referred in this case as analytical sieving. The same sieve should not be used for both purposes as the sieves differ depending on the type of analysis to be performed. Thus, an analytical sieve must not be used for powder separation or deagglomeration taking into mind that this procedure normally forces powders to pass through the sieve, hence compromising structure of the analytical sieves, which will ultimately lead to poor results. [46], [47]

Usually, a sieving analysis requires a stack of 2 to 6 sieves with different aperture sizes, a top cover and a fines collector. The sieves are normally made from wire woven and must be stacked following an ascending order of opening size. Therefore, the sieve with the largest aperture should be placed at the top, while the one with the smallest aperture has to be positioned at the bottom. In a general way, the technique consists of placing a sample with a predetermined weight on the top sieve that will be retained into different sieve fractions. [48], [49] The whole structure is put into motion (manually or by an instrument) which promotes particles to pass through the sieves and end up on the sieve whose aperture size will be smaller than the particle size of the particle. Thus, if a particle passes through a 100 μm but is retained on a sieve with an aperture of 75 μm , particle size will be in-between 75 and 100 μm . However, it cannot have a particle size of 100 μm considering that for a particle to pass through a certain sieve, it has to present a smaller dimension than the actual sieve size. Once the structure remains in motion for a standardized period of time, and then the particles retained on each sieve is weighted and presented as a percentage of the total amount of sample. [38] The results can be represented either by plotting 'particle size versus the amount retained or cumulative retained on the sieves to obtain a particle size distribution' and therefore, a mass-based distribution is attained. [49] In this case, a median of 50 μm suggests that 50% of the total amount of the sample is composed by particles that can pass through a sieve with an aperture of 50 μm . [38]

As mentioned before, sieving can be done manually or by an instrument. However, manual sieving is not considered the best option because it can result on the acquisition of unreliable data as the analysis performance can vary between different operators. Sieving by means of an instrument, also known as automatic sieving, utilizes either air entrainment or mechanical agitation methods to promote the motion of the particles. Mechanical agitation methods is considered to be more intense when compared to the air entrainment method. The first utilizes

movements as shaking and tapping, while the second performs sieving using air or sonic movement which leads to particle motion without leading to screen blinding (clogging of the screen aperture). [49]

Sieving is a relatively simple technique and requires a minimal sample preparation. It is applicable over a broad range of sizes (20 μm to 125 mm) and is mostly used as an off-line technique although an on-line approach has been designed for process and quality control monitoring. [46] Despite minimal sample preparation, a relatively large quantity of sample is needed to perform the analysis which makes it inappropriate for pricey materials and materials that are only available in small quantities. Additionally, measurements for odd-shaped particles are extremely difficult as sieve analysis does not consider the effect of particle shape. One of the most significant drawbacks is the sieves susceptibility to the blinding phenomena, which can greatly influence the mass distribution and consequently the accurateness of the PSD. Thus, high maintenance and a rigorous cleaning procedure are required. [38], [50]

1.3.1.1.3. Image analysis

Microscopy-based techniques provide a powerful tool for particle characterization as it is accepted as the most direct measurement of particle size, distribution and morphology. Over time, two different approaches have been developed in terms of image analysis: static and dynamic image analysis. Both involve the direct observation of particles in a two-dimensional image however they differ regarding the way how the sample is introduced into the measuring zone. The choice of which technique to use is influenced by the size of the particles to be analyzed. [51], [52] Dynamic image analysis is used for measurements of particle over the range of 30 up to 3000 μm , while static image analysis is adequate for measurement of systems sized between 0.5 and 1000 μm . [35] When performing a static image analysis, the particles to be analyzed rest on a slide, while on dynamic image analysis, particles flow during measurements. Despite the differences, many basic functions operate on the same way with either one of the approaches. The particles are placed on the measurement zone and a digital (CCD) camera captures images. The captured images are then analyzed in order to distinguish the particles from the background which will ultimately allow to measure numerous size and shape parameters for each individual particle. [34], [51], [52]

Samples analyzed by static image analysis normally sit on a slide that is moved by an automated stage. The slide is then scanned, and the resulting images of the particles are collected by a microscope and digital camera. Most static image analysis measurements are performed on powders (to be used on solid oral dosage forms) which require a sample preparation step before the analysis. In most cases, the sample preparation corresponds to the breakage of agglomerates or the dispersion of the particles on the slide that can be

achieved by using positive pressure on a rigid surface. Once the sample preparation step is concluded, the slide is scanned, and a series of image are processed through the device's software. The software allows particles to be separated from the background by defining a parameter with a specific threshold value (e.g. contrast threshold – particle/background contrast). Additionally, several software functions can be used to improve the image definition. Many steps used on static image analysis are also utilized on dynamic image analysis, however there are a number of exceptions. [53] Within the dynamic approach, the sample preparation step differs completely as the particles are in motion during the measurement. In this particular case, a sample director can be used to orientate particles towards the measurement site or an ionizer can be included on the sample preparation steps in order to reduce possible static interactions between particles improving the flowability of the sample itself. When the sample reaches the measurement site, the particles are dropped between a backlight and two CCD cameras (basic camera and zoom camera). The backlight is responsible for generating and projecting the particles shadow which is recorded at a rate of 60 frames (or more) per second, followed by the image analysis. The basic camera records the larger particles, while the zoom camera provides enables a higher resolution for a fine range of particles. The two-camera system will ultimately provide maximum precision over the whole measuring range. [54]

Image analysis enables the measurement of size and shape-related parameters of particles through the analysis of a two-dimensional image. Every parameter measurement is stored separately. Regarding the measurement of PSD, the diameter is the most important parameter to take into account. Several measurements of particle size are described on Subchapter 1.3. [48]

Recent technological advances in dynamic image analysis enable the reconstruction of three-dimensional images of particles by using multiple light sources e.g. photometric stereo imaging. The photometric stereo imaging (PSI) technique has been used for at-line measurement of granules and on-line measurement during granulation and dry milling. In resemblance to the older image analysis techniques, a digital image is obtained and processed. The digital image will consist of pixels that contain information regarding the brightness of a particular point in the image. Thus, the digital image will be presented as a black and white image and a grey-scale value between 0 and 255 will be associated to each individual pixel, where 0 and 255 correspond to black and white, respectively. Considering that particles surface can be characterized by the grey-scale value of the pixel at a certain location, a three-dimensional projection is achievable, and its area can be calculated. Simple calculations using the area value will ultimately allow the acquisition of a volume-based PSD and the related D values of the particles present on the captured image. [38], [55]

1.3.1.2. In-line methods

1.3.1.2.1. Acoustic emission

Acoustic emission (AE) is a well-suited technique for continuous measurement of particle size and size distribution. It is one of very few techniques capable of sizing particles within a range of 0.01 μm to 1 mm. AE measurements are broadly applied within granulation process which is an essential step in the pharmaceutical industry. [56] There are several pharmaceutical manufacturing processes that cause vibrations. These vibrations can be translated into useful information concerning both chemical and physical parameters such as particle size. In general, AEs are measured at a high frequency range (70 – 500 Hz) as it allows an easy propagation through solid materials and a rapid attenuation in air. [57] Thus, the audible noise from the background produced by the mechanical vibrations is suppressed. [58]

The AE methods presents numerous advantageous such as the continuous on-line measurement of the signal, high sensitivity, slight influence on the flow channel and simple instrumentation. Acoustic measurements also offer a relatively inexpensive real-time response and can be performed in hazardous process environments without engaging supplementary protection. [58] Additionally, the AE is an appropriate method to be applied in-line on a fluid bed granulation (FBG) environment due to its minimum invasiveness. [37] In this case, the sensor has to be of a small dimension and easily mounted outside of the granulator in order to enable noninvasive measurements during granulation. However, the fluidizing air flow rate in combination with external uncontrollable factors can compromise the sensitivity of the technique. [58]

Measurements using the AE method are based on signals generated by particle-chamber collisions due to the creation of a natural (e.g. flow channel bend) or artificial obstacle introduced into the flow. The solid particles hit against the obstacle which results on an acoustic emission signal that is collected by a piezoelectric acoustic emission sensor, also known as an AE transducer. A waveguide is used to generate and transmit the AE signal. The AE transducer is attached to the outer endpoint of the waveguide and will feed the signal to a signal conditioning and data acquisition system (Figure 5). [59]

The impact force carries information about particle since it is affected by the size of the impinging particle. Once the AE signal is collected and the peaks of the impulsive signals detected, the particle size distribution. Through physical modelling of the particle impact, a relationship between peak AE voltage and particle size can be defined. [59]

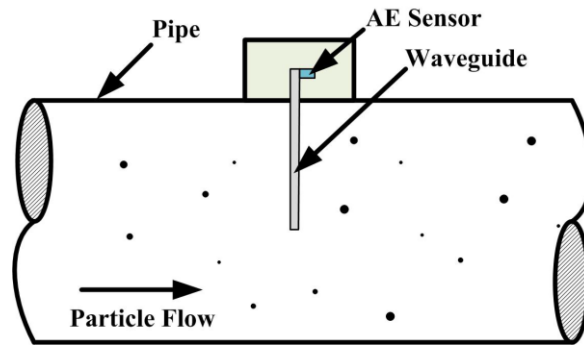


Figure 5: Schematic illustration of particle measurement through AE sensing. [59]

1.3.1.2.2. Methods based on chord length measurements

Spatial Filtering Velocimetry (SFV) and Focused Beam Reflectance Measurement (FBRM) are in-process particle size techniques that measure chord length in place of actual particle size. The chord length of a particle can be designated as a straight-line segment whose endpoints both reach the surface of the particle. (Figure 6) These techniques use a laser beam that randomly passes through the particle and a chord length is derived. The number of times an individual particle is measured takes the form of a particle size distribution. [38]

For spherical particles, the highest possible value for chord length is the diameter of the particle. Thus, the measured chord length is not dependent of the particle orientation in regard to the laser beam. Oppositely, the shape and orientation of a particle has an influence on chord length measurement when analyzing non-spherical particles. [60]

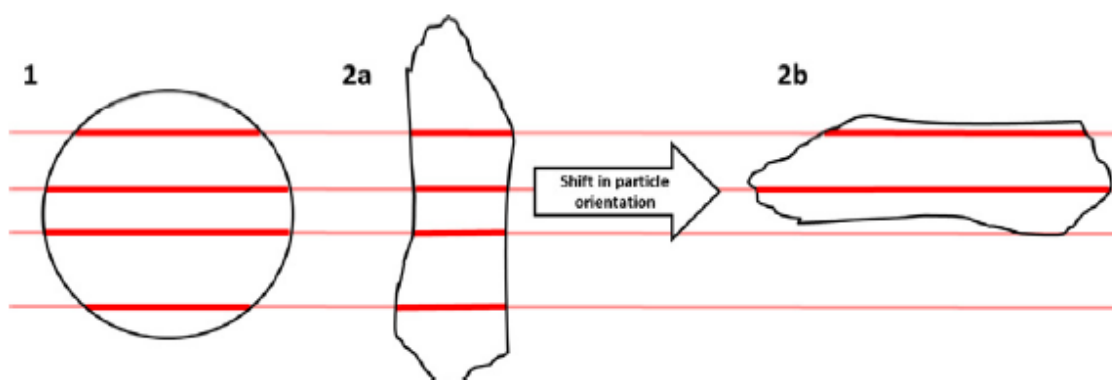


Figure 6: Examples of the measurement of chord length (bold red line) when a laser beam crosses (1) a spherical particle and (2a and 2b) non-spherical particle in two distinct positions. Illustration of the influence of particle orientation on chord length. [38]

The interpretation of chord length distribution (CLD) is of considerable importance to obtain actual particle size distribution (PSD), whose value can be significantly different from CLD. Apart from the fact that particle size is easier to interpret when compared to chord length, it permits the comparison to particle size measured by other techniques as most instruments present their results as PSD. Despite SFV and FBRM use a laser beam for their measurements, chord length is obtained in a distinct way on both techniques. FBRM calculates chord length from the reflected laser light detected by the probe, while SFV calculates chord length from the shadows generated by the particles crossed by a laser beam. Apart from the measurement mechanism, the techniques also differ in terms of probe design. The measurement (sapphire) window of FBRM probe (e.g. FBRM® C35 by Mettler-Toledo) is positioned at the tip of the probe, whereas the SFV probe (e.g. Parsum® IPP70 by Malvern) has its measuring gap inside the probe between two measurement windows. [38] For the FBRM® C35 system, the implementation of the probe on the process environment is significantly important. Particles placed a few hundred micrometers away from the probe are more likely not to be measured, reason why it is required for particles to flow over the sapphire window. [61] Parsum® IPP70 can perform real-time size measurements for particle over the dynamic range of 50 up to 6000 μm , while FBRM is more adequate for the measurement of systems sized between 3 and 3000 μm . [62], [63]

There are several advantages of using the SFV and FBRM techniques such as the fact that no sampling and calibration is required and the real-time measurement at high particle loadings (ideal for fluid bed monitoring). [63]

1.3.1.2.2.1. Spatial filtering velocimetry

Spatial filtering velocimetry (SFV) is a technique used for the concurrent measurement of particle size and velocity. The basic operation of SFV is to observe the shadow of particles moving in-between two sapphire windows (measuring gap) of the probe. During SFV measurements, a laser beam passes through the moving particles resulting in the cast of shadows on the opposite side of the measuring gap, on which there are two fiber-optic receivers for detecting the velocity and the time-of-flight of each individual particle. The velocity sensor is a spatial frequency filter that consists of linear optical fibers, while the time-of-flight detector is a single optical fiber placed after it. The shadow cast onto an array of optical fibers generates a burst signal whose frequency along with the known lattice constant of the array will permit the calculation of the velocity of each individual particle. The addition of a single optical channel generates a secondary signal (time-of-flight) as the beam passes through the moving particles. By knowing the velocity and the time-of-flight for each particle, chord length can be determined, and is then stored in an adjustable-length ring buffer. The ring buffer

detains the total number of particles and is continuously updated by replacing old particle measurements by recent ones. This continuous update will allow the calculation of particle size distribution. Therefore, a higher number of particles in the buffer is preferable considering that a lower value is associated to more unreliable size results. [63]–[65]

The SFV techniques has been successfully used to obtain granule size information during fluid bed granulation (FBG) utilizing an in-line, at-line and off-line experimental approach which demonstrates the technique’s ability to uninterruptedly monitor the granule size distribution during processing (Figure 7). [63]

A system based on the SFV principle is the Parsum® IPP70 probe developed by Malvern. The Parsum® instrument is an in-line particle sizing probe designed to measure the particle size and size distribution in pharmaceutical processes. It can be utilized for particle characterization of dense particle flows that can be found in fluidizing bed processes. The Parsum® measurement software allows a flexible interface that is capable of reporting size after converting raw CLD into a number or volume-based PSD through an algorithm in the system’s software. [62], [66]

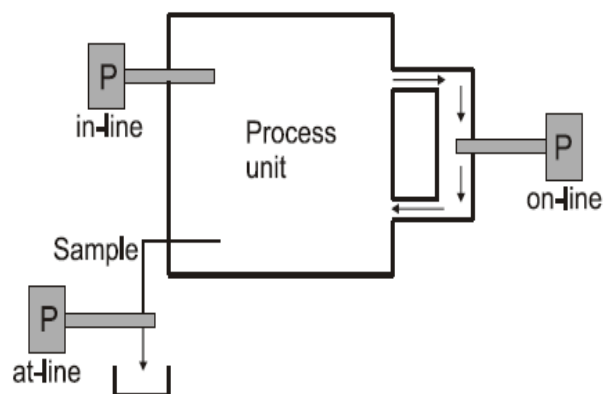


Figure 7: Illustration of three types of measurements with the probe systems. [63]

1.3.1.2.2.2. Focused beam reflectance measurements

Focused beam reflectance measurement (FBRM) is an in-line technique designed for monitoring chord lengths. The FBRM probe operates based on the principle of laser back-scattering. In a FBRM method, a tightly-focused laser beam is projected through the sapphire window of the probe, as shown in Figure 8a. When the laser beam contacts a particle passing near the probe window, light is reflected and detected as it propagates back through the probe. The light reflectance continues until the rotating focused beam reaches the opposite edge of the particle. The light back-scattered towards the probe is utilized to determine particle chord length and particle chord length distribution. The particle chord length is calculated through the

software by multiplying the optical rotating laser scan speed of the laser by the duration of time for which the beam is reflected. The laser scan speed can be regulated between 2 to 8 m/s depending on the particle size distributions, and dispersion concentrations and flow rates of the sample. [38], [67] A high speed of the laser scan allows the assessment of thousands of particle chord lengths per second, generating a chord length distribution (CLD) which is a function of the actual PSD (Figure 8b). The results are presented as a number-based CLD, i.e., the number of particles within a size (chord length) class. Additionally, the apparatus software enables the extraction of D-values from the number-based CLDs. [68]

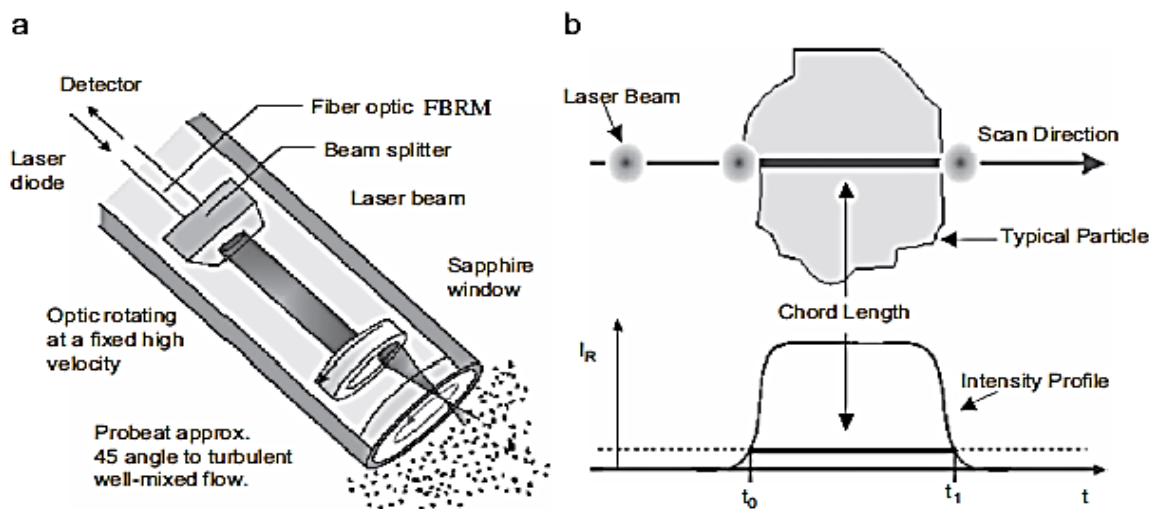


Figure 8: (a) The FBRM probe technique; (b) Measurement of a particle chord length using the FBRM technique. [68]

The measuring instrument consists of three parts: a computer for data assemble and analysis, a measurement unit and the measurement probe itself. FBRM is a user-friendly instrument that requires nominal maintenance and calibration requirements. Its most significant disadvantage is the fouling phenomena that can occur on the probe window. This is caused by dispersed material that sticks to the probe window which results on the same particles being counted several times, compromising the quality of the monitoring system itself. [69]

The FBRM® C35 technology developed by Mettler Toledo, a global leader in PAT for in-situ particle characterization within the pharmaceutical industry, addresses window fouling as a potential issue in numerous applications. Accordingly, the fouling drawback was overhauled by including a patented scraper unit that keeps the probe window clean during real time in-process measurements enabling measurements to be performed in highly concentrated particle systems. [61] In contrast to the FBRM® C35 probe, the Parsum® IPP70 is designed to perform in-line measurements of adhesive or wet material. In this case, the measurement

windows are kept clean due to an internal and external pressurized air connection existing on the probe. [62]

As a particle chord distribution differs from particle size, several studies have been done to establish a relationship between CLD and PSD. The Parsum® IPP70's software results can be presented as PSD as it performs the CLD-PSD conversion itself. In the other hand, using the FBRM®35, the results are expressed as chord length. The simplest way to perform a CLD-PSD conversion is through the development of a PSD-CLD model in order to calculate a CLD correspondent to a known PSD and shape. Once the PSD-CLD model is attained, it should be inverted to obtain a PSD based on a CLD value (CLD-PSD model). [38]

1.4. ConsiGma™-25 continuous manufacturing system

A truly continuous granulation line is the ConsiGma™-25 system developed by GEA Pharma Systems, Collette™ (Wommelgem, Belgium. The ConsiGma system consists of three modules: a continuous twin-screw granulation module, a six-segmented cell fluid bed dryer and a product control unit (also known as granule conditioning unit) (Figure 9). In addition, the ConsiGma line allows complementary blending, tableting and coating by attaching a blender, a tablet press, and a coater, respectively, to the product control unit (Figure 10). However, the thesis was not focused on these three additional unit operations. [70]–[74]

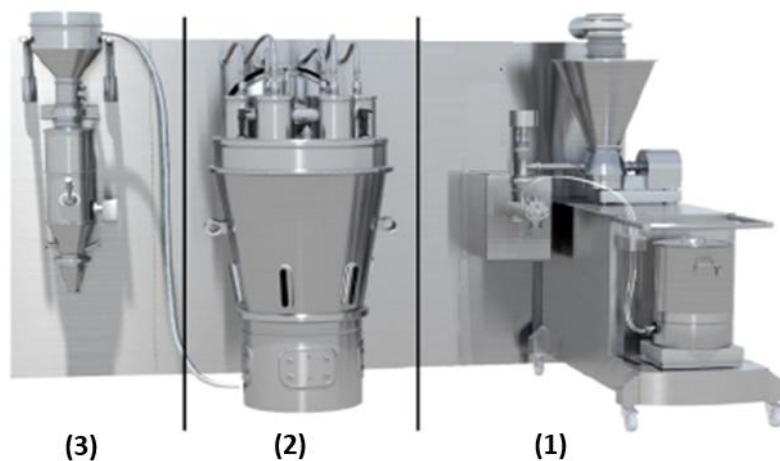


Figure 9: ConsiGma™-25 continuous manufacturing line. (1) Continuous twin-screw granulation module; (2) Six-segmented cell fluid bed dryer; (3) Product control unit. [4]

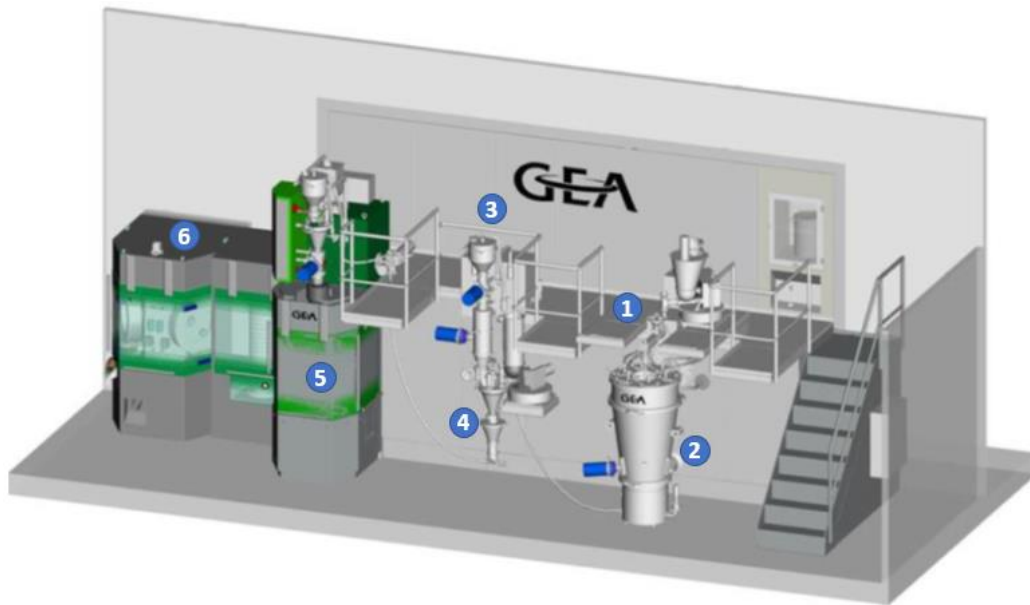


Figure 10: ConsiGma™-25 continuous line: 1. Twin-screw granulator; 2. Six-cell segmented fluid bed dryer; 3. Product control unit; 4. Blender (external phase); 5. Tablet press; 6. Tablet coater (Courtesy of GEA Pharma Systems). [4]

1.4.1. Continuous twin-screw granulator

The continuous granulation module consists of a powder dosing unit (i.e. powder feeder), a liquid addition module and the twin-screw granulator (TSG) itself (Figure 11). The powder dosing unit operates based on the loss-in-weight principle, and continuously feeds a pre-blended mixture consisting of excipients and active pharmaceutical ingredient (APIs) into the granulator. Alternatively, several feeders can act simultaneously, each one dosing a different ingredient (excipient or API) to the feeder which homogenizes the material before entering the granulator. Furthermore, before reaching the granulator, the pre-blended mixture is passed through a rotational bridge breaker which prevents bridging and ensures an extra mixing step of feed before entering the granulator.

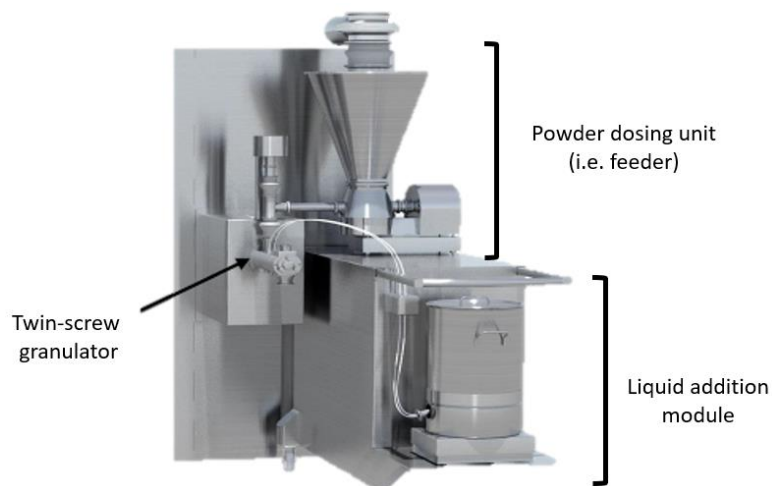


Figure 11: Continuous granulation module. [4]

The granulation unit consists of a barrel enclosing two co-rotating screws, containing either conveying or kneading elements for transportation and mixing purposes, respectively. The screws consist of a long transport zone and two kneading zones (also known as mixing zones). Each kneading zone contains six kneading elements in an angle of 60° and are separated from each other by a short transport zone, that has the same length as a mixing zone. The modular structure of the screws makes it possible to vary the number of kneading elements, therefore allowing to modify the length of the mixing zone (Figure 12).

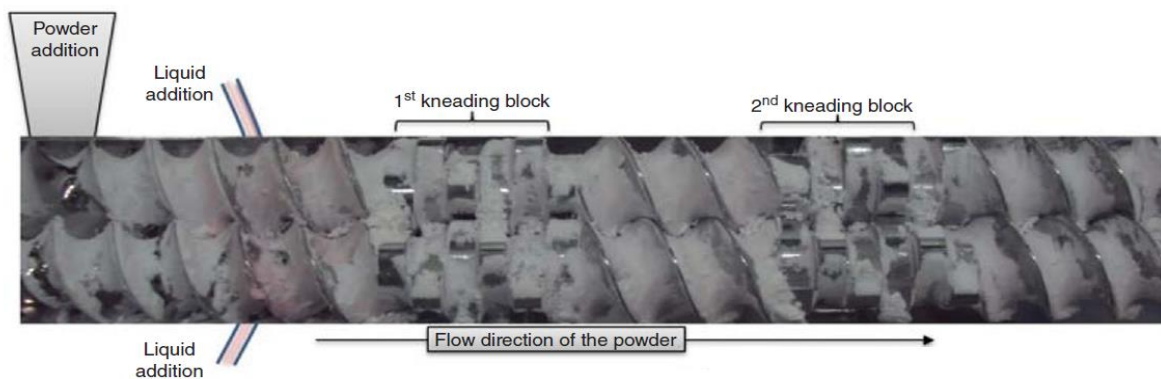


Figure 12: Screw configuration with 12 kneading elements (two mixing blocks, each containing six kneading elements) indicating the geometry of the screws used in a TSG. [72]

The barrel of the continuous granulator can be divided into three segments: a feed segment, a work segment and a discharge segment (Figure 13). In the feed segment, the powder is fed into the barrel containing screws with conveying elements (transport zone). The dry powder is blended while being transported to the work segment. In the work segment, granulation occurs due to the intensive mixing of the powder with the granulation liquid. The change of particle morphology from small (micro-structure) to large (macro-structure) is done by the kneading elements present on both mixing zones. The granulation liquid is fed into the granulator right before the first mixing zone through two injection nozzles, one for each screw, using a peristaltic pump (loss-in-weight principle). The wet granules produced are unloaded from the barrel in the discharge segment and are pneumatically transferred to the six-segmented cell fluid bed dryer. [70]–[74]

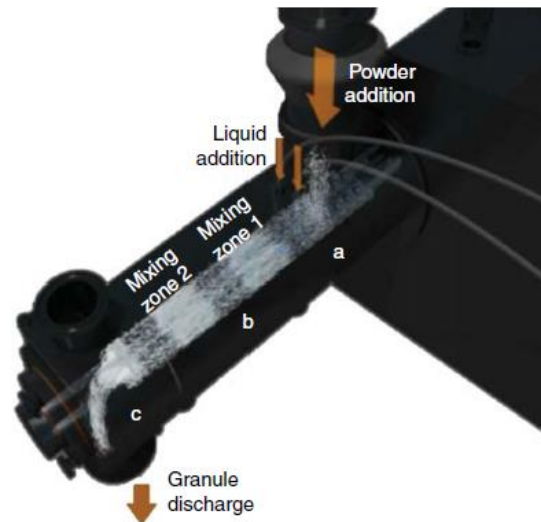


Figure 13: The feed segment (a), work segment (b) and discharge segment (c) of a TSG during operation. [72]

1.4.2. Six-segmented cell fluid bed dryer

The granulation and drying units of the ConsiGma™-25 line (Ghent, Belgium) are lined up horizontally, reason why the granules are pneumatically transported from the granulation barrel to the top of the six-segmented fluid bed dryer. For new generation systems, the twin-screw granulation is placed on top of the dryer allowing the gravitational transfer of wet granules to the dryer.

The fluid bed dryer consists of six identical cells which are sequentially charged and discharged, one after the other, ensuring a continuous flow of incoming wet granules and outgoing dry granules (Figure 14 and Figure 15). The granules are dried by hot air, whose flow (m^3), humidity (%RH) and temperature ($^{\circ}C$) can be controlled while the actual temperature inside the individual cell is monitored. The number of cells is user-defined depending on the quantity of material used. The material inside a cell can vary between a minimum of 0.5 and a maximum of 1.5 kg. The airflow, which is set from bottom-to-top, is regulated by a push/fan system while a fan/blower system regulates the pressure within the dryer. Several HEPA filters are placed at the air outlets of the dryer to ensure that there is no material exiting the system. The cells dry for a predefined period, and after discharge, remain inactive until they are once again filled. After a set drying period, the granules are vacuum discharged from the drying segment through a rotational outlet valve and are transferred to the product control unit. [70]–[74]

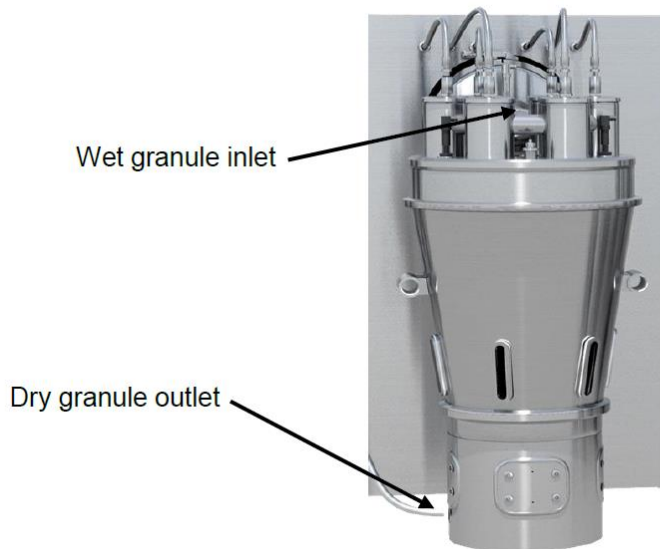


Figure 14: Six-segmented cell fluid bed dryer. [4]



Figure 15: Inside view of the six-segmented cell fluid bed dryer. [4]

1.4.3. Product control unit

The dry granules discharged from the cells are then transported to the product control hopper with an integrated mill (Figure 16). The granules are gravitationally fed, at a constant flow, to the mill inlet. The resulting milled material is discharged gravitationally, and can undergo further processing, such as blending, tableting and coating. [70]–[74]



Figure 16: Product control unit. [4]

1.5. Artificial neural networks

An artificial neural network (ANN) is a computational technique designed to simulate the information processing ability of a human brain, although in a much simpler way. However, it still resembles the human brain in various aspects. ANNs have the ability to process a broad amount of data and acquire knowledge through learning procedures (also known as network training). After the network has undergone the learning procedure, it is capable of storing information, which can be further applied to unknown data. For these reasons, ANNs are considered highly useful for classification and prediction purposes based on pattern recognition. [75]

All ANNs are characterized by their architecture and training process. The architecture of a given ANN determines how the neurons are arranged within the network. The network is usually divided into three segments known as: input layer, hidden layer(s) and output layer. On the other hand, the training process aims the adjustment of the connections between neurons, which will ultimately allow to approximate the output of the network being trained to the desired value. [76]

An ANN consists of a number of processing elements (PE), called neurons, that are connected by coefficients (weights), forming the neural structure. The neuron receives one or more inputs from an external source or from an output of another neuron, and produces its own output. The outputs of all the neurons of the neural structure will ultimately propagate through the network towards the final layer (output layer) where the final output is obtained. Each inter-neuron

connection has a processing weight, which is acquired during the training process of the neural network. The processing weight is indicative of the relevance that every single input linked to the neuron. [77]

As shown in Figure 17, the inputs (x_1 , x_2 and x_3) have a connection weight associated to them (w_1 , w_2 and w_3). The inputs are multiplied by the connection weight, then the set of inputs are summed (activation function) and fed into a transfer function ($f(\sum x_i w_i)$) in order to produce an output (y). [78]

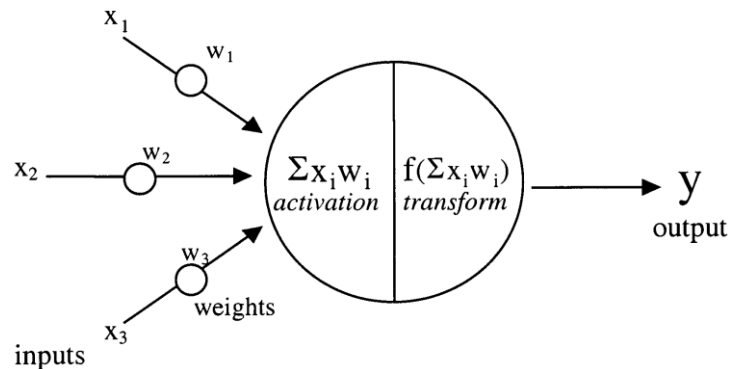


Figure 17: Structure of an artificial neuron. [79]

In addition to the inputs, another element with a weight associated to it must be considered within the neural structure. This additional element is usually called a bias and allows the activation function to be shifted (left or right) depending on its weight value. In other words, it determines whether or not the activation function of a given neuron will propagate forward throughout the network. Considering the integration of a bias, before the activation is applied, the bias values must be added to the summed weighted inputs. Alike the several weights of the network, biases undergo the training procedure, which means that their weight values will suffer a readjustment. [77], [80]

Taking into consideration the aim of the present thesis, all discussion regarding neural networks will be focused on multilayer ANNs. In general, multilayer ANNs can be divided in two main categories concerning the architecture of the network: feedforward neural networks and the recurrent neural networks. The categories differ from each other in terms of the type of inter-neuron connection used on the neural structure. When using a feedforward neural network the signal travels throughout the network in one single direction: from input to output. There are no feedback loops, i.e., there is no feedback from the outputs of the neurons to towards the inputs. On the other hand, recurrent neural networks make use of feedback loops which allow the signal to travel in both directions. [81]

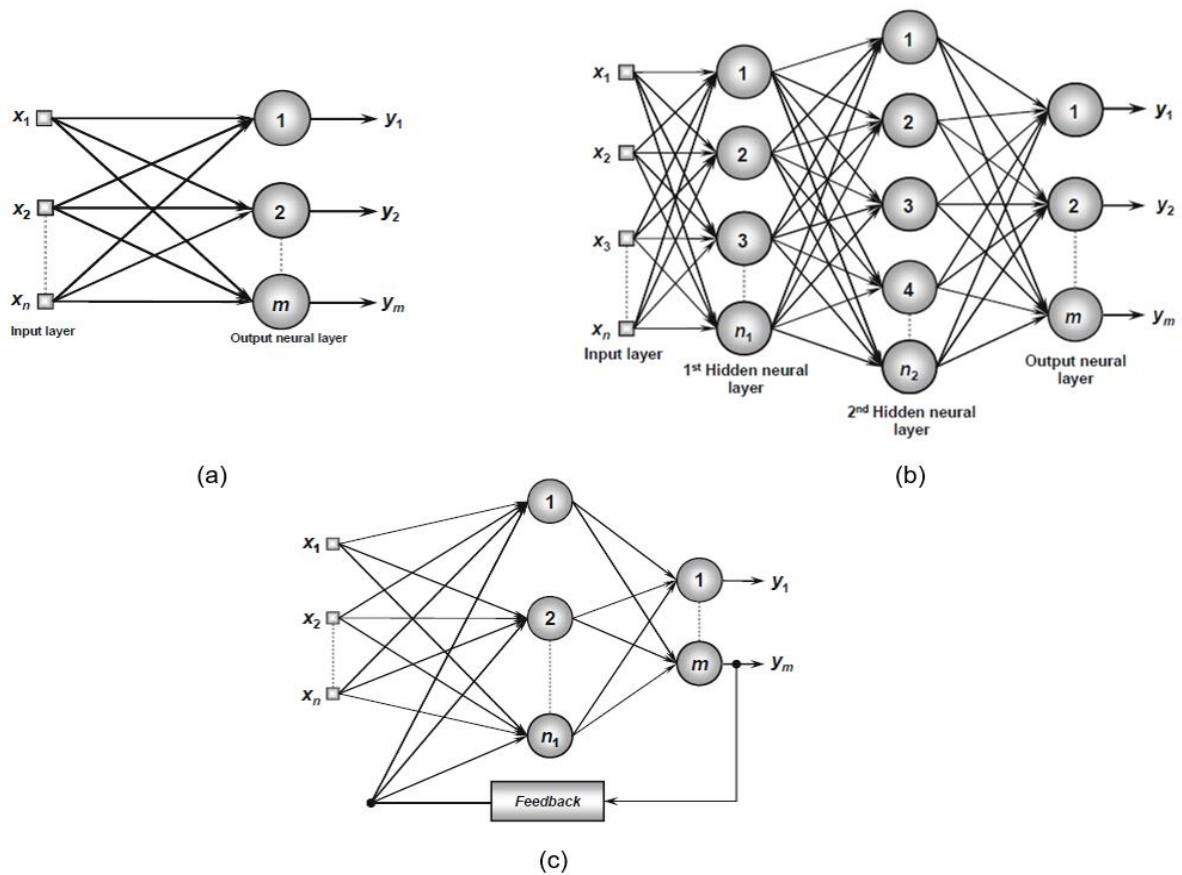


Figure 18: Example of neural networks. (a) single-layer feedforward network; (b) multilayer feedforward network; (c) recurrent network. (adapted from [76])

1.5.1. Multilayer artificial neural networks

In a multilayer feedforward neural network, the signal follows a unidirectional flow from the input towards the output layer, which means that there is a straightforward association between inputs and outputs. Depending on the number of layers, this type of network can be denominated as single layer or multilayer feedforward neural network. [81]

1.5.1.1. Single-layer feedforward artificial neural network

In Figure 18a, a feedforward neural network consisting of one layer is shown. This type of network is composed by n inputs and m outputs, integrated in the input and output layers, respectively. Despite two layers are included in single-layer feedforward ANN, the input layer is not taken into consideration as computation is only performed on the output layer. The input signals (x_1, x_2, \dots, x_n) propagate towards the output layer through the inter-neuron connections (weights) and the neurons there located ($1, 2, \dots, m$) produce the final output signals (y_1, y_2, \dots, y_n). The number of neurons will always correspond to the number of outputs computed by the network. [76]

1.5.1.2. Multilayer feedforward artificial neural network

Contrarily to a single-layer feedforward network, a multilayer feedforward network is composed by one or more hidden layers in-between the input and output layers. The number of hidden layers and the number of neurons which is composed by are dependent on the problem being mapped by the ANN, in addition to the condition of the data, quantitatively and qualitatively wise.

In Figure 18b a neural network with two hidden layers with an unequal number of neurons is shown. The network is referred as a n - n_1 - n_2 - m network as there are n inputs, n_1 and n_2 neurons on the first and second hidden layer, respectively, and m output neurons. Both Figure 18a and Figure 18b display a “fully connected” network, which means that each neuron, placed in every layer, is connected to any other neuron of the layer ahead. In case some inter-neuron connections are not observed, the network is designated as “partially connected”. Similarly to a single-layer feedforward neural network, this type of network will compute the same number of output signals as the number of neurons located at the output layer. [76], [81]

1.5.2. Recurrent artificial neural network

In recurrent ANNs, the outputs of the neurons are utilized as feedback inputs of the previous layers, or of the same layer (Figure 18c). These networks have the capability of elaborating data through the time, i.e., they can be used on time-variant systems, as time series prediction. For this reason, recurrent networks are considered to be dynamic as they acknowledge that a system remains in constant change and progress over time and that a relationship between current and past events exists. Thus, using the recurrent ANN, the output is analyzed as a function of the previous output value, which means that the final output produced by the network will correspond to an integration of not only the input values but also of the previous states of the system. [76]

1.5.2.1. Non-linear autoregressive network with exogenous inputs

The non-linear autoregressive network with exogenous inputs (NARX) is a class of recurrent networks well suited for time-series modelling. The NARX is a dynamic network and has feedback connections towards previous layers within the network. This recurrent network can be described by the following equation:

$$y(t) = f(x(t-1), \dots, x(t-d), y(t-1), \dots, y(t-d))$$

Where the value of the output signal ($y(t)$) is a function of past values of itself ($y(t - 1), \dots, y(t - d)$) and previous values of (exogenous) input signals ($x(t - 1), \dots, x(t - d)$). The NARX model is commonly used in time-series modelling as a predictor, with the goal of predicting the next value of a certain input signal. [82] One of the reasons why this type of neural network is broadly used remains in the fact that it can present different architectures, as shown in Figure 19. It is possible to create a NARX network with a series-parallel (open loop) architecture which is extremely useful for training, and then rearrange it into a parallel (closed loop) architecture. This rearrangement presents two main advantages. Firstly, the input provided to the feedforward network is more precise, and secondly, as the network presents a feedforward architecture, it can be trained using the back-propagation algorithm, which will ultimately enable a faster and more efficient training process when compared to a parallel architecture. In regard to the series-parallel architecture, training is performed using the true output rather than feeding back the estimated output, which is characteristic of a parallel architecture. However, a series-parallel architecture is only able to perform “one-step ahead” predictions, reason why a rearrangement is highly appropriate as the parallel architecture enables “multi-step ahead” predictions. [83]

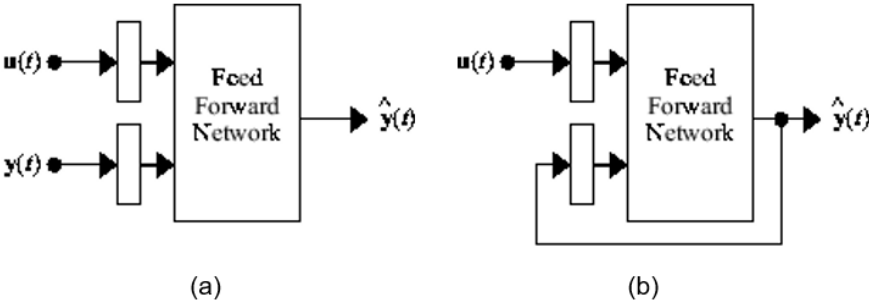


Figure 19: NARX neural network. (a) Series-Parallel Architecture. (b) Parallel Architecture. [82]

1.5.3. Training process

As previously mentioned, one of the most significant characteristics of ANNs is their ability to acquire knowledge regarding the system behavior through learning procedures. Once the network is capable of recognizing existing input-output relationships from a complete dataset, it can produce an output that will closely correspond to the expected output of a given set of inputs. [75]

The goal of the training process (also known as learning) is to achieve the best linear/non-linear relationship between inputs and outputs of a complete dataset, which is done by the adjustment of the weight/bias values associated to the neurons. During the training procedure,

the ANN will attain discriminant features from the dataset which will allow to determine input-output relationships. [78]

Normally, the complete dataset is split into two subsets, called training subset and test subset. The training and test subsets consist of 60 to 90% and 10 to 40%, respectively, of the samples composing the complete dataset. The training subset is used in the learning procedure of neural network, while the test subset is utilized to assess predictive ability of the network. [76] Once the training-test division is done, a percentage of the training dataset is chosen to integrate the calibration and validation subsets. Thus, the training process includes both a calibration and a validation step. Whereas the calibration subset is used for training, i.e., weight adjustment, the validation subset is utilized to make sure that the overfitting phenomena does not occur. [84] A model is considered overfit when it can classify very well the data in the calibration subset but is unable to generalize and perform accurate classification on data that it was not trained on. The overfitting phenomena is among the most critical issues when training a neural network. [85]

Each cycle of presentation of all the samples of the training subset is named training iteration (epoch). Each training iteration converts the weights somewhat more efficient in terms of converting inputs into outputs, which involves the enhancement or weakening of the interneuron connections. [78] During training, the model will be classifying each input from the validation subset as well, however no weight adjustment is performed. In this case, the classification will be done based on what the model has learned regarding the data that is being used for training. The iterative process should be ceased when an inflection point is detected, i.e., when the validation dataset acquires an error value higher than the last one assessed. However, many different early-stopping implementations can be defined. The weight values of inter-neuron connections at that epoch are recorded and can then be applied to the test subset. [86] The testing process will be used to predict the output values of new unseen data (test subset), which will ultimately provide a realistic performance assessment of the trained neural network model. [87]

The learning procedure can be executed using two different approaches, a supervised or an unsupervised training/learning (Figure 20).

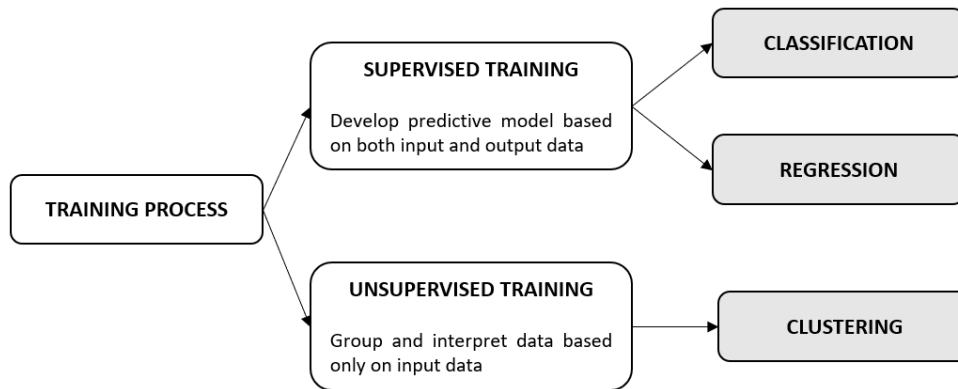


Figure 20: Types of training. [86]

1.5.3.1. Supervised training

The supervised approach is the most commonly used, being highly indicated for classification and regression purposes. It utilizes known input and output data to train the network for it to be able to generate acceptable predictions in response to new unseen data. Therefore, the output values must be known, and the data used during training has to be well-established, i.e., correctly labelled. Classification methods are utilized to develop a predictive model. Classification methods are used to classify the input data into classes, while regression methods are responsible for continuously predicting output values. [88]

1.5.3.2. Unsupervised training

Unsupervised training, on the other hand, is usually used to detect patterns and structures in the input data, reason why it is extremely suitable in exploratory data analysis. The most common task within this type of training is clustering, which consists of separating the input data into different groups according to the similarities detected between them. [88]

1.6. Objectives

This thesis aims at evaluating the possibility of estimating the mean particle size of dried granules produced by the ConsiGmaTM-25 continuous manufacturing system using a software sensor (inferential sensor) resorting to process variables logged at a very high rate. Given the underlying dynamic nature of the continuous system and the probable non-linear relationships, the type of modelling strategy was based on an autoregressive multilayer feedforward neural network. The neural network was calibrated resorting to process data (e.g., feed-rates, temperatures, pressures) logged by the ConsiGmTM-25 against the median

particle size (d50) obtained also in real-time by a focused beam reflectance measurement (FBRM). The FBRM probe was positioned immediately after one of the multiple drying chambers used by ConsiGma25-TM. The objective is to assess the feasibility of a software sensor for estimating this important material property paving the way to the possibility of estimating the same property on different process locations and, eventually, replacing the need for physical equipment, that is known to represent a substantial fraction of the investment when setting up a PAT monitoring strategy on pharmaceutical processes.

2. Materials and methods

2.1. Pharmaceutical formulation

A pharmaceutical dry premix containing two APIs, powdered cellulose, maize starch, pregelatinized starch and sodium starch glycolate was granulated with distilled water in the ConsiGma™-25 system.

2.2. Manufacturing process

The experiments were performed in the continuous production line ConsiGma™-25 line (GEA Pharma Systems, Collette™ Wommelgem, Belgium), previously described in Subchapter 1.4. During the runs, the powder dosing unit fed the dry premix to the granulator at a speed of 20 kg/h. The liquid addition module fed the granulation liquid (water) at a rate of 50 g/min. The screw speed and barrel temperature were set at 900 rpm and 25°C, respectively. The six cells were filled for 180 seconds sequentially, one after each other, ensuring a continuous operation. The drying time was set to 790 seconds in total, including the 180 seconds cell filling time. During the last seconds of drying, granules were pneumatically discharged to the product control unit after which the cell remained inactive for 290 seconds until new wet granules were introduced for a new drying cycle (Figure 21). At the product control unit, the dried material was milled and subsequently discharged from the system. The air handling unit, responsible for preparing the air entering the dryer according to the defined setpoints, contains a dehumidifier inside which unit removes moisture from the incoming air. In addition, a push/fan system regulated the air flow inside the dryer while a fan/blower system controlled the pressure. Both the air exiting the dryer and the product control unit had to pass through different HEPA filters in order to prevent particulate material to be carried out of the system.

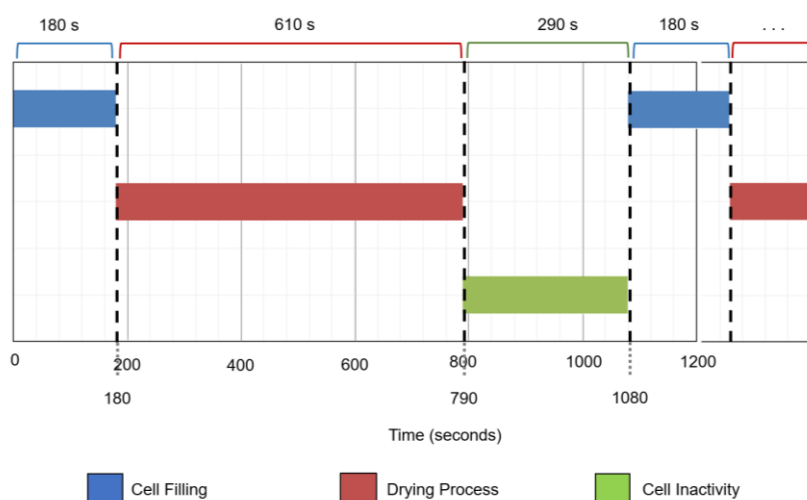


Figure 21: Schematic representation of time lengths of cell filling, drying process and cell inactivity time.

2.3. In-process measurements

In multiple locations of the ConsiGma™-25 system, fifty sensors were continuously measuring variables (e.g., temperatures, pressures, etc.) essential to the control system of the process. These were logged every second. These process variables, summarized in Annex 1, incorporate user-set variables (setpoints) as well as other variables (open loop variables) that are simply measured, i.e., are not set by the user. Although the setpoints are pre-defined, variances around their set point value may occur due to disturbances which will then be corrected by the system itself by means of independent proportional-integral-derivate (PID) controllers. The set value for each setpoint is also described in Annex 1.

2.3.1. In-line particle size analysis

A FBRM probe (FBRM™ C35, Mettler-Toledo) was used for measuring particle size distribution (d50 profile) every 10 seconds. The probe was placed, at an angle of approximately 45°, inside dryer cell no. 4 located at the six-segmented cell fluid bed dryer unit.

2.4. Continuous manufacturing runs

As observed in Table 1, a total of sixteen continuous manufacturing runs were produced during August of 2014. Eight of the sixteen runs (Run 8-15) were performed in normal operating conditions (NOC) and, therefore, are known as reference runs. For the eight remaining runs (Run 1-7, 16), a disturbance was imposed. Thus, for each disturbed run, a different setpoint was changed at the time dryer cell no. 1 was filled for the fourth time (3240 seconds; sampling point no. 324) and altered back to the original set value when the same cell was filled for the seventh time (6480 seconds; sampling point no. 648), as shown in Figure 22. The time length of the disturbance (three fills) was selected to guarantee that the effect of the disturbances could be visibly identified, and that a new steady state would be observed. The inclusion of runs with an imposed disturbance in the present work was related to the need of an evaluation of the impact that a certain disturbance can have on the particle size value. However, runs were not defined in accordance to an experimental design.

For Run 1 the imposed disturbance was the increase of the dryer air flow (V4) from 360 to 400 m³/h. In Run 2, the granulator barrel temperature (V23) was increased from 25 °C to 35°C. Despite the setpoint being set at 25°C, the logged average temperature varied around 28°C. When the setpoint was changed to 35°C, the temperature increased to 36°C. For both Run 3 and Run 4, there was not a provoked disturbance. Run 3 differs from the NOC runs, due to the occurrence of the caking phenomena. Regarding Run 4, the system was not cleaned after the previous run (Run 8). In Run 5, the temperature of the air entering in the dryer was changed

from 50 °C to 60 °C. Another set point changed was the granulation liquid mass flow (Run6 V46) from 58 to 66.7 g/min. For Run 7 the powder dosing unit mass flow (V37) was changed between 25 to 21.7 kg/h. The final setpoint changed was the granulator screws speed (Run16 V19) that was altered between 700 and 900 rpm.

Table 1: Sixteen continuous manufacturing runs.

Run	Description	Date
1	Airflow	19.08.2014
2	Barrel Temperature	20.08.2014
3	Caking Reference	14.08.2014
4	Dirty Reference	13.08.2014
5	Drying Temperature	19.08.2014
6	Liquid	12.08.2014
7	Powder	20.08.2014
8	Reference 1	12.08.2014
9	Reference 2	13.08.2014
10	Reference 3	13.08.2014
11	Reference 4	13.08.2014
12	Reference 5	14.08.2014
13	Reference 6	15.08.2014
14	Reference 7	15.08.2014
15	Reference 8	21.08.2014
16	Speed	18.08.2014

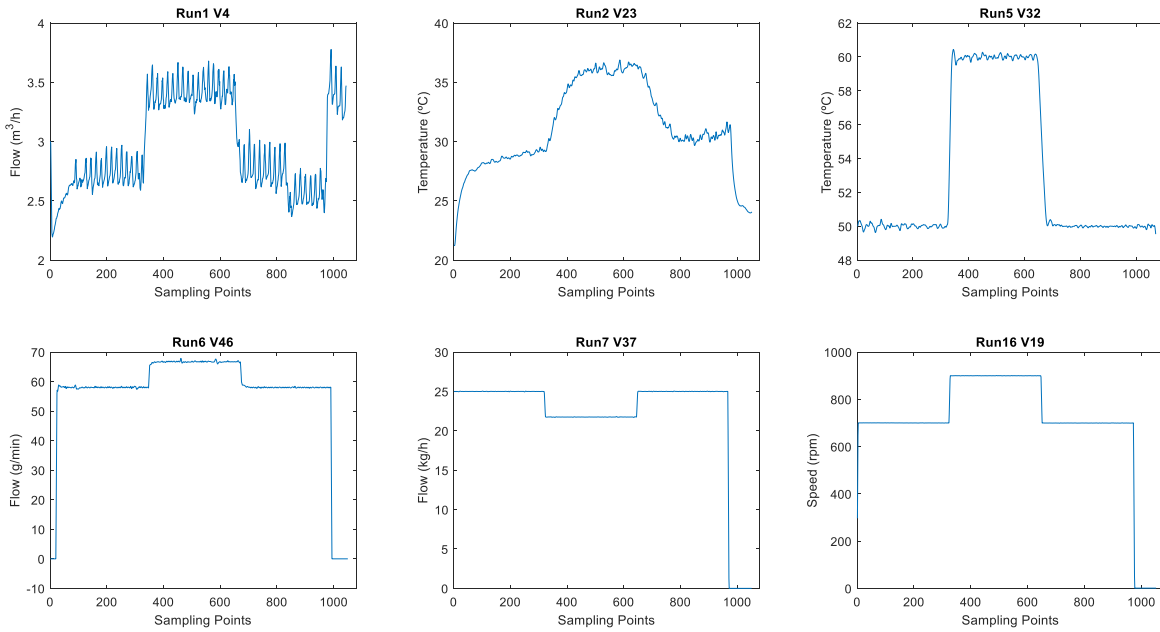


Figure 22: Disturbances imposed on Runs 1, 2, 5, 6, 7 and 16.

2.5. Data collection

The collected data from each run of the continuous production line was represented by two two-dimensional data arrays, X_n and Y_n , being n correspondent to the run. Since a total of sixteen runs were performed, thirty-two data arrays were used in this work, sixteen of them associated to in-process measurements and the other sixteen to the d_{50} measurements. A two-dimensional array X_n ($A \times B$) indicates that B process variables were measured at A time intervals. Additionally, a data array Y_n ($C \times D$) was also used, being D correspondent to the d_{50} value measured at C sampling times. Whereas the data array X_n includes fifty process variables measured every second within multiple locations of the ConsiGma system, the data array Y_n consists of the d_{50} value measured every 10 seconds.

Table 2 and Table 3, respectively, display useful information in regard to data arrays X_n and Y_n . This information includes the number of times a measurement was performed, the time at which the process variables/ d_{50} were first and lastly assessed and, the total duration of sampling. It is acknowledgeable that the number of sampling points is much superior on data array X_n when compared to Y_n . This is mainly due to the fact that the process variables were assessed every second, in contrast with the d_{50} value which was measured every ten seconds. On the other hand, the process variables and d_{50} measurements were not performed exactly at the same time. While the in-process variables were measured throughout the entire length of the run, i.e., from the beginning until the shut-down of the system, particle size was only assessed during a time-section of the run. By taking Run 1 as an example, it is noticeable that the total run length corresponds to three hours, twenty-six minutes and thirty-two seconds,

which translates on 12 393 seconds corresponding to 12 3393 sampling points. Differently, the d50 value was assessed for two hours, fifty-three minutes and fifty seconds as the FBRM probe, started recording values, approximately, thirty minutes after the run began and stopped, two minutes prior to the shutdown of the system. In this case, the d50 value was measured for 10 440 seconds, however the number of sampling points corresponds to 1044 as measurements were performed every 10 seconds.

Nevertheless, it is noticeable that for Run 3 the d50 measurements were performed for a longer period of time when compared to the in-process variables measurements. This suggests that despite shutting down the ConsiGma system, the FBRM probe continued its operation for about two more minutes.

Table 2: Starting and ending time of the fifty in-process measurements performed within the three modules of the ConsiGmaTM-25 system.

Run	Number of Sampling Points	Start Time	End Time	Total Duration
1	12 393	13:11:54	16:38:26	03:26:32
2	12 357	08:24:33	11:50:29	03:25:56
3	4 066	07:45:52	08:53:37	01:07:45
4	3 799	12:45:18	13:48:36	01:03:18
5	11 930	08:27:32	11:46:21	03:18:49
6	11 341	14:42:15	17:51:15	03:09:00
7	11 306	14:09:41	17:18:06	03:08:25
8	7 626	08:33:27	10:40:32	02:07:05
9	4 835	09:12:22	10:32:56	01:20:34
10	4 926	11:22:04	12:44:09	01:22:05
11	5 029	15:07:57	16:31:45	01:23:48
12	4 870	12:41:14	14:02:23	01:21:09
13	7 442	07:59:16	10:03:17	02:04:01
14	8 538	14:02:58	16:25:15	02:22:17
15	6 153	09:05:14	10:47:46	01:42:32
16	12 909	13:03:11	16:38:19	03:35:08

Table 3: Starting and ending time of the d50 measurements performed by the FBRM probe inserted inside the dryer cell no.4.

Run	Number of Sampling Points	Starting Time	Ending Time	Total Duration
1	1044	13:42:29	16:36:19	02:53:50
2	1052	08:54:32	11:49:42	02:55:10
3	437	08:00:54	09:13:34	01:12:40
4	371	12:57:18	13:58:58	01:01:40
5	1126	08:48:05	11:55:35	03:07:30
6	1050	14:52:28	17:47:18	02:54:50
7	1113	14:23:04	17:28:24	03:05:20
8	618	08:55:25	10:38:15	01:42:50
9	336	09:27:52	10:23:42	00:55:50
10	387	11:35:05	12:39:25	01:04:20
11	409	15:18:11	16:26:11	01:08:00
12	436	12:50:31	14:03:01	01:12:30
13	679	08:10:44	10:03:44	01:53:00
14	777	14:14:57	16:24:17	02:09:20
15	398	09:37:26	10:43:36	01:06:10
16	1052	13:41:41	16:36:51	02:55:10

2.6. Data processing

All data arrays designated in the previously subchapter endured several steps of data processing. As the data assessed within all sixteen runs was utilized to predict future values of d50, a data processing step was highly recommendable. In contrast to raw data, processed data will allow the development of a robust model which will ultimately permit the attainment of good predictions of the d50 value. The several data processing steps described throughout Subchapters 2.6, 2.7 and 2.8 were executed using Matlab (R2016b) software.

2.6.1. Data alignment

Taking into consideration that the number of sampling points of the data arrays X_n and Y_n are not the same, a data alignment was performed. As the d50 measurements were performed in-between the process variables measurements, the alignment was done by preserving the

sampling points of Y_n . Once the exact time of every sampling point of Y_n was selected, the same sampling times were selected on X_n with the subsequent exclusion of the unselected sampling points. Whereas data array Y_n remained unchanged, array X_n had its number of sampling points narrowed to the number of points of its corresponding Y_n array. As a result, each run will be associated to an array X_n and Y_n with the number of sampling points depicted on Table 3, which ultimately represents a measurement performed every 10 seconds.

2.6.2. Data filtering

Once the data alignment was completed, a data filtering step was performed in two different stages: (1) zero removal and (2) 'NaN' (missing data) removal. At a first stage, the sampling points for which the d50 value corresponded to zero were removed. The removal of those same sampling points was performed in the X_n array. The second stage of data filtering consisted of removing 'NaN's present in X_n and, accordingly, the removal of those sampling points was done to the Y_n array. Throughout all data processing steps, the same sampling points were preserved in both X_n and Y_n arrays. Therefore, every time a sampling point was removed from either one of the arrays, the removal of that same point was executed on the corresponding X_n or Y_n array. This was done to ensure that both arrays of each run presented the same length once the processing step was finalized.

2.7. Data organization

Once the several steps of data processing were completed, all thirty-two data arrays were fragmented in smaller slots of data. The fragmentation was done based on the d50 profile (Y_n), which translated on the number of drying cycles performed on each run. Taking into account, that the length of all Y_n arrays is superior to the duration of one individual drying cycle (1080 seconds), Y_n will be composed of the d50 profile of different drying cycles. Figure 23 shows the d50 profile of Run 1, where nine drying cycles occurred, reason why the array was fragmented in nine smaller slots of data. The time intervals of the fragmentations were recorded, and the same division was done to its correspondent X_n array.

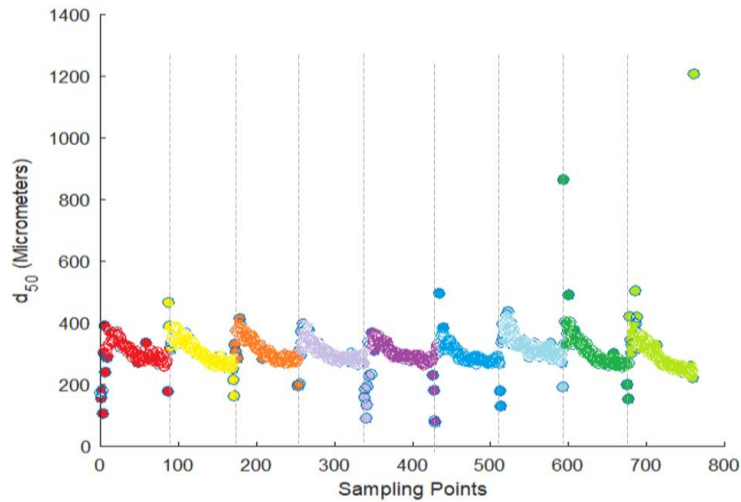


Figure 23:d50 profile (Run 1).

2.8. Supplementary data processing

Once the data fragmentation according to the number of drying cycles displayed was completed, a further data processing step was performed due to the existence of deviations within the smaller data arrays. For each run, each slot of data was analyzed, and a removal of outliers was completed. The removal was done by executing a script that eliminated sampling points for which its corresponding d50 value did not lie within a defined interval of values. Furthermore, a few sampling points from the beginning and/or end of each slot of data were also removed. Data slots with a low number of sampling points were excluded.

2.9. Modelling strategy

In this work, a non-linear autoregressive with exogenous inputs (NARX) neural network was utilized to predict the d50 value for a time t given past values of itself and process variables (exogenous). In order to generate accurate predictions of the d50 value, several steps for network optimization were performed, characterized by the determination of the following: (1) Input delay, (2) Input selection, (3) Run selection and (4) Training methodology. The optimization of the network was executed by means of the Matlab (R2016b) software and the Neural Networks Toolbox (version 9.1). A generic representation of the topology of a NARX neural network is shown in Figure 24.

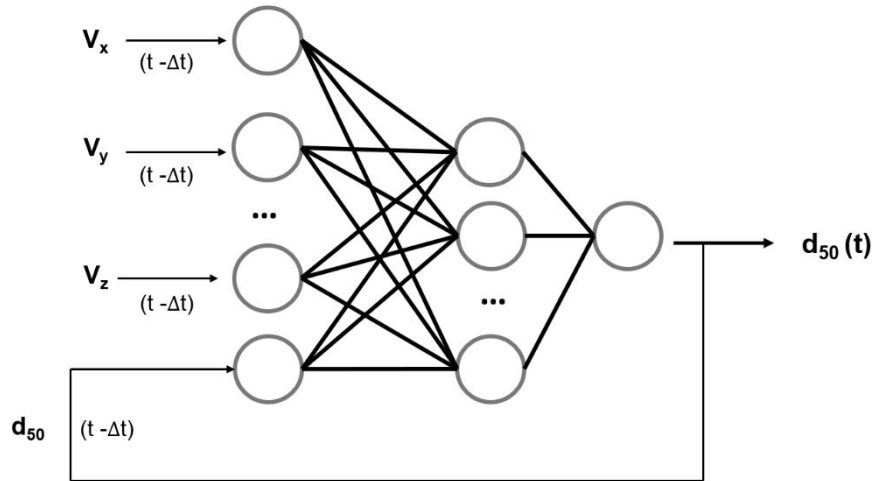


Figure 24: Generic representation of the NARX network.

2.9.1. Input delay

In this work, the effect of the existing time lags was minimized through a dataset adjustment based on the location where each univariate process parameter is measured. The delay value for each input variable included on the model was assigned based on the article “Linking granulation performance with residence time and granulation liquid distributions in twin-screw granulation: An experimental investigation” written by Kumar A., et al. [89] For this purpose, several assumptions were made for each process parameter based on the residence time of the granules in the twin-screw granulator, wet granules transfer line and fluid bed dryer.

2.9.2. Input selection

In this work, an input selection was performed with the overall goal of selecting a subset of variables that is considered to be relevant to the problem (i.e. d_{50} value). Although the subset corresponds to a representation that utilizes fewer variables, it will still express most of its information. This procedure is commonly known as data compression and it enables the reduction of unnecessary or irrelevant information in the data, which in turn will allow the neural network being optimized to perform the predictions of the d_{50} value in a more efficient way. Data compression was performed using two distinct approaches: (1) manual approach and (2) empirical approach. In the manual approach, a total of eighteen variables were excluded based on prior knowledge regarding the ConsiGma™-25 continuous line. Once completed the manual selection, a back-wise input selection was performed on the remaining thirty-two variables. The input selection technique included a total of thirty-one rounds, in which a sequential removal of the most irrelevant variables was executed. In each round, a model was performed as many times as the number of variables being evaluated. Thus, as thirty-two

variables were included in round 1, also thirty-two feedforward neural networks were used in this round. Each neural network used as an input a specific subset of variables composed by thirty-one variables to produce an output (i.e. d50 value). The mathematical model for which a better prediction was observed, i.e., that presented a lower RMSEP was selected and the variable not included in the input subset was identified. This procedure ultimately allowed to verify which subset of variables provided the best fit to the property of interest or, in other words, which variable that once excluded allowed the neural network to perform better predictions. Once the missing variable is identified, round 2 is executed using the same procedure described above, however, in this case, thirty-one neural networks were used to perform the output predictions. This procedure was carried out until one single variable is left which, in theory, corresponds to the variable that affects more significantly the d50 value predictions.

2.9.3. Run selection

In this work, the sixteen runs were split into two subsets, named training subset and test subset. The training subset was used in the learning procedure itself, while the test subset was used to assess the predictive ability of the network. A large amount of training data is essential to build a good empirical model, however it must be sufficiently representative of the data that is expected to be obtained during real-time operation of the analyzer (i.e. FBRM probe). In other words, the training subset must cover the range of states of the sample during the operation of the analyzer, which in turn will allow the network to have a good performance on its predictions. Therefore, a meticulous selection for the training subset must be carried out so that some states are not over-represented and others under-represented.

In order to perform the training-test division, two principal component analysis (PCA) were performed. The PCA models were used for data visualization, more specifically to reveal patterns in data such as clusters and outliers, along with their consistency between runs. The first PCA model was calibrated with the eight reference runs (Run 8-15), whereas the second PCA model made use of the runs for which a disturbance was imposed (Run 1-7,16).

Considering that the overall data was arranged as a three-mode array X_n (sixteen runs, fifty variables and the number of sampling points shown in Table 4), an unfolding step was performed to generate two-dimensional arrays. As a result of the unfolding step, two two-dimensional arrays were created, one with 2572 rows and a second with 4733 rows (Figure 25). Apart from the fifty process variables, another column corresponding to the d50 value (Y_n array) was added to both arrays. The final arrangement of both arrays is shown in Figure 25a and b. Before performing the PCA, both unfolded matrixes were mean centered and auto-scaled.

Table 4: Total number of rows for each two-dimensional array.

Description	Run	Number of Sampling Points	Total
Reference Runs	8	397	2572
	9	222	
	10	261	
	11	258	
	12	251	
	13	397	
	14	530	
	15	256	
Runs with an imposed disturbance	1	761	4733
	2	741	
	3	169	
	4	167	
	5	737	
	6	667	
	7	729	
	16	762	

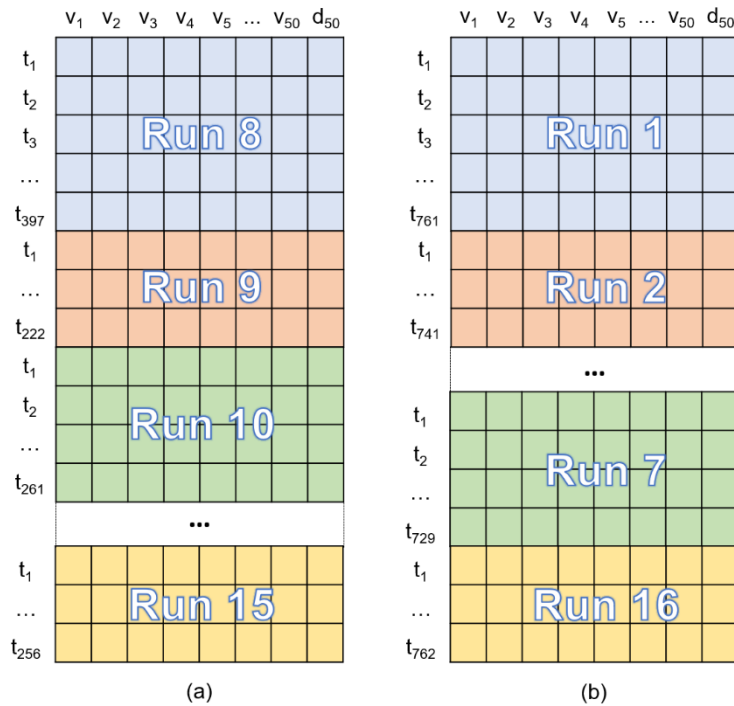


Figure 25: Final arrangement of each two-dimensional array (a) reference runs; (b) runs with an imposed disturbance.

2.9.4. Training methodology

The first essential step of network training is the train-test run division. Based on the results of the run selection described in the previous subchapter, twelve runs were selected for training, whereas four runs were used to test the predictive ability of the network. All train runs were divided in three different sets: calibration, validation and test. The division was automatically performed by the algorithm (50% for training, 25% for validation and 25% for testing). Considering that the data used in this work is not continuous, i.e., presents dynamics, the training procedure was performed using slots of data correspondent to drying cycles in alternative to the usage of the complete run dataset. The training procedure is composed by several iterations. In each iterative step, a randomly obtained drying cycle (from the calibration set) was presented to the network and an adjustment of its parameters occurred. During training, a total of three-hundred iterations were performed, meaning that three-hundred randomly selected cycles were presented to the network (Figure 26). As the iterative process progressed, the network becomes successively more capable of estimating data from the validation set in spite of not being used to adjust the parameters of the network. The end-point of the training process was defined by the increase of the validation error (inflection point). Once the validation error started increasing, the network started losing the ability of generalizing and classifying data that was not used for training (calibration and test set). Once ceased the training, the weights values of the interconnections were recorded, and the test set was applied. Considering that the network was trained with three-hundred randomly selected drying cycles, a total of one-hundred neural networks were created and trained (different initialization and runs/cycles order). The one hundred networks were tested with the entire calibration runs/cycles and the worst 25% in terms of RMSEC were excluded, while the remaining 75% were maintained. The final prediction for each model corresponds to the average of the predictions obtained from each selected network (75%). Further details regarding the training of the neural networks are described in Annex 3.

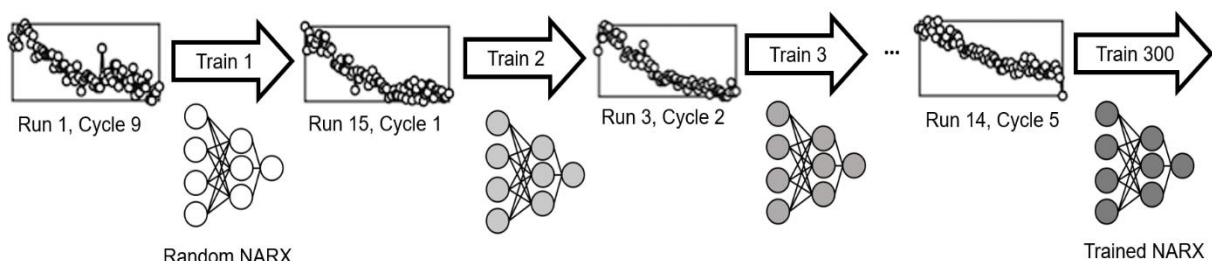


Figure 26: Example of the iterative steps occurring during the training of the neural network.

3. Results and Discussion

3.1. Data filtering

At a first stage of data filtering, sampling points for which the d50 value corresponded to zero were removed. The existence of values equal to zero within the Yn arrays is most certainly related to the setup of the FBRM probe. As mentioned before, the FBRM measurements are acquired when a laser beam enters in contact with the granule passing near the probe window. Thus, a d50 value equal to zero suggest that at that exact second, no granules were positioned near the tip of the probe. As demonstrated in Run 3, FBRM measurements kept being performed even though the system had already been shut-down. Once the system was shut-down, the flow of the dryer air inlet within the dryer cell is ceased. Consequently, the granules remain at the bottom of the dryer cell which prevents them from being detected by the FBRM probe. After removing the sampling points on the Yn array, the same points were removed on Xn array.

The second stage of data filtering consisted of the 'NaN' removal. For certain sampling points of the Xn arrays, the value of all fifty process variables was not acquired. This is likely due to punctual failures of the monitoring/control system established within the continuous line as for some of those sampling points, a d50 value was acquired. The sampling points removed from the Xn array were removed in its corresponding Yn array.

The total number of sampling points removed during the two stages of data filtering, is shown in Table 6. Table 6 depicts the number of sampling points of the Xn and Yn arrays of each run and the corresponding sampling duration.

Table 5: Total number of sampling points removed after the two stages of data filtering.

Run	Number of Sampling Points (Before Data Filtering)	Number of Sampling Points (After Data Filtering)	Number of Sampling Points Removed
1	1044	761	283
2	1052	741	311
3	437	169	268
4	371	167	204
5	1126	737	389
6	1050	667	383
7	1113	729	384
8	618	397	221
9	336	222	114

10	387	261	126
11	409	258	151
12	436	251	185
13	679	397	282
14	777	530	247
15	398	256	142
16	1052	762	290

Table 6: Total duration of both Xn and Yn arrays within each run.

Run	Number of Sampling Points	Total Duration
1	761	02:06:50
2	741	02:03:30
3	169	00:28:10
4	167	00:27:50
5	737	02:02:50
6	667	01:51:10
7	729	02:01:30
8	397	01:06:10
9	222	00:37:00
10	261	00:43:30
11	258	00:43:00
12	251	00:41:50
13	397	01:06:10
14	530	01:28:20
15	256	00:42:40
16	762	02:07:00

3.2. Data organization

After data processing, all thirty-two data arrays were fragmented into smaller slots of data. For each run, the fragmentation was done based on the d50 profile shown in the Yn array. As already stated in Subchapter 2.2, one drying cycle has the total duration of 1080 seconds which corresponds to approximately 108 sampling points. Although the duration of all drying

cycles must be equal to 1080 seconds, most of the cycles take less time to be concluded. In Figure 23 it is possible to state that during Run 1, nine drying cycles take place, each one of them with the approximate duration of 1000 seconds (100 sampling points). Once the drying cycles are identified, the start and end point of each drying cycle is established and, based on that information the fragmentation on Y1 is performed. For Run 1, Y1 will be divided into nine smaller slots of data, each one of them corresponding to one drying cycle. The exact same fragmentation is performed in X1, which will permit that for the time length of each slot of data, information regarding the fifty process variables and particle size is acquired.

Table 7 shows the number of drying cycles within each run based on the observation of the d50 profile of its respective Yn array, as well as the number of sampling points of each cycle. The fragmentation procedure described above was done to every single one of the sixteen runs. Figure 27 illustrates the smaller slots of data that resulted from the fragmentation of the Yn array of each run. A close-up of some drying cycles is presented in Annex 4.

Table 7: Number of drying cycles and number of sampling points of each cycle.

Run	Number of Drying Cycles	Drying Cycle no.									
		1	2	3	4	5	6	7	8	9	10
1	9	86	86	81	87	89	84	79	84	85	-
2	9	83	84	82	82	80	84	82	85	79	-
3	2	88	81	-	-	-	-	-	-	-	-
4	2	82	85	-	-	-	-	-	-	-	-
5	9	89	86	82	82	83	83	76	78	78	-
6	8	80	80	80	70	120	78	82	77	-	-
7	10	89	82	82	80	21	58	76	79	81	81
8	5	79	80	81	79	78	-	-	-	-	-
9	3	88	82	52	-	-	-	-	-	-	-
10	3	87	88	86	-	-	-	-	-	-	-
11	3	84	91	83	-	-	-	-	-	-	-
12	3	84	83	84	-	-	-	-	-	-	-
13	5	81	82	78	79	77	-	-	-	-	-
14	7	84	88	82	82	78	80	36	-	-	-
15	3	87	87	82	-	-	-	-	-	-	-
16	9	83	82	81	79	81	83	79	81	80	-

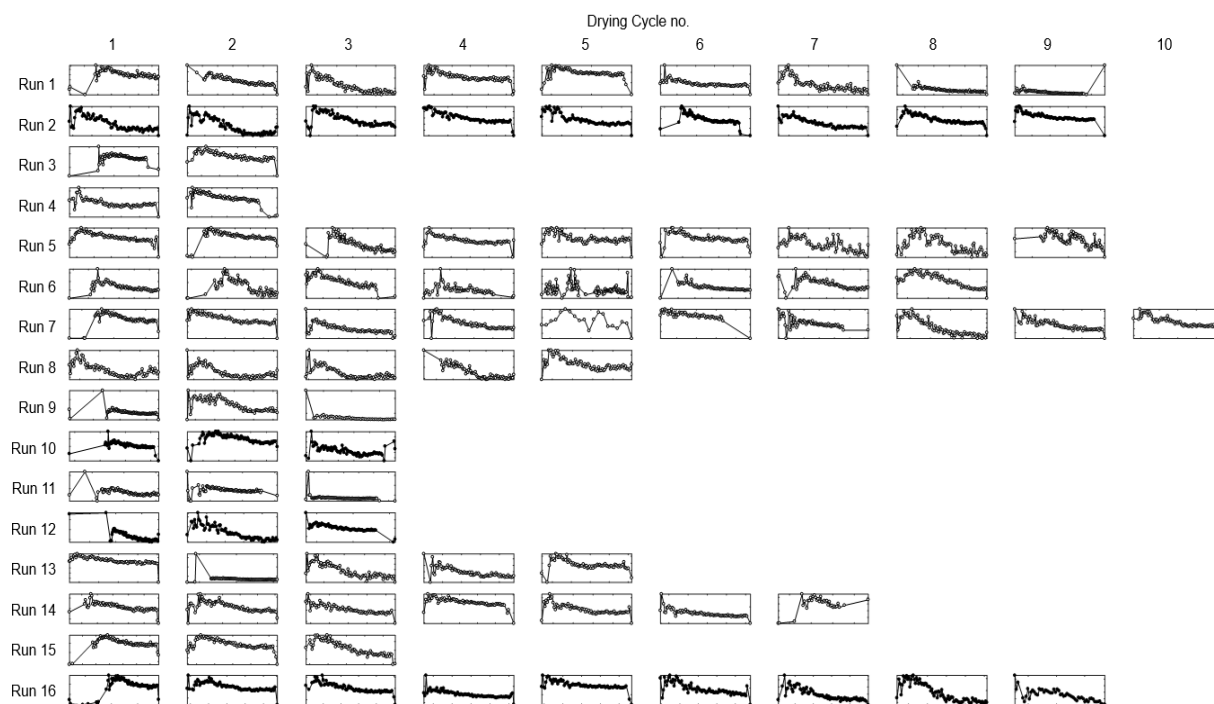


Figure 27: d50 profile of each drying cycle of every run.

By observing Figure 23 and each slot of data represented in Figure 27, it is noticeable that, at a first stage, the d50 value increases abruptly. This is highly indicative of the beginning of the drying cycle as the granules formed in the inside the granulator barrel are inserted into the dryer cell no.4. Once the filling of dryer cell is completed, the drying process itself begins. At this point, a 'down-to-up' hot air source is supplied which will maintain the granules in constant recirculation inside of the dryer cell and, ultimately, promote granule-granule collisions. During the drying process, mass and heat transfer operations occur. For drying to take place, it is required that the heat transfers to the granules, so that they can acquire the latent heat necessary to the evaporation of the granulation liquid (i.e. water). On the other hand, a mass transfer occurs by the diffusion of the water to the evaporation surface of the granules. After the subsequent evaporation of the water from the surface, a diffusion of the resulting vapor into the stream of the passing air occurs. The water evaporation that occurs during the drying process results on the weakening of the bonds that preserve the structure of the granules. As it is known, they are formed due to the agglomeration of smaller particles during granulation, being the granulation liquid the main responsible for promoting the adherence between smaller particles. Therefore, the size reduction over time is most probably related to the combination of two main events: (1) weakening of the granules' structure due to water evaporation and (2) granule-granule collisions promoted by the hot air source.

The beginning of a new drying cycle is represented by the rapid increase of the d50 value. As the FBRM probe is not deactivated in-between drying cycles, it detects new wet granules as they are being filled in the dryer cell. Once the cell is filled, the drying process begins once again.

3.3. Supplementary data processing

Once the data fragmentation according to the number of drying cycles displayed in Table 7 was completed, a further data processing step was performed due to the existence of deviations within the smaller data arrays.

By analyzing each slot of data, the existence of deviations is clear as a few data points lay far from the rest of the distribution. These deviations are commonly known as outliers and may be indicative of experimental errors or even variability in terms of granules' size within the whole measurement. However, the size variability theory can be easily discarded as it is highly unlikely that the granule passing by the probe at those exact instants presents a much higher or lower particle size in comparison to the remaining granules. By closely observing Figure 23, it is acknowledgeable that most outliers are situated on the beginning and ending of each drying cycle. This fact demonstrates that the existence of deviations is most likely related to the sensitivity of the FBRM probe. The deviated data points appear when the filling and discharge of the granules within the dryer cell take place, which may be indicative that these two events affect the stability of the probe positioned inside of the cell. An unstable probe will poorly assess particle size, which results on a d50 value associated to a high level of error. Although the majority of the outliers were observed at the starting and ending phase of each drying cycle, a couple of deviated points in certain data slots were detected during the drying process itself. Nevertheless, most data points that diverged in a more significant manner from the remaining observations were removed. The same sampling points were removed from the corresponding Xn arrays.

Table 8 shows the number of sampling points for each data slot within each run once the outliers' removal was completed. Both drying cycle no. 5 of Run 7 and drying cycle no. 7 of Run 14 presented a low number of sampling points (Figure 29), and therefore, its corresponding Xn and Yn arrays were removed from the whole dataset (Table 9). The drying cycles used for the optimization of the neural network are shown in Figure 28.

Table 8: Number of sampling points of each drying cycle after the outliers' removal.

		Drying cycle no.									
Run	1	2	3	4	5	6	7	8	9	10	
1	78	76	76	80	74	75	75	74	78	-	
2	75	76	76	74	75	70	76	79	74	-	
3	75	76	-	-	-	-	-	-	-	-	
4	69	75	-	-	-	-	-	-	-	-	
5	77	76	74	75	79	75	72	74	74	-	
6	69	76	73	50	49	74	73	74	-	-	
7	76	76	73	73	19	56	51	74	77	73	
8	73	71	76	74	66	-	-	-	-	-	
9	82	76	46	-	-	-	-	-	-	-	
10	76	76	77	-	-	-	-	-	-	-	
11	75	72	75	-	-	-	-	-	-	-	
12	76	80	79	-	-	-	-	-	-	-	
13	78	77	74	72	72	-	-	-	-	-	
14	77	78	75	76	73	75	26	-	-	-	
15	75	75	74	-	-	-	-	-	-	-	
16	77	76	76	77	75	78	75	78	75	-	

Table 9: Total number of sampling points after the removal of drying cycles no.5 (Run 7) and 7 (Run 14).

		Drying cycle no.									Total Number of Sampling Points
Run	1	2	3	4	5	6	7	8	9		
1	78	76	76	80	74	75	75	74	78	686	
2	75	76	76	74	75	70	76	79	74	675	
3	75	76	-	-	-	-	-	-	-	151	
4	69	75	-	-	-	-	-	-	-	144	
5	77	76	74	75	79	75	72	74	74	676	
6	69	76	73	50	49	74	73	74	-	538	
7	76	76	73	73	56	51	74	77	73	629	
8	73	71	76	74	66	-	-	-	-	360	
9	82	76	46	-	-	-	-	-	-	204	
10	76	76	77	-	-	-	-	-	-	229	
11	75	72	75	-	-	-	-	-	-	222	
12	76	80	79	-	-	-	-	-	-	235	
13	78	77	74	72	72	-	-	-	-	373	
14	77	78	75	76	73	75	-	-	-	454	
15	75	75	74	-	-	-	-	-	-	224	

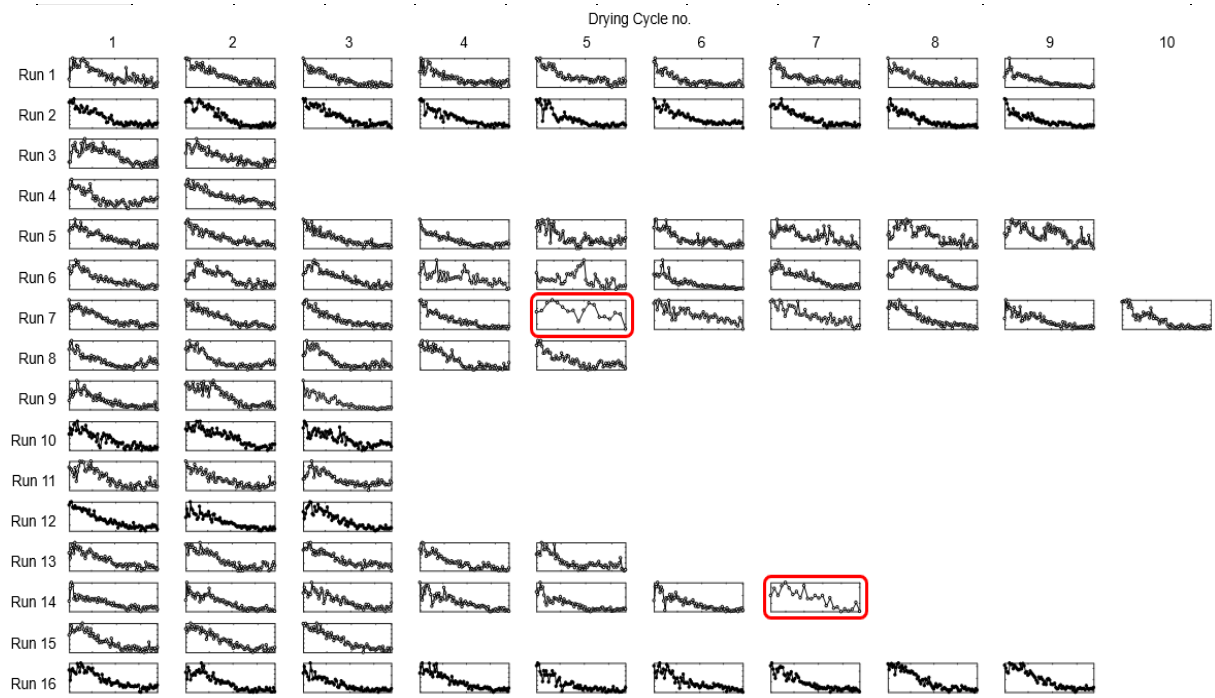


Figure 29: d50 profile of each drying cycle of every run after the supplementary data processing.

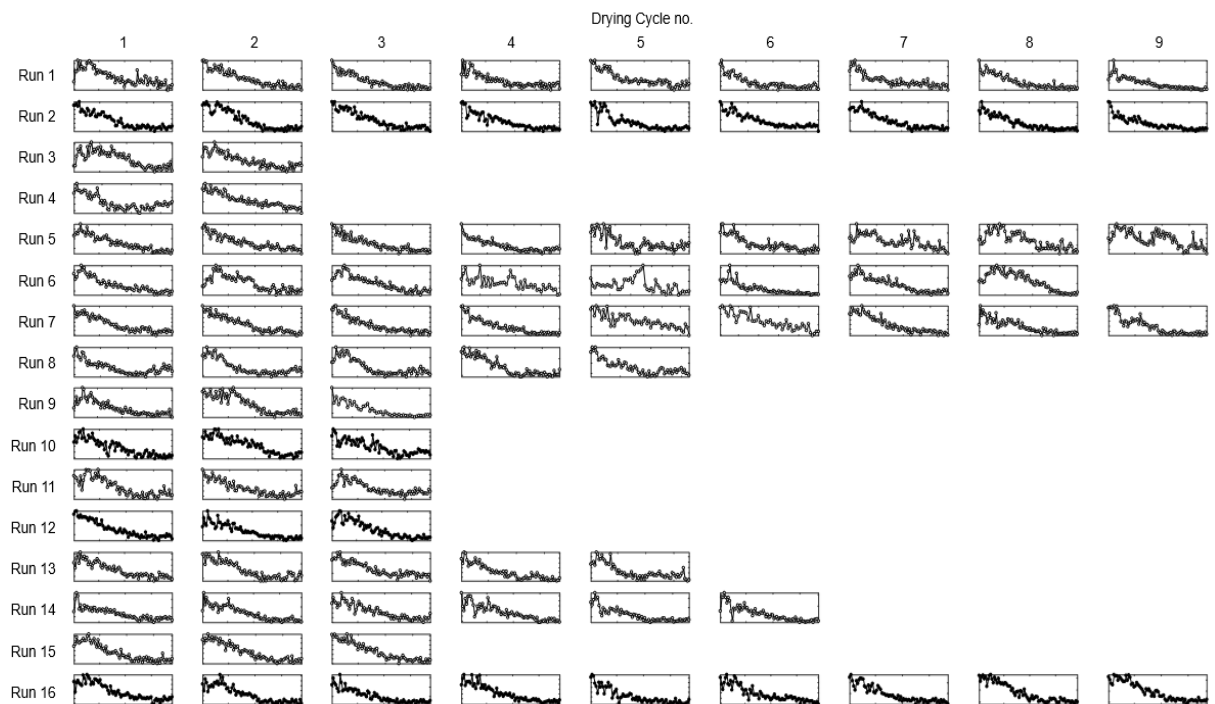


Figure 28: d50 profile of each drying cycle of every run after the removal of drying cycle no. 5 of Run 7 and drying cycle no. 7 of Run 14.

3.4. Modelling strategy

3.4.1. Input delay

The granulator unit of the ConsiGma cannot be considered a perfect plug-flow reactor as axial mixing occurs inside of the granulator barrel. Thus, residence time in the twin-screw granulator cannot be characterized by a single scalar value and instead is represented as a distribution. An experimental investigation by Kumar A. et al focused on the study of RTD in the twin-screw granulator by monitoring the granules at the granulator outlet using NIR-CI. In this study, several operating conditions were utilized during granulation to assess its impact on RTD. As it can be observed in Figure 30, the maximum value registered for mean residence time was of 6.5 seconds, which corresponded to a throughput of 25 kg/h, L/S of 8%, screw configuration with 12 kneading discs at 60°C and a screw speed of 500 rpm. It is also noticeable that all RTDs reside below 10 seconds, which indicates a fast transport within the granulator barrel. Differently from the granulator unit, the wet granule transfer line can be seen as an ideal plug-flow due to the fast transfer of the wet granules to the six-segmented cell fluid bed dryer unit. It is indeed so fast that usually no more than 1 second is conceded to compensate the transfer of wet granules.

Since the time distance between two sampling points corresponds to 10 seconds, the residence time in the twin-screw granulator was roughly approximated to 10 seconds (in alternative to the registered time of 6.5 seconds). As the wet granules transfer from the twin-screw granulator unit to the six-segmented cell fluid bed dryer is nearly instantaneous, a delay was not considered. For measurements performed within the fluid bed dryer, a delay was not attributed.

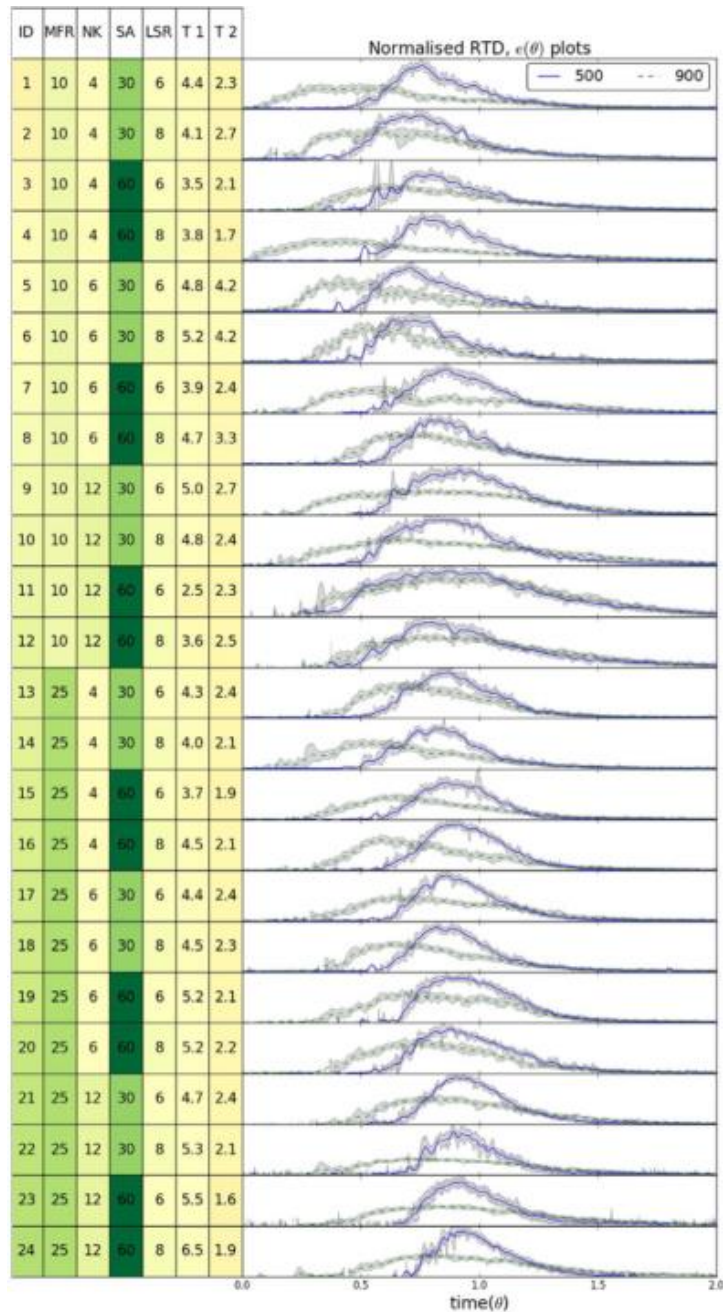


Figure 30: Normalized RTD (right) profile with a shaded region denoting the standard deviation at different screw speed (500, 900 rpm) during various experiments (ID) using twin screw granulation [SA: stagger angle ($^{\circ}$), NK: number of kneading discs (-), MFR: material throughput (kg/h), LSR: liquid-solid ratio (%). T1: mean residence time at 500 rpm (s), T2: mean residence time at 900 rpm (s)]. [89]

In alternative to individually assigning a delay to each variable included on the structure of the neural network, a dataset adjustment was executed. Thus, for every single variable a number of sampling points were removed depending on the delay assigned to it.

Figure 31 corresponds to a schematic representation of the adjustment procedure of a dataset containing 10 sampling points given the different delays (0 and 10 seconds) to be utilized on the real dataset.

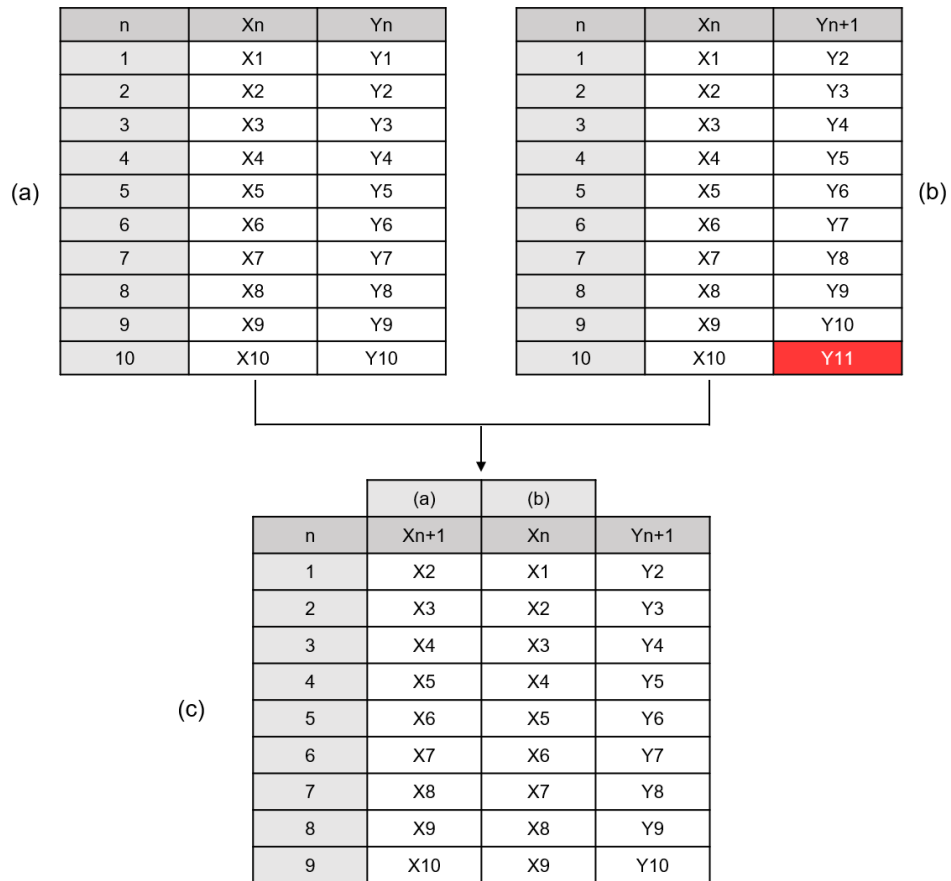


Figure 31: Schematic representation of the logical procedure behind the data alignment upon the delay implementation.

Figure 31a represents an array where no delay is implemented, and thus, no alteration on the structure of the array is done. Differently, on Figure 31b a delay of 10 seconds is considered which means that a variable measured on sampling point no. 1, will be characteristic of the particle size assessed on sampling point no. 2. Thus, the alignment is done by removing the first sampling point of the Yn array. Once this first row is removed, it is noticeable that the variable measured at sampling point no. 10 is aligned with a non-measured particle size correspondent to sampling point no. 11 (highlighted in red). Therefore, a delay of 10 seconds requires the removal of the first and last row of the Xn array. Figure 31c corresponds to the combination of two tables represented in Figure 31a and Figure 31b, and ultimately represents all the adjustments to be performed when a delay is appointed to a variable. It is important to refer that for the Xn array for which a delay was not considered, as well as for the Yn array, the first sampling point was excluded with the purpose of maintaining the same number of sampling points within the whole dataset.

As previously mentioned, Figure 31 is purely representative of the logical procedure behind the dataset alignment as the number of sampling points vary within the different slots of data. Table 10 shows the number of sampling points of each slot of data once a delay was assigned

to each variable. Once finalized the adjustment procedure, the complete dataset is utilized on the input selection step.

Table 10: Total number of sampling points after the delay implementation.

Run	Drying cycle no.									Total Number of Sampling Points
	1	2	3	4	5	6	7	8	9	
1	77	75	75	79	73	74	74	73	77	677
2	74	75	75	73	74	69	75	78	73	666
3	74	75	-	-	-	-	-	-	-	149
4	68	74	-	-	-	-	-	-	-	142
5	76	75	73	74	78	74	71	73	73	667
6	68	75	72	49	48	73	72	73	-	530
7	75	75	72	72	55	50	73	76	72	620
8	72	70	75	73	65	-	-	-	-	355
9	81	75	45	-	-	-	-	-	-	201
10	75	75	76	-	-	-	-	-	-	226
11	74	71	74	-	-	-	-	-	-	219
12	75	79	78	-	-	-	-	-	-	232
13	77	76	73	71	71	-	-	-	-	368
14	76	77	74	75	72	74	-	-	-	448
15	74	74	73	-	-	-	-	-	-	221
16	76	75	75	76	74	77	74	77	74	678

3.4.2. Input selection

3.4.2.1. Manual input selection

As for the manual approach, a total of eighteen variables were excluded on a primary selection. All user-set variables (setpoints) are shown in Figure 32. Although the setpoints are pre-defined, a variance that goes far from the set value is observed on V4, V6, V23, V32 and V47. These different variances are likely related to disturbances that were not able to be corrected by the control system itself. As the value of the five different variables do not fluctuate around the setpoint, they were included on the empirical input selection to assess the effect of the variance on the granules size produced. In contrast, setpoints represented by V19, V37 and V46, remain constant over time and, therefore, are not included on the next input selection phase. From the fifty variables, six variables, namely V3, V10, V21, V34, V40 and V48, were not measured throughout the whole sampling time, being for that reason omitted from the empirical input selection. As illustrated in Figure 33, V1, V5, V18 and V22 remained unchanged through sampling, reason why they were not taken into consideration. V16 and V17

correspond, respectively, to the pressure measured before and after HEPA suction to the product control unit. Taking into account that the d50 value to be modelled is assessed within dryer cell no. 4 of the fluid bed dryer unit, V16 and V17 are not considered to have an effect on the value to be predicted. Thus, V45 was accordingly excluded it corresponds to the differential pressure of V16 and V17. In addition, V15 was not considered on the empirical input selection as its values lie close to the standard atmosphere value which refers to the exact pressure of 101 325 Pa (1 atm). Through the analysis of the progression of V15 over the sixteen runs, it is observable that the atmospheric pressure measured resides around 1009 mbar, which is equivalent to approximately 100 900 Pa (Figure 34). Given this, it was considered that the atmospheric pressure measurements did not present a significant difference from the normal pressure value, reason why V15 was not included on the next phase of the input selection. Apart from V15, also V35 was excluded as the weight of the granulation liquid tank proportionally decreases over time (Figure 34) The proportional decrease of the weight of the tank is justified by the fact that the granulation liquid (i.e. water) is added to the TSG at a constant rate. This comes in line with the constant speed (approximately 130 rpm) at which the water is pumped into the granulator (V1).

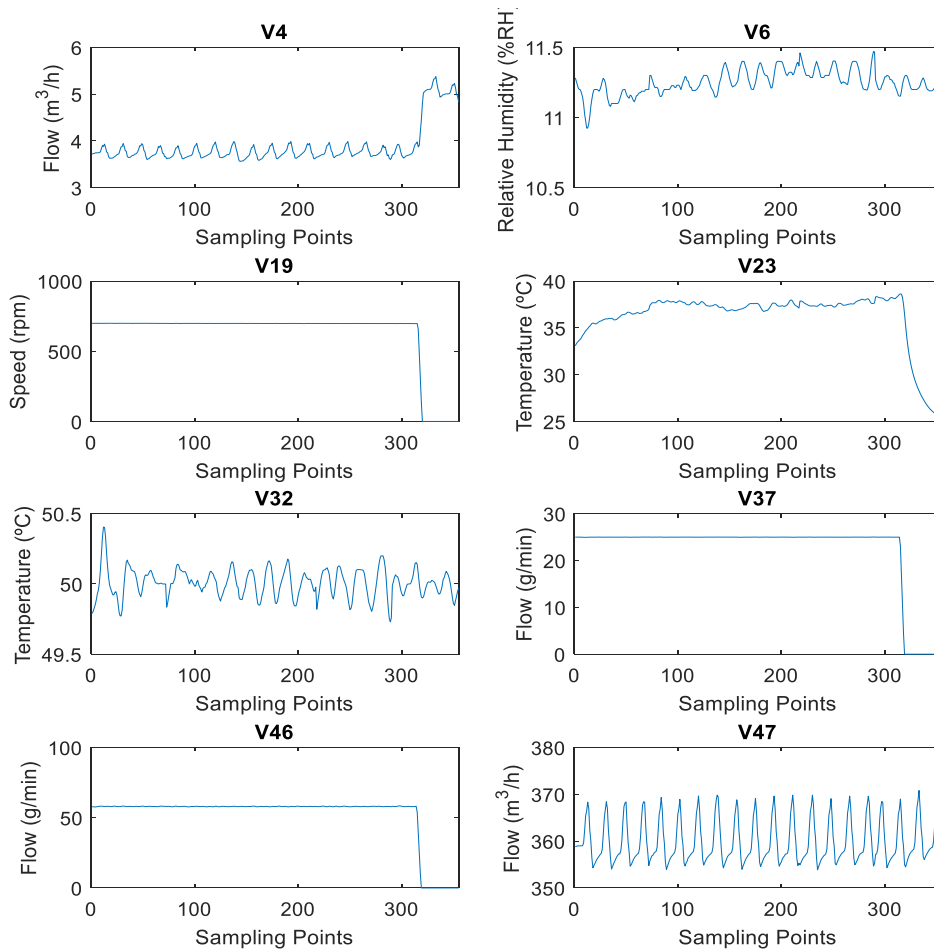


Figure 32: User-set variables for Run 8. V4: Flow air inlet wet granule transfer; V6: Relative humidity dryer air inlet; V19: Speed granulator drive; V23: Temperature granulator barrel; V32: Temperature dryer air inlet; V37: Mass flow powder dosing 1; V46: Mass flow granulation liquid; V47: Flow dryer air inlet.

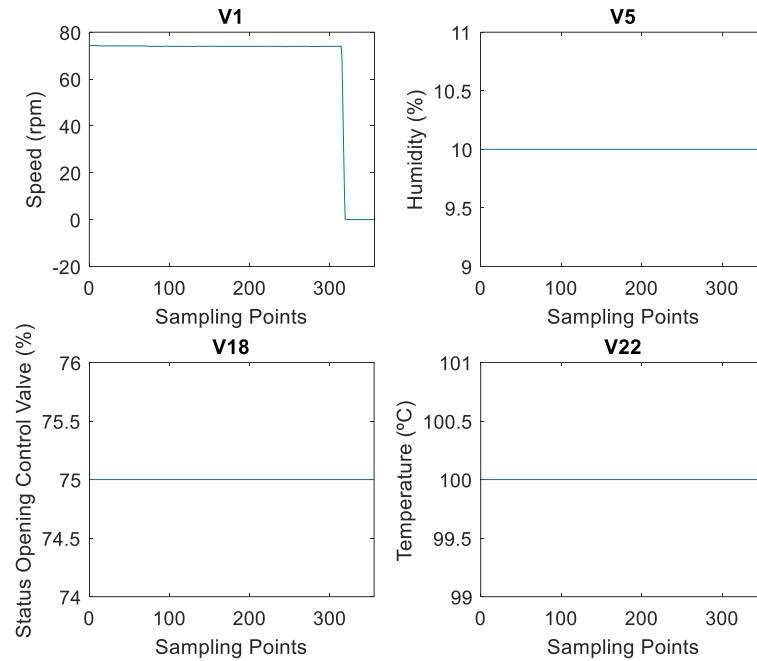


Figure 33: V1, V5, V18 and V22 for Run 8. V1: Liquid pumps speed; V5: Humidity air handling unit control; V18: Actual status opening control valve pressure dryer air inlet; V22: Temperature filter dryer air handling unit.

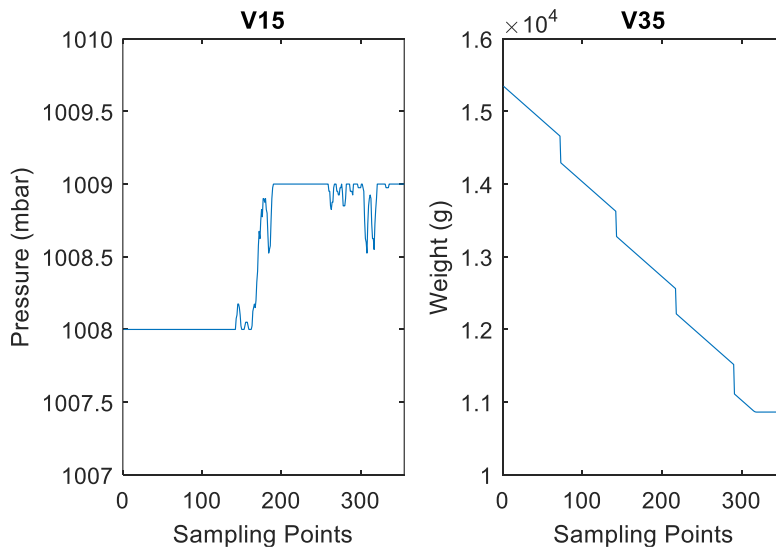


Figure 34: V15 and V35 for Run 8. V15: Pressure atmospheric pressure; V35: Weight granulation liquid tank.

3.4.2.2. Empirical input selection

The results of the back-wise input selection were presented based on the RMSEP associated to the exclusion of each one of the thirty-two variables included in the empirical selection. As seen in Figure 35, the variables ordered from left-to-right correspond to the variables that were (sequentially) removed in each one of the thirty-one rounds performed during the empirical

input selection. Based on the results, four variables (V28, V30, V32 and V44) seem to be the ideal to integrate the structure of the NARX network as it corresponds to the subset of variables that is associated to the lowest RMSEP value (about 20.5 micrometers). It is noticeable that when V33 was removed, the RMSEP decreased, however this value slightly increased in the next round, in association with the removal of V44. Thus, the subset of variables composed by V28, V31, V32 and V44 is considered to enable the neural network to perform its predictions in a more accurate way. Although these four variables are considered as a subset, the way how each individually variable correlates with the particle size measured by the FBRM probe is not so straightforward. Therefore, an assessment of the influence of each variable on particle size is highly advisable.

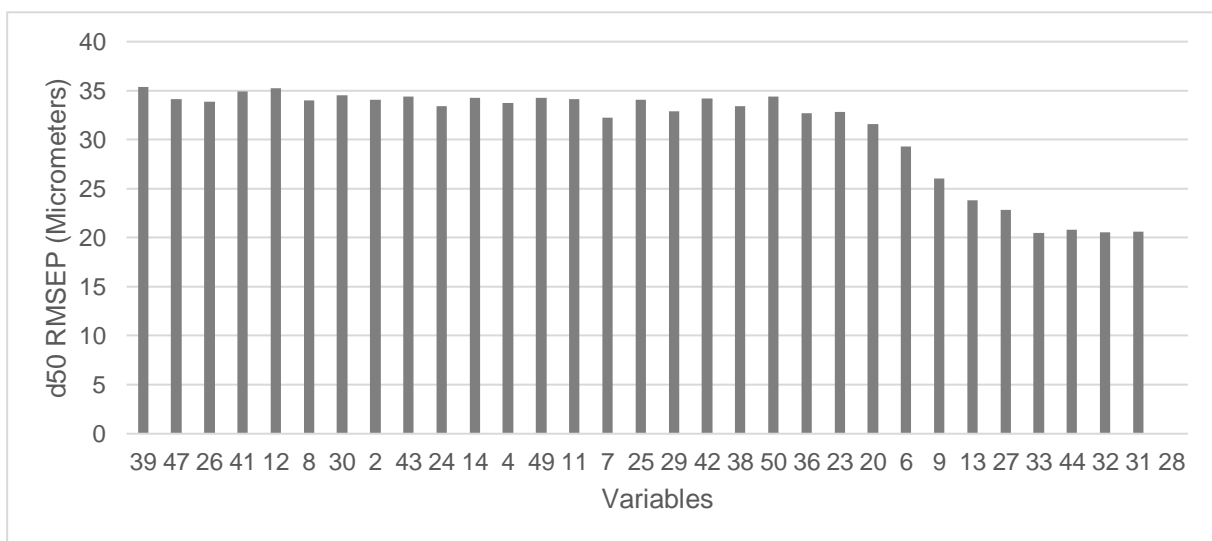


Figure 35: d₅₀ RMSEP in each round of the empirical input selection. X-axis represents the variable removed at each round.

As previously shown in Figure 9 and Figure 10, the ConsiGma™-25 system presented a horizontal set-up, reason why the wet granules were pneumatically transferred from the outlet of the TSG to the top of the six-segmented dryer. As seen in Figure 36, the differential pressure over the wet granules transfer line (V44) presents a negative value throughout the whole sampling duration, a behavior which is observed within every single one of the sixteen runs. However, it also is possible to identify several abrupt decreases of pressure throughout the run. One of the main causes for pressure drops is the gas (flow) acceleration, as confirmed by Figure 37. This figure illustrates the behavior of V4 and V44 of Run 8 during the first drying cycle. It is very much clear that as the gas airflow begins to increase, a decrease on the pressure of the wet transfer line is observed. Other causes for pressure drops can be associated to granule collisions that may occur during the pneumatic transfer. As previously seen in Figure 23, the d₅₀ profile is characterized by an initial increase correspondent to the

filling of the cell prior to the drying process. Although a clear increasing tendency was observed, a few deviations were easily identified as, at some sampling points, the d50 value decreased and subsequently increased. In Subchapter 3.3, the deviations were linked to sensitivity of the FBRM probe at the time the granules were inserted inside the dryer cell, however it is possible to affirm that the deviations observed during filling can also be related to the collisions mentioned above. The mutual collisions of granules and collisions between granules and the wall of the transfer line and the wall of the dryer during filling are responsible for breakage events that result on granules particle size reduction, reason why lower d50 values are given by the FBRM device. In brief, the pressure drops detected in V44 can be used to identify the occurrence of breakage events, and, therefore, is highly correlated to the initial phase of the d50 profile within each run.

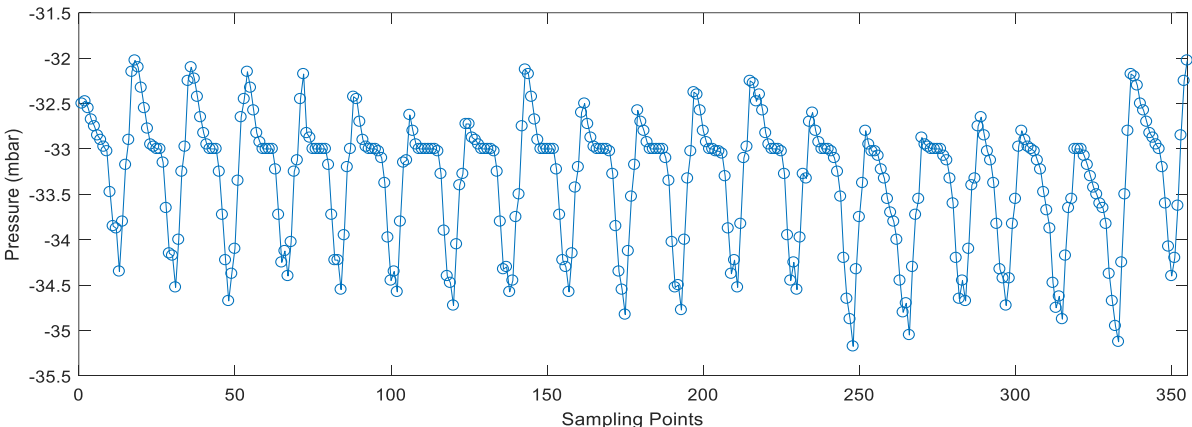


Figure 36: Differential pressure over the wet granule transfer line (V44) during Run 8.

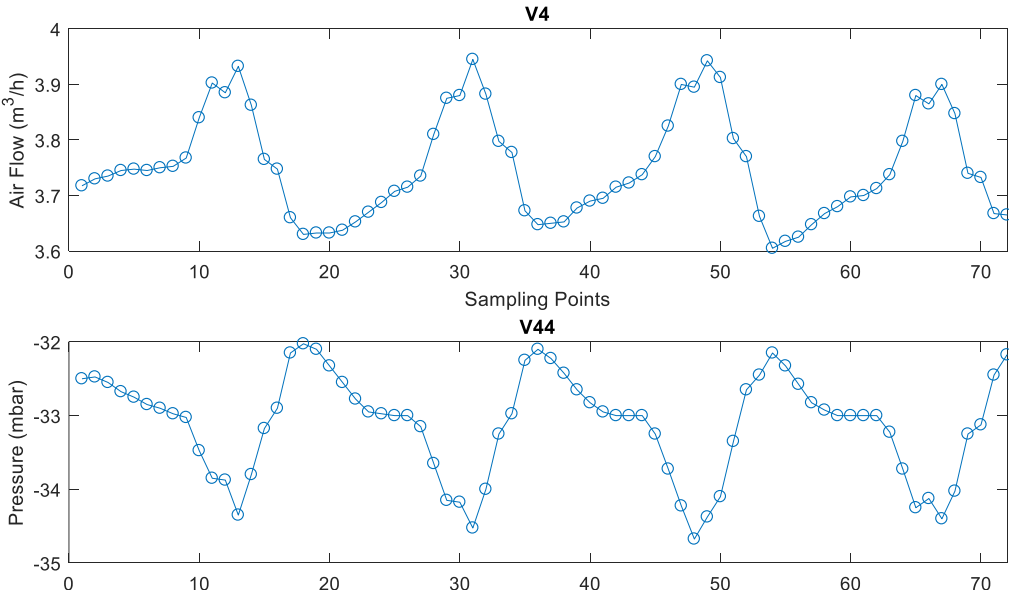


Figure 37: Initial seventy-two sampling points for V4 and V44 during Run 8.

In spite of the body of the ConsiGma™-25 dryer being segmented into six identical dryer cells, a single ‘down-to-up’ air stream enters the dryer, being subsequently divided over the different cells. This single air stream only enters the bottom of the dryer cells which are activated, i.e., that are filled with granules. By analyzing Figure 38, it is noticeable that the temperature profiles of V26-31 are highly repeatable, being the only significance difference the fact that they are spaced in time. This means that despite of the existence of six individual dryer cells, the drying process occurring inside each one of them can be considered identical. Therefore, it becomes important to determine which temperature of dryer cell is more appropriate to be included in the predictive model.

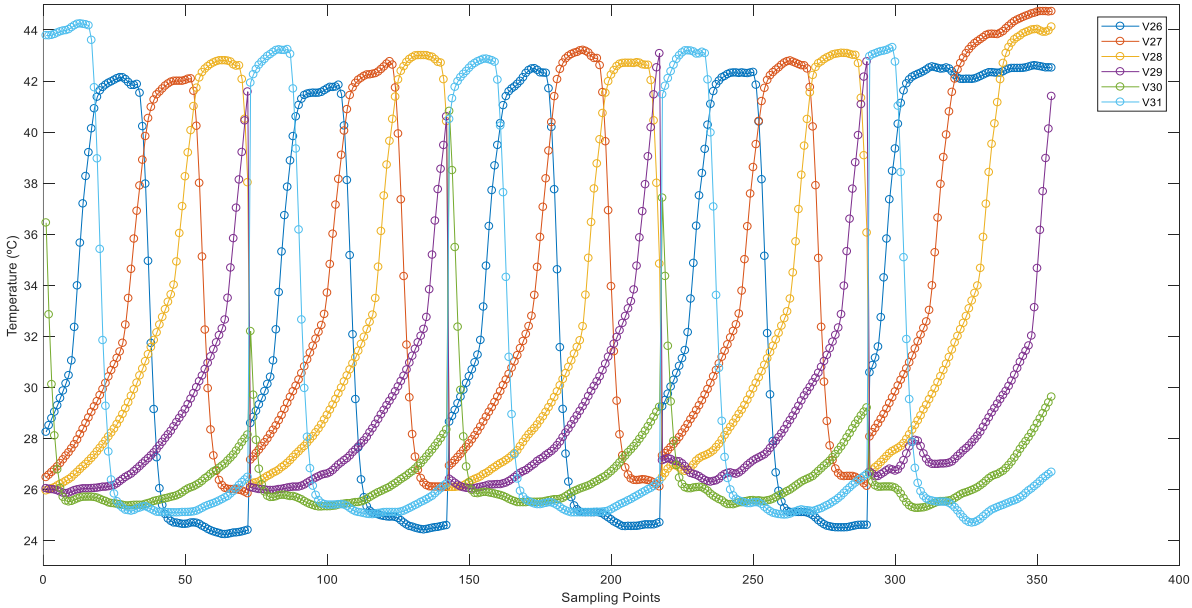


Figure 38: Temperature of dryer cells no. 1, 2, 3, 4, 5 and 6 during Run 8.

Figure 39 and Annex 6: illustrate a comparison between the d_{50} profile and the temperature profile for each dryer cell (V26-31). This comparative step was completed to determine which variable (V26-31) is correctly aligned in time to the d_{50} values. Based on the graphical representations, it is affirmable that V29 represents the temperature of the dryer cell most closely spaced in time to the particle size assessed. As previously mentioned, during a drying cycle, the d_{50} value decreases throughout time, while an increase in terms of temperature within the dryer cell is expected. This behavior is only seen within V29, as the temperature of the dryer cell starts increasing at the point the d_{50} value starts decreasing. This comes in line with the fact that the FBRM probe is located inside dryer cell no.4.

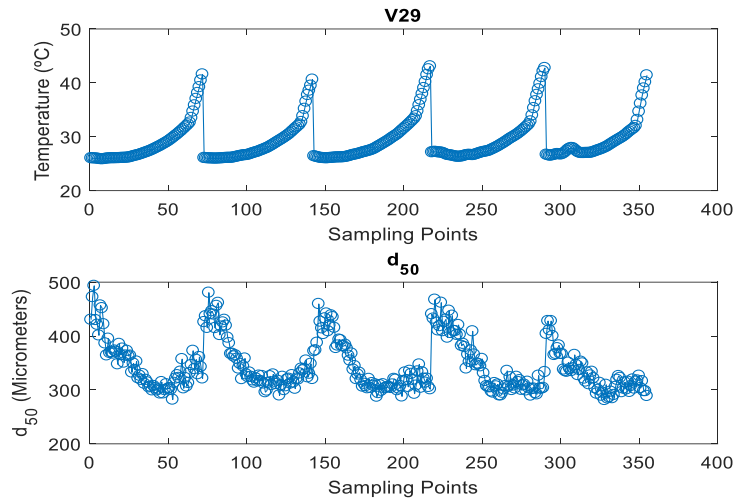


Figure 39: Temperature of dryer cell no. 4 and d50 profile during Run 8.

As seen in Figure 40, a closer inspection of the temperature of the dryer air inlet (V32) showed that, despite the setpoint being set at 50°C, the logged average temperature varied around 49.8°C and 50.4°C. It is known that a high temperature of the dryer air inlet (V32) promotes a higher heat transfer from the gas phase to the granules, which ultimately leads to a higher diffusion rate of the water inside the granules to the passing air stream. Therefore, it is possible to correlate the temperature of the air supply with the particle size assessed. The air inlet temperature will influence the moisture content of the granules, which is determinant on the physical integrity of the granules being dried, since a higher water content in the granular structure can lead to particle size enlargement, and vice versa.

After a meticulous review of the subset of variables resultant from the empirical variable selection, V28 and V31 were not considered to be appropriate to be included on the neural structure. Since V29 was proven to be more suitable than V28 and V31, V29, V32 and V44 were selected to integrate the structure of the NARX network. The location within the ConsiGma™-25 continuous line at which the monitoring of these variables was performed is schematically shown in Annex 6.

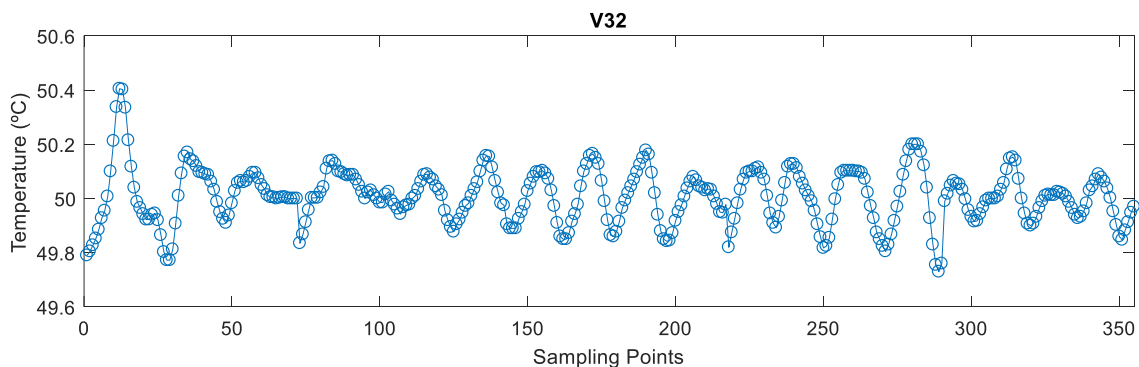


Figure 40: Temperature of the dryer air inlet outlet (V32) during Run 8.

3.4.3. Runs selection

The analysis of the two main principal components as a score plot in both Figure 41 and Figure 42, allows the identification of a main trajectory, though some variations are observed.

For both scores' plots, it can be acknowledgeable that the transition from the lower quadrants to the upper quadrants is related to the start-up phase of the process, being the steady state found around the origin the of score plot for the majority of the runs. In Figure 41, the scores plot of the reference runs is shown. It can be observed that most runs naturally group at the origin of the plot, except for Run 8 and 15 that vary in its PC1. The same behavior is seen in Figure 42, where a transition from the lower-left quadrant towards the origin of the scores plot is observed. In this case, Run 6 clearly stands out as from the remaining runs as few of its sampling points lie outside the 95% confidence ellipse. The variations between runs are mainly related to the operational conditions since the process was run for different periods of time and during different days.

As mentioned before, the training dataset must incorporate samples that are representative of all states and, therefore, the runs that present a distinct behavior in comparison to the remaining ones were considered for the training subset. For the test subset, four runs whose steady state lied around the origin were randomly selected. Given the visualization of the scores' plots, a 75%-25% train-test division was performed, which means that twelve runs were used for training and four runs were chosen to integrate the test subset, as represented in Table 11.

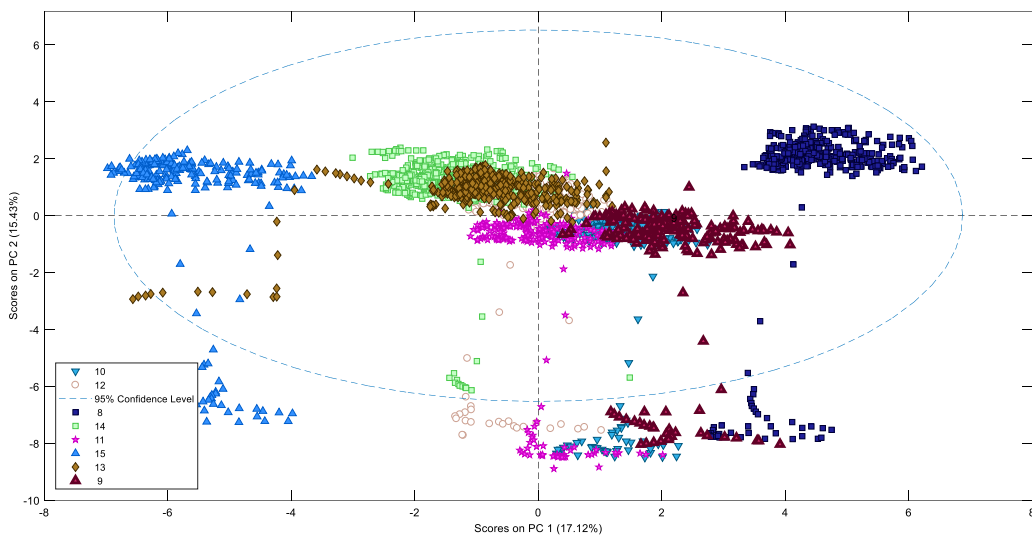


Figure 41: PCA score plot from the first two principal components of the reference runs.

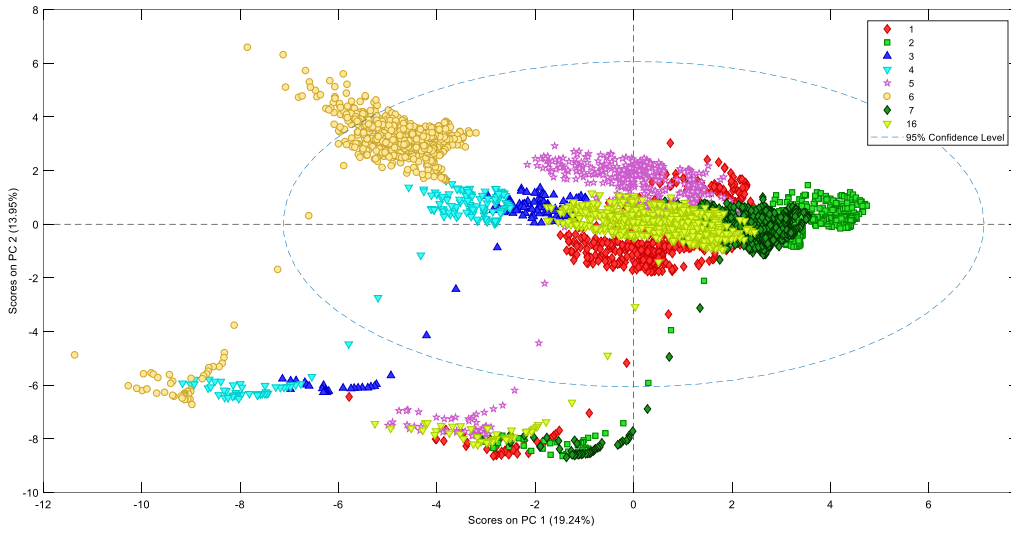


Figure 42: PCA score plot from the first two principal components of the reference with an imposed disturbance.

Table 11: Runs chosen to integrate the training and test subset.

Run	Train	Test
1	X	
2		X
3	X	
4	X	
5	X	
6	X	
7	X	
8	X	
9	X	
10		X
11	X	
12		X
13	X	
14	X	
15	X	
16		X
Number of runs	12	4

3.5. Modelling strategy

The optimized NARX neural network is composed by one hidden layer consisting of three hidden nodes and has one feedback connection towards the input layer. The final topology of the optimized NARX neural network is shown in Figure 43. This recurrent network can be described by the following equation:

$$d_{50}(t) = f(V_{29}(t), V_{32}(t), V_{44}(t), d_{50}(t - 10s))$$

Where the value of the output signal ($d_{50}(t)$) is a function of past values of itself ($d_{50}(t - 10s)$) and previous values of (exogenous) input signals ($V_{29}(t)$, $V_{32}(t)$, $V_{44}(t)$). The exogenous inputs selected to integrate the neural structure were considered without a delay value, whereas the feedback connection of d_{50} value was assigned with a 10 second delay.

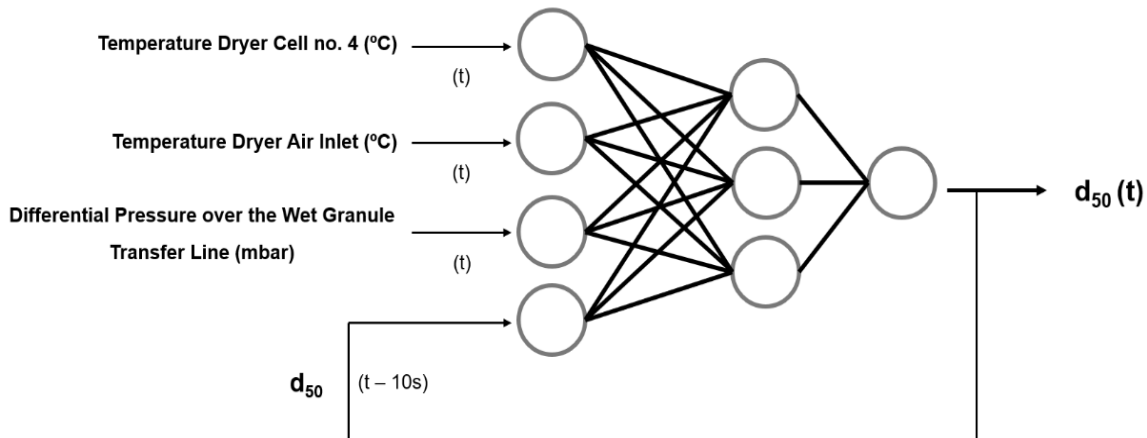


Figure 43: Final topology of the optimized NARX neural network.

3.6. ANN model calibration

The three-hundred iterations performed during the training process of the neural networks, did not made use of drying cycles of runs 5 and 6 (on the calibration and validation sets). As seen in Table 12 and Annex 7, most of the drying cycles of runs 5 and 6 present irregular fluctuations throughout its duration. As irregular variations do not follow a particular model, they cannot be accurately predicted. In Table 12, the RMSEP values for each drying cycle of runs 5 and 6 is shown. In exception of the drying cycles no. 1 and 2 of Run 5, the RMSEP associated to each cycle is significantly high, which translates on an overall high RMSEP for runs 5 and 6. Based on the RMSEP values, it is affirmable that including the drying cycles of runs 5 and 6 on the training process would not be beneficial in terms of the final performance of the network. The usage of a cycle associated to a high RMSEP value during learning would induce the

model to perform poor predictions, which would result on the generation of an output (d50 value) significantly dissimilar to the experimentally observed. Thus, the training of the network was performed using the drying cycles of ten runs (Runs 1,3-4,7-9,11,13-15) for calibration and validation (Figure 44).

Table 12: Median RMSEP for each drying cycle of runs 5 and 6. Average RMSEP and standard deviation of runs 5 and 6.

Drying Cycle	Run	
	5	6
1	25.5	41.7
2	16.3	83.5
3	6034.3	85.7
4	8144.2	168.4
5	8191.0	275.5
6	8155.4	85.6
7	152.1	79.9
8	207.5	180.6
9	170.7	-

Average RMSEP (µm)	3455.2	125.1
Standard Deviation(µm)	4015.5	76.9

Table 13 and Figure 45 display the median RMSE and standard deviation of the calibration and testing sets. In spite of the usage of distinct drying cycles for training and testing, the median RMSEP value for both sets are quite comparable, however the standard deviation is much higher for the calibration set in relation to the testing set. This is indicative of the variability within the drying cycles used for the training of the network, which in turn could have been compensated by the usage of a superior number of drying cycles. In the other hand, a lower standard deviation value for the testing set indicates that the drying cycles used for testing presented a median RMSE close to the overall average of the testing set. This means that while drying cycles used for training might present a very distinct behavior, the cycles utilized for testing display a more similar behavior, i.e., present a lower variability.

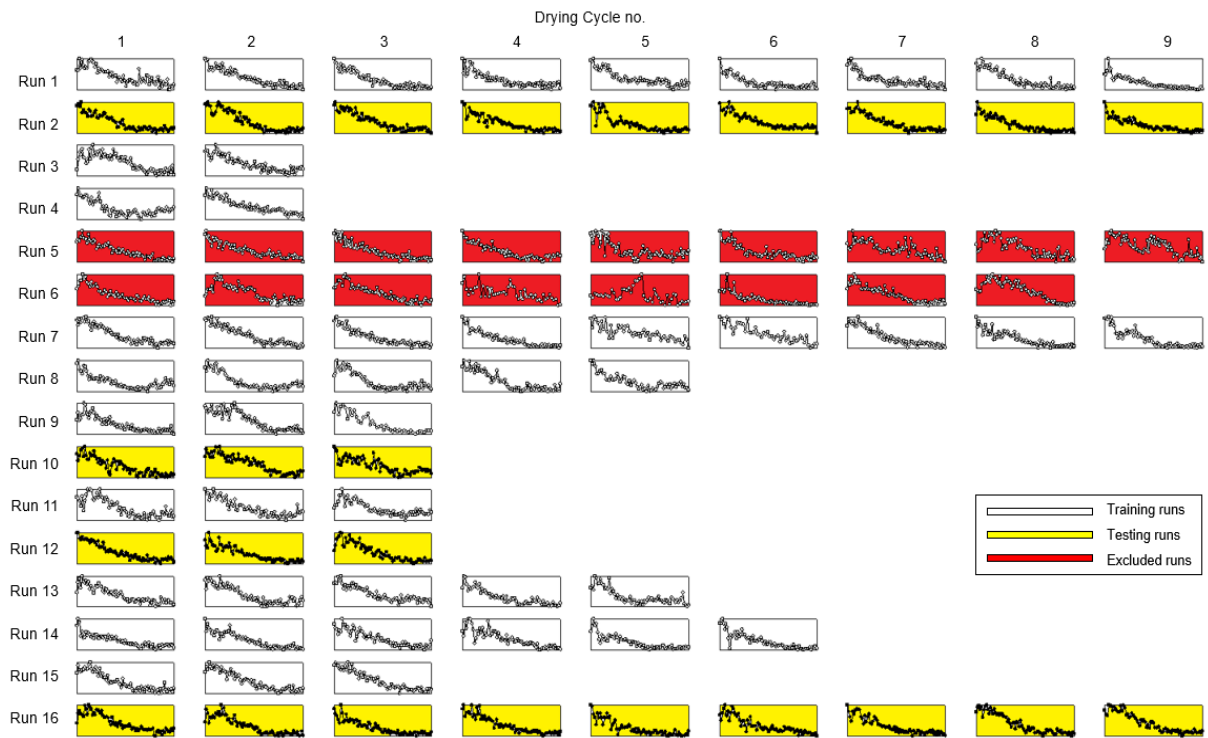


Figure 44: Drying cycles selected for training and testing.

Table 13: Median RMSE and standard deviation of the calibration and testing set.

	Median RMSE (μm)	Standard Deviation (μm)
Calibration set	20.4	14.4
Testing set	21.0	3.8

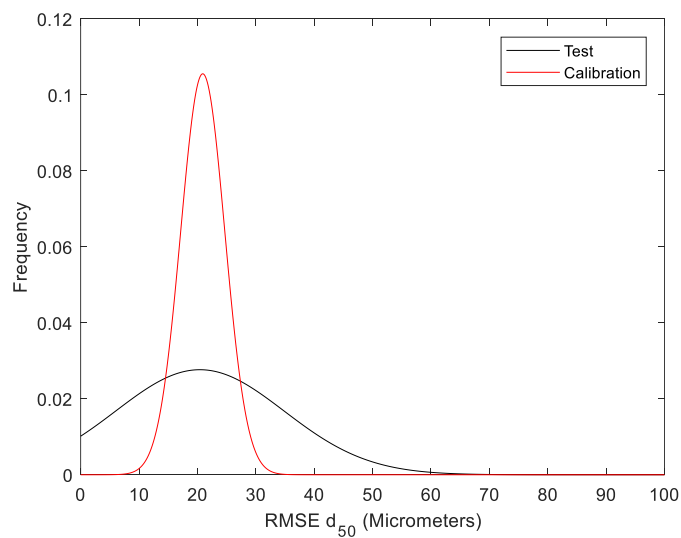


Figure 45: Distribution of RMSE for the calibration and testing set.

In Table 14, the RMSEP for each drying cycle of every run is shown. Despite the usage of drying cycles of four runs to test the optimized network, a RMSEP value for both cycles used during training and testing was obtained. The RMSEP of the testing cycles/run, however, were estimated based on the network learning process that made use of cycles exclusively from the training runs. Thus, it would be expected for the RMSEP value for the training cycles/runs to be lower than for the testing cycles/runs, as its own data was used during the training process.

Table 14: Median RMSEP (μm) for each drying cycle of runs 1-4,7-16.

Run	Drying cycle no.								
	1	2	3	4	5	6	7	8	9
1	17.7	13.4	13.1	17.0	12.3	14.2	27.6	15.1	38.4
2	20.8	20.9	17.9	21.8	25.2	23.2	19.3	25.5	23.0
3	45.2	37.1	-	-	-	-	-	-	-
4	19.2	14.6	-	-	-	-	-	-	-
7	15.6	11.8	18.6	13.0	27.0	18.9	16.6	19.3	15.3
8	55.4	59.6	54.4	63.7	40.2	-	-	-	-
9	21.6	19.9	29.0	-	-	-	-	-	-
10	19.6	19.5	20.5	-	-	-	-	-	-
11	41.2	14.8	31.9	-	-	-	-	-	-
12	35.9	27.6	15.0	-	-	-	-	-	-
13	17.4	25.1	14.8	34.9	40.7	-	-	-	-
14	27.7	22.7	15.9	15.0	23.3	19.3	-	-	-
15	15.2	39.0	10.3	-	-	-	-	-	-
16	14.4	14.2	16.8	17.1	16.7	20.0	18.0	21.8	16.3

In Table 15, it is seen that a lower RMSEP value for the training runs was not necessarily obtained. In fact, the highest overall RMSEP values regard runs 3 and 8, which were included in the calibration and validation sets. As randomly obtained drying cycles are used during the training process of the network, it is possible that a network can end up being very well or badly trained. For this reason, several neural networks are usually created and trained as the performance of a single network lacks significance. In this work, one-hundred networks were developed and the 25% of them that presented the worst performance were excluded. In general, the overall RMSEP for every run is acceptable, being runs 3 and 8 the ones that presented a higher RMSEP value in comparison to the remaining ones. The RMSEP presented for each run corresponds to the average of the RMSEP of each drying cycle included in that same run. Thus, a higher RMSEP for a particular run is not necessarily related to a poor prediction of the all cycles within the run. Taking as an example Run 11, it is observable that the overall RMSEP corresponds to 29.3 μm , the third highest RMSEP value after runs 3 and

8. Nevertheless, the error of d50 prediction for the drying cycle no.4 is considerably low (14.8 μm) based on the overall results for all cycles.

Table 15: Average RMSEP for runs 1-4,7-16.

Run	RMSEP (μm)	Standard Deviation (μm)
1	18.8	8.7
2	22.0	2.5
3	41.2	5.7
4	16.9	3.3
7	17.3	4.4
8	54.7	8.9
9	23.5	4.8
10	19.9	0.6
11	29.3	13.4
12	26.2	10.5
13	26.6	11.1
14	20.6	4.8
15	21.5	15.4
16	17.3	2.4

In Figure 46 **Figure 46**, it is seen that the testing runs (highlighted in yellow), fell below the average RMSEP for the testing set, however Run 12 presented a slightly higher RMSEP value due to a less accurate prediction of cycle no. 1. In regard to the training runs, runs 3 and 8 were the ones that presented a more distinguish RMSEP value in relation to the average RMSEP for the calibration set. This comes in line with the fact that both runs were identified as the less accurately predicted within the complete assembly of cycles. Also, runs 11 and 13 remained above the average RMSEP for the calibration set, which is due to the less accurate prediction of the cycles no. 1 and 3 and cycles no. 4 and 5 of Run 11 and Run 13, respectively.

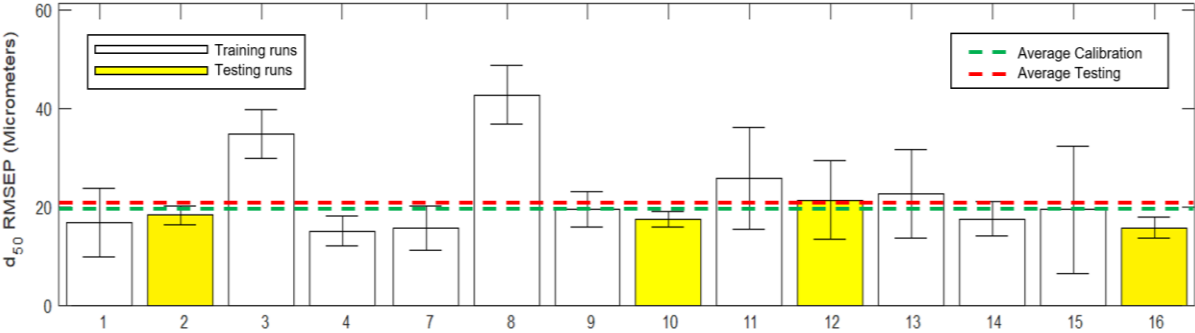


Figure 46: RMSEP for runs 1-4, 7-16.

In Figure 47, a close-up of the d50 prediction for the drying cycles no.3 and 2 of runs 15 and 16, respectively, are shown. These graphical representations correspond to the drying cycles for which a lower RMSEP was attained. Despite the inability of the network on producing the exact same experimental values, it is perceptible that the trend of the d50 value within the duration of the drying cycles was clearly detected by the network. Figure 48 depicts the extremely close prediction of the experimental data of the testing cycles/runs and most of the training cycles/runs. This is highly indicative that the network was successfully trained and presents the ability of accurately predicting the d50 value within the different cycles.

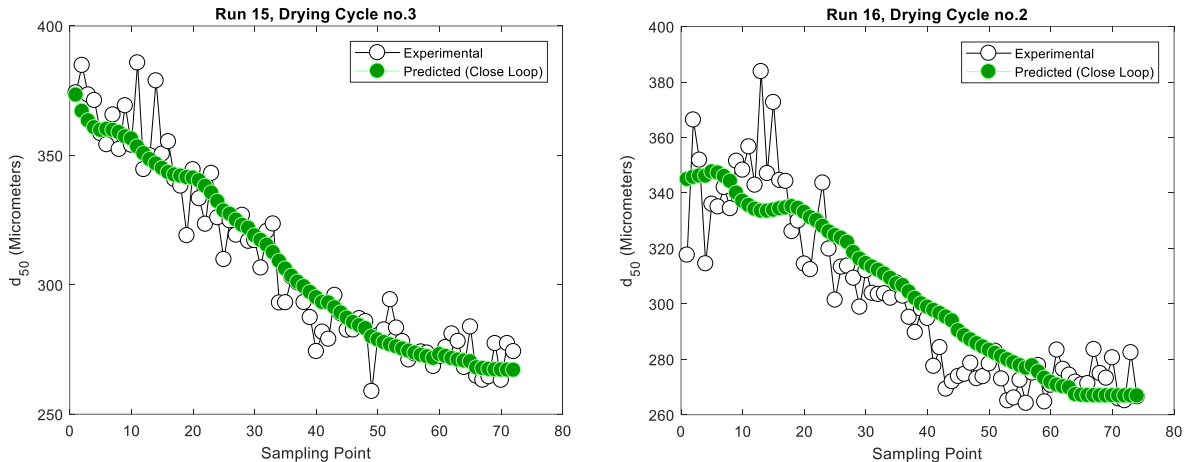


Figure 47: d50 prediction for drying cycle no.3 of Run 15 (training run) and drying cycle no.2 of Run 16 (testing run).

Table 16 and Table 17 provide an overall insight regarding the performance of the network in terms of the predictability of the drying cycles included on the testing runs. In Table 16, the average d50 value for each drying cycle of the testing set and for the whole run is presented. In Table 17, a comparison between the average d50 within the four runs is compared to the average RMSEP value obtained for the same runs. Based on the information contained in the tables, it was possible to calculate the percentual RMSEP for each testing run. According to the results, it is observable that the RMSEP for each testing run does not deviate in such a significant proportion (<10%) from the average d50 value. Overall, an average RMSEP of 6.9% was obtained for the optimized neural network, which indicates that the model can perform accurate predictions of the experimental data that was not used during its optimization.

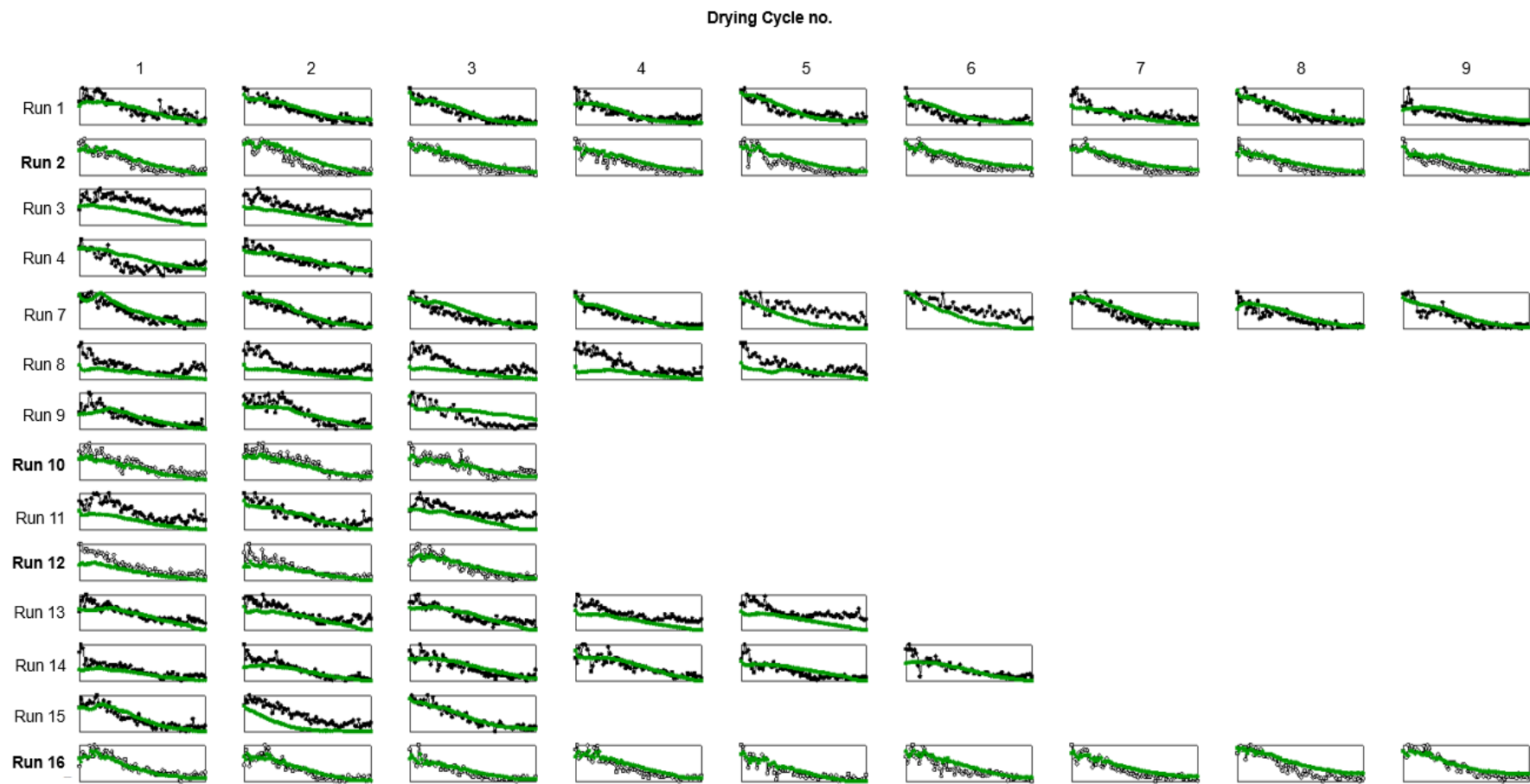


Figure 48: d50 predictions for the drying cycles of runs 1-4,7-16.

Table 16: Average d50 value (μm) for the testing runs.

Run	Drying cycle no.									Average experimental d50 (μm)
	1	2	3	4	5	6	7	8	9	
2	309.4	302.6	306.2	299.7	294.4	294.3	296.0	299.9	289.9	300.2
10	312.0	310.8	308.3	-	-	-	-	-	-	310.4
12	322.6	317.0	300.4	-	-	-	-	-	-	313.3
16	307.2	302.2	300.3	299.4	300.8	294.2	293.0	287.7	295.4	297.8

Table 17: Average RMSEP (%) for the testing runs.

Run	RMSEP (μm)	Average d50 (μm)	RMSEP (%)
2	22.0	300.2	7.3
10	19.9	310.4	6.4
12	26.2	313.3	8.4
16	17.3	297.8	5.8
		Average RMSEP (%)	6.9

4. Conclusions

The non-linear autoregressive network with exogenous inputs is a class of recurrent networks well-suited for modelling granules size distribution. The in-process measurements provided by univariate sensors implemented in the continuous line can be correlated to the size distribution (d50) of the granules assessed inside the dryer cell. However, not all process variables will affect equally the attribute measured by the analytical tool (i.e. FBRM). Process variables, such as temperature of dryer cell, temperature of the dryer air inlet and the pressure of the wet granule transfer line, are evidently determinative factors in the prediction of the particle size distribution of granules.

In order to evaluate the performance of the model in terms of its predictive ability, the RMSEP value was determined for each drying cycle. As the result of the best seventy-five neural networks were selected in this work, the median value was used for the RMSEP determination in alternative to the mean value. The usage of the median is proven to be more robust than the use of the mean value, as it is not affected by the presence of extreme (outliers) values and provides a more realistic insight on the results of the training of the seventy-five neural networks.

The model presented the ability to predict the d50 value from the beginning to the end of the several drying cycles. The accuracy of the artificial neural network was determined by a RMSEP of 6.9%, which demonstrates the capability to produce close results to the experimental data of the cycles/runs included on the testing set. However, the predictive ability of the neural network could not be extended to more atypical cases, such as runs 5 and 6. Thus, a change in the temperature of the air entering the dryer (50 to 60°C) and mass flow of the granulation liquid (58 to 66.7 g/min) is considered to affect with significance the particle size in such way that the model is unable to perform correctly its predictions. The model was not able to predict most of the cycles from both those runs, which reflected on an extremely high RMSEP value. Furthermore, the RMSEP value increased on drying cycles that showed a slight irregular behavior, which means that the computational technique does not offer enough sensitivity to predict abnormal variations within certain drying cycles.

The network was successful in learning, however the quality of the predictions performed can be rather debatable. Particle size is one of the most important quality attributes in the manufacturing of tablets, as it is indicative of the progress of the manufacturing run and directly related to the quality of the end product. Thus, a precise monitoring strategy is required to ensure that no problems arise in terms of performance, stability and appearance of the end product. As seen, the prediction of the d50 value throughout the several drying cycles did not correspond exactly to the experimental data, however an average error of 6.9% (for the testing set) is very low. Therefore, it is affirmable that the sensor (i.e. neural network) developed

through software is not suitable if a precise monitoring is desired. In the other hand, if a mean error of 6.9% (21 μm) is proven not to be significant, the software sensor can be considered as an alternative to the physical FBRM sensor.

Nevertheless, this work opens up the possibility for further improvements of the predictive model. A higher number of experimental runs/cycles could be useful for the training process, in order to enable the network to identify and predict with more ease irregular fluctuations of the d50 value over the drying cycle. Furthermore, a more realistic optimization strategy could be performed for all process parameters in simultaneous through the implementation of a genetic algorithm, for example. Changes in terms of network topology, such as the number of hidden layers and hidden nodes, can also be considered.

Ultimately, a future aim would be to replace an analytical tool, such as the FBRM, by a novel software approach. Overall, this thesis presents several factors, which are meant to positively change the mindset towards the introduction of computational power in the pharmaceutical industry as an essential part of the strategy for continuous manufacturing process monitoring.

5. References

- [1] M. Teżyk, B. Milanowski, A. Ernst, and J. Lulek, "Recent progress in continuous and semi-continuous processing of solid oral dosage forms: A review," *Drug Dev. Ind. Pharm.*, vol. 42, no. 8, pp. 1195–1214, 2015.
- [2] Z. Brennan, "FDA Allows First Switch From Batch to Continuous Manufacturing for HIV Drug," *Regularoty affairs professionals society*. 2016.
- [3] K. Plumb, "Continuous processing in the pharmaceutical industry: Changing the mind set," *Chem. Eng. Res. Des.*, vol. 83, no. 6 A, pp. 730–738, 2005.
- [4] A. Filipa, "Process analytical technology for batch and continuous pharmaceutical processes ' supervision," no. February, 2017.
- [5] S. L. Lee *et al.*, "Modernizing Pharmaceutical Manufacturing: from Batch to Continuous Production," *J. Pharm. Innov.*, vol. 10, no. 3, pp. 191–199, 2015.
- [6] G. Allison *et al.*, "Regulatory and quality considerations for continuous manufacturing May 20-21, 2014 continuous manufacturing symposium," *J. Pharm. Sci.*, vol. 104, no. 3, pp. 803–812, 2015.
- [7] S. Byrn *et al.*, "Achieving continuous manufacturing for final dosage formation: Challenges and how to meet them May 20-21, 2014 continuous manufacturing symposium," *J. Pharm. Sci.*, vol. 104, no. 3, pp. 792–802, 2015.
- [8] S. Chatterjee, "Chatterfee. (2012), FDA. FDA perspective on cont manufacture," *IFPAC Annu. Meet.*, p. 21, 2012.
- [9] S. Massey, "Making the Switch: Continuous Manufacturing vs. Batch Processing of Pharmaceuticals," *Life Sci. Blogs*, pp. 2016–2018, 2016.
- [10] S. L. Lee, "Modernizing the way drugs are made: A transition to continuous manufacturing," *US Food&Drug Administration*. 2017.
- [11] A. Pellek and P. Van Arnum, "Continuous Processing: Moving with or against the Manufacturing Flow," *Pharm. Technol.*, vol. 9, no. 32, 2008.
- [12] M. J. Mollan and M. Lodaya, "<Continuous Processing in Pharmaceutical Manufacturing.pdf>," 2004.
- [13] S. T. Santos, F. F. Gouveia, and J. C. Menezes, "PAT paves the way for continuous manufacturing," *Pharm. Technol.*, 2015.
- [14] C. G., "FDA's PAT initiative," *Pharm. Technol. Eur.*, vol. 16, no. 10, pp. 34–36, 2004.
- [15] D. Wu and D. L. Olson, "Enterprise risk management: Coping with model risk in

- a large bank," *J. Oper. Res. Soc.*, vol. 61, no. 2, pp. 179–190, 2010.
- [16] ICH, "Ich Harmonised Tripartite Guideline," *ICH Harmon. Tripart. Guidel.*, vol. 8, no. August, pp. 1–28, 2009.
- [17] R. S. Chaudhary, A. Pazhayattil, and J. Spes, "Continuous Manufacturing: A Generic Industry Perspective," *Pharm. Tech.*, 2017.
- [18] R. Hernandez, "Continuous manufacturing: A changing processing paradigm," *BioPharm Int.*, vol. 28, no. 4, pp. 20–41, 2015.
- [19] K. Langhauser, "Janssen's Historic FDA Approval," *Pharm. Manuf.*, 2017.
- [20] E. Palmer, "GSK doubles down on Singapore continuous processing plant," *Fierce Pharma*, 2015.
- [21] J. Butschli, "AstraZeneca invests in continuous wet granulation unit." 2013.
- [22] A. L. Robertson, "From Pharmaceutical Substance to Product-An Industrial Perspective on Continuous Processing," 2013, no. September.
- [23] M. Kopcha, "'Continuous Manufacturing' - Common Guiding Principles Can Help Ensure Progress," *U.S. Food Drug Adm.*, 2017.
- [24] Pharmaceutical Technology Editors, "Vertex Receives FDA Approval for Continuously Manufactured Drug Product," *PharmTech.com*, 2018.
- [25] Pharmaceutical Technology, "FDA Approves Tablet Production on Janssen Continuous Manufacturing Line," *PharmaTech.com*, vol. April 12, p. 312414, 2016.
- [26] M. LaTorre-Snyder, "The Benefits of Continuous Manufacturing," *Pharm. Process.*, 2016.
- [27] L. Lachman, H. Lieberman, and J. Kanig, "Teoria e Prática na Indústria Farmacêutica," *Fundação Calouste Gulbenkian*, vol. I, no. 3, pp. 83–112, 2015.
- [28] C. Tremblay and D. Zhou, "A Study of Efficient Drying Parameters for Bed Dryers," no. 179, pp. 1–8, 2015.
- [29] L. Briens and M. Bojarra, "Monitoring Fluidized Bed Drying of Pharmaceutical Granules," *AAPS PharmSciTech*, vol. 11, no. 4, pp. 1612–1618, 2010.
- [30] "Fluid Bed Dryer Uses And Applications," *Gen. Kinemat.*, 2018.
- [31] "Advantages & Disadvantages of Fluid Bed Dryer in Pharmaceutical Industry," *SaintyCo Pharma Process Packag.*, 2018.
- [32] A. Choudhary, "Principle and Working of Fluidized Bed Dryer (FBD)," *Pharm. Guidel.*, 2015.
- [33] G. GmbH, "Fluidized Bed Drying." 2013.

- [34] D. Science, "Practice Guide," *Fire Res.*, no. August, pp. 1–165, 2014.
- [35] Horiba Scientific, "A guidebook to particle size analysis," pp. 1–32, 2017.
- [36] H. G. Brittain, "Shape , Size , and Distribution, part I: Representations of particle shape, size, and distribution," *Pharm. Phys.*, vol. 1, no. December, pp. 1–6, 2001.
- [37] T. Närvänen, *Particle Size Determination during Fluid Bed Granulation*. 2009.
- [38] A. F. T. Silva *et al.*, "Particle sizing measurements in pharmaceutical applications: Comparison of in-process methods versus off-line methods," *Eur. J. Pharm. Biopharm.*, vol. 85, no. 3 PART B, pp. 1006–1018, 2013.
- [39] Particle Sciences. Drug Development Services, "Particle size distribution and its measurement," *Tech. Br.*, vol. 2, pp. 1–2, 2009.
- [40] "Particle size," *Malvern Panalytical*, 2018.
- [41] "Laser Diffraction (LD)," *Malvern Panalytical*.
- [42] "Light Diffraction Measurement of Particle Size," *U.S. Pharmacop.*, no. 29.
- [43] "Mie theory -The first 100 years," *Malvern*, 2010.
- [44] R. M. Jones, "Particle size analysis by laser diffraction: ISO 13320, standard operating procedures, and Mie theory," *Am. Lab.*, no. 35, pp. 44–47, 2003.
- [45] S. J. Blott, D. J. Croft, K. Pye, S. E. Saye, and H. E. Wilson, "Particle size analysis by laser diffraction," *Geol. Soc. London, Spec. Publ.*, vol. 232, no. 1, pp. 63–73, 2004.
- [46] "Particle Size Distribution Estimation by Analytical Sieving," *U.S. Pharmacop.*, no. 35, pp. 336–339, 2012.
- [47] A. Rawle, M. I. Limited, E. B. Park, and G. Road, "Basic Principles of Particle," *Surf. Coatings Int. Part A Coatings J.*, vol. 44, no. 0, pp. 1–8, 2003.
- [48] H. G. Brittain, "Particle-size distribution, part III: Determination by analytical Sieving.," *Pharm. Phys.*, vol. 3, no. December, pp. 1–5, 2002.
- [49] H. Heywood, "Evaluation of powders," *J. Pharmacol.*, vol. 15, p. 56T–74T, 1963.
- [50] M. Levin, "Sieving Method," *Am. Lab.*, 2005.
- [51] R. P. King, "Measurement of Particle Size Distribution by Image Analyser," in *Powder Technology*, vol. 39, 1984, pp. 279–289.
- [52] C. Shanthi, R. K. Porpatham, and N. Pappa, "Image Analysis for Particle Size Distribution," vol. 6, no. 3, pp. 1340–1345, 2014.
- [53] J. Ross, "Introduction to Image Analysis," *Horiba Sci.*, pp. 1–26, 2012.
- [54] Sympatec GmbH, "Dynamic Image Analysis," no. 42, pp. 1–16, 2017.

- [55] N. Sandler, "Photometric imaging in particle size measurement and surface visualization," *Int. J. Pharm.*, vol. 417, no. 1–2, pp. 227–234, 2011.
- [56] F. Alba, G. M. Crawley, J. Fatkin, D. M. J. Higgs, and P. G. Kippax, "Acoustic spectroscopy as a technique for the particle sizing of high concentration colloids, emulsions and suspensions," *Colloids Surfaces A Physicochem. Eng. Asp.*, vol. 153, no. 1–3, pp. 495–502, 1999.
- [57] A. Burggraeve, T. Monteyne, C. Vervaet, J. P. Remon, and T. De Beer, "Process analytical tools for monitoring, understanding, and control of pharmaceutical fluidized bed granulation: A review," *Eur. J. Pharm. Biopharm.*, vol. 83, no. 1, pp. 2–15, 2013.
- [58] M. Uher and P. Benes, "Measurement of particle size distribution by acoustic emission method," *XX IMEKO World Congr. Sept. 9-14*, no. 102, pp. 2–6, 2012.
- [59] Y. Hu, X. Huang, X. Qian, L. Gao, and Y. Yan, "Online particle size measurement through acoustic emission detection and signal analysis," *IEEE Trans. Instrum. Meas.*, vol. 64, no. 5, pp. 1100–1109, 2014.
- [60] A. V. Pandit and V. V. Ranade, "Chord length distribution to particle size distribution," *AIChE J.*, vol. 62, no. 12, pp. 4215–4228, 2016.
- [61] "Measure Particle Distribution In-Process: FBRM C35 Technology," *Mettler Toledo*, 2009.
- [62] "Inline Particle Measurement: Parsum," *Malvern Instruments Ltd.*
- [63] P. Dieter, D. Stefan, E. Günter, and K. Michael, "In-line particle sizing for real-time process control by fibre-optical spatial filtering technique (SFT)," *Adv. Powder Technol.*, vol. 22, no. 2, pp. 203–208, 2011.
- [64] D. Petrak, S. Dietrich, G. Eckardt, and M. Köhler, "In-line particle sizing for process control by an optical probe based on the spatial filtering technique (SFT) - revised personal version," *Int. J. Sci. Technol. Powders Part. Mater.*, vol. 22, no. 2, pp. 1–18, 2010.
- [65] E. Petrova, *Innovation and Marketing in the Pharmaceutical Industry*, vol. 20. 2014.
- [66] "Measuring principle: Fibre-optic spatial filter method," *Parsum GmbH*, 2017.
- [67] A. R. Heath, P. D. Fawell, P. A. Bahri, and J. D. Swift, "Estimating average particle size by focused beam reflectance measurement (FBRM)," *Part. Part. Syst. Charact.*, vol. 19, no. 2, pp. 84–95, 2002.
- [68] D. Greaves *et al.*, "Measuring the particle size of a known distribution using the

- focused beam reflectance measurement technique,” *Chem. Eng. Sci.*, vol. 63, no. 22, pp. 5410–5419, 2008.
- [69] V. Kumar, M. K. Taylor, A. Mehrotra, and W. C. Stagner, “Real-Time Particle Size Analysis Using Focused Beam Reflectance Measurement as a Process Analytical Technology Tool for a Continuous Granulation–Drying–Milling Process,” *AAPS PharmSciTech*, vol. 14, no. 2, pp. 523–530, 2013.
- [70] G. P. Systems, “Operating manual for Collette machine number: 07CG025002R,” pp. 1–87.
- [71] M. Fonteyne *et al.*, “Real-time assessment of critical quality attributes of a continuous granulation process,” *Pharm. Dev. Technol.*, vol. 18, no. 1, pp. 85–97, 2013.
- [72] A. Kumar, K. V. Gernaey, I. Nopens, and T. De Beer, “Twin-screw Granulation Process Development: Present Approaches, Understanding and Needs,” *Contin. Manuf. Pharm.*, pp. 283–311, 2017.
- [73] O. Goldstein, “ConsiGma™ - A platform for Continuous Solid Dosage manufacturing enabling Quality by Design and Lean Manufacturing,” 2017.
- [74] J. Vercruysse *et al.*, “Stability and repeatability of a continuous twin screw granulation and drying system,” *Eur. J. Pharm. Biopharm.*, vol. 85, no. 3 PART B, pp. 1031–1038, 2013.
- [75] D. J. Sarma and S. C. Sarma, “Neural Networks and their Applications in Industry,” *DESIDOC Bull. Inf. Technol.*, vol. 20, no. 1, pp. 29–36, 2000.
- [76] I. N. da Silva, D. Hernane Spatti, R. Andrade Flauzino, L. H. B. Liboni, and S. F. dos Reis Alves, “Artificial Neural Networks,” pp. 21–29, 2017.
- [77] M. Wesolowski and B. Suchacz, “Artificial Neural Networks: Theoretical Background and Pharmaceutical Applications: A Review,” *J. AOAC Int.*, vol. 95, no. 3, pp. 652–668, 2012.
- [78] S. Ibrić, J. Djuriš, J. Parojčić, and Z. Djurić, “Artificial neural networks in evaluation and optimization of modified release solid dosage forms,” *Pharmaceutics*, vol. 4, no. 4, pp. 531–550, 2012.
- [79] S. Agatonovic-Kustrin and R. Beresford, “Basic concepts of artificial neural network (ANN) modeling and its application in pharmaceutical research,” *J. Pharm. Biomed. Anal.*, vol. 22, no. 5, pp. 717–727, 2000.
- [80] MathWorks, “Neural Network Toolbox.” 2016.
- [81] M. H. Sazli, “A brief review of feed-forward neural networks,” *Commun. Fac. Sci.*

- Univ. Ankara*, no. January 2006, pp. 11–17, 2006.
- [82] MathWorks, “Design Time Series NARX Feedback Neural Networks.” .
- [83] V. Ćirović, D. Aleksendrić, and D. Mladenović, “Braking torque control using recurrent neural networks,” *Proc. Inst. Mech. Eng. Part D J. Automob. Eng.*, vol. 226, no. 6, pp. 754–766, 2012.
- [84] T. Shah, “About Train, Validation and Test Sets in Machine Learning,” *Towards Data Science*. 2017.
- [85] MathWorks, “Improve Neural Network Generalization and Avoid Overfitting.” .
- [86] L. Prechelt, “Early stopping - But when?,” *Lect. Notes Comput. Sci. (including Subser. Lect. Notes Artif. Intell. Lect. Notes Bioinformatics)*, vol. 7700 LECTU, pp. 53–67, 2012.
- [87] P. Radhakrishnan, “When to stop training your Neural Network?” 2017.
- [88] MathWorks, “Introducing Machine Learning,” *Mach. Learn. with MATLAB*, p. 12, 2016.
- [89] A. Kumar *et al.*, “Linking granulation performance with residence time and granulation liquid distributions in twin-screw granulation: An experimental investigation,” *Eur. J. Pharm. Sci.*, vol. 90, pp. 25–37, 2016.

6. Supplementary material

Annex 1: Parameters logged by the ConsiGma™-25 system during processing; ▲ – User-set variables (setpoints); ■ – Variables included in the mathematical model for input selection.; ▼ – Variables included in the structure of the NARX network.


Variable	Measurement	Units	Setpoint value	ConsiGma™-25 unit	Depicted Underneath Tag *
1	Liquid pumps speed	rpm	-	Liquid addition module (granulator)	FC03031
2	Speed air handling unit fan control ■	%	-	Air handling unit (dryer)	FIC06021
3	Vacuum pump motor – variable frequency drive	%	-	Vacuum pump (dryer)	FIC09031
4	CB flow air inlet wet granule transfer ▲■	m ³ /h	3.6	Wet granule transfer line (dryer)	XFE07011
5	Humidity air handling unit control	%	-	Air handling unit (dryer)	MIC06021
6	Relative humidity dryer air inlet ▲■	% RH	6	Dryer	ME06021
7	Relative humidity dryer air outlet ■	% RH	-	Dryer	ME06022
8	Torque- granulator drive ■	Nm	-	Granulator	NET04021
9	Differential pressure for the air inlet wet granule transfer ■	mbar	-	Wet granule transfer line (dryer)	PDET07011
10	Differential pressure for the filter outlet air handling for dryer	mbar	-	Air handling unit (dryer)	PDET08015
11	Pressure dryer top ■	mbar	-	Dryer	PET06011
12	Pressure dryer air inlet ■	mbar	-	Dryer	PET06021
13	Pressure dryer air outlet (before HEPA filter) ■	mbar	-	Dryer	PET06022
14	Pressure dryer air outlet (after HEPA filter) ■	mbar	-	Dryer	PET06023
15	Pressure atmospheric pressure	mbar	-	Dryer	PET07016
16	Pressure before HEPA suction to product control	mbar	-	Product control unit	PET09031
17	Pressure after HEPA suction to product control	mbar	-	Product control unit	PET09032
18	Actual status opening control valve pressure dryer air inlet	%	-	Dryer	PV06021
19	Speed granulator drive ▲	rpm	700	Granulator	SET04021
20	Temperature filter dryer air handling unit ■	°C	-	Air handling unit (dryer)	TE08014
21	Temperature air handling unit control	°C	-	Air handling unit (dryer)	TIC06021

22	Temperature filter dryer air handling unit	%	-	Air handling unit (dryer)	TE08014
23	Temperature granulator barrel ▲ ■	°C	25	Granulator	TE04011
24	Temperature tank granulator barrel temperature control unit ■	°C	-	Temperature control unit (granulator)	TE05015
25	Temperature inlet granulator jacket ■	°C	-	Temperature control unit (granulator)	TE05021
26	Temperature dryer cell 1 ■	°C	-	Dryer	TE06011
27	Temperature dryer cell 2 ■	°C	-	Dryer	TE06012
28	Temperature dryer cell 3 ■	°C	-	Dryer	TE06013
29	Temperature dryer cell 4 ■ ▼	°C	-	Dryer	TE06014
30	Temperature dryer cell 5 ■	°C	-	Dryer	TE06015
31	Temperature dryer cell 6 ■	°C	-	Dryer	TE06016
32	Temperature dryer air inlet ▲ ■ ▼	°C	50	Dryer	TE06021
33	Temperature dryer air outlet ■	°C	-	Dryer	TE06022
34	Temperature mill screen	°C	-	Product control unit	TE09021
35	Weight granulation liquid tank	g	-	Liquid addition module (granulator)	WE03031
36	Mass flow powder dosing 1 (average) ■	kg/h	-	Powder dosing unit (granulator)	XFI02011
37	Mass flow powder dosing 1 (calculated) ▲	kg/h	25	Powder dosing unit (granulator)	XFI02011
38	Speed motor powder dosing 1 ■	rpm	-	Powder dosing unit (granulator)	X02011
39	Weight powder dosing 1 (net) ■	kg	-	Powder dosing unit (granulator)	X02011
40	Mass flow powder dosing 2	kg/h	-	Powder dosing unit (granulator)	X02021
41	Differential pressure dryer hole plate & bed ■	mbar	-	Dryer	XDPI06011
42	Differential pressure over the dryer filters ■	mbar	-	Dryer	XDPI06012
43	Differential pressure filter dryer air outlet ■	mbar	-	Dryer	XPDI06021
44	Differential pressure over the wet granule transfer line ■ ▼	mbar	-	Wet granule transfer line (dryer)	XDPI07011
45	Differential pressure exhaust HEPA suction to product control	mbar	-	Product control unit	PDET09031
46	Mass flow granulation liquid (calculated) ▲	g/min	58	Liquid addition module (granulator)	XFI03031
47	Flow dryer air inlet ▲ ■	m ³ /h	360	Dryer	XFE06021

48	Air inlet wet granule transfer (average)	m ³ /h	-	Wet granule transfer line (dryer)	XFE07011
49	Power granulator drive ■	W	-	Granulator	XJI04021
50	Temperature outlet granulator ■	°C	-	Temperature control unit (granulator)	TE0502A

*Based on the GEA operating manual for Collette™ machine number: 07CG025002R.shown in Annex 2.

Annex 2: GEA operating manual for Collette™ machine number: 07CG025002R.

OPERATING MANUAL <i>for Collette™ machine number: 07CG025002R</i>		 GEA Pharma Systems N.V. Collette™
Document file name and revision: OM07CG025002R00.docx	Customer: Universiteit Gent - Belgium Machine type: ConsiGma™ 25 Project reference: V001001327	

2.6.2.1.2. Overview Screen

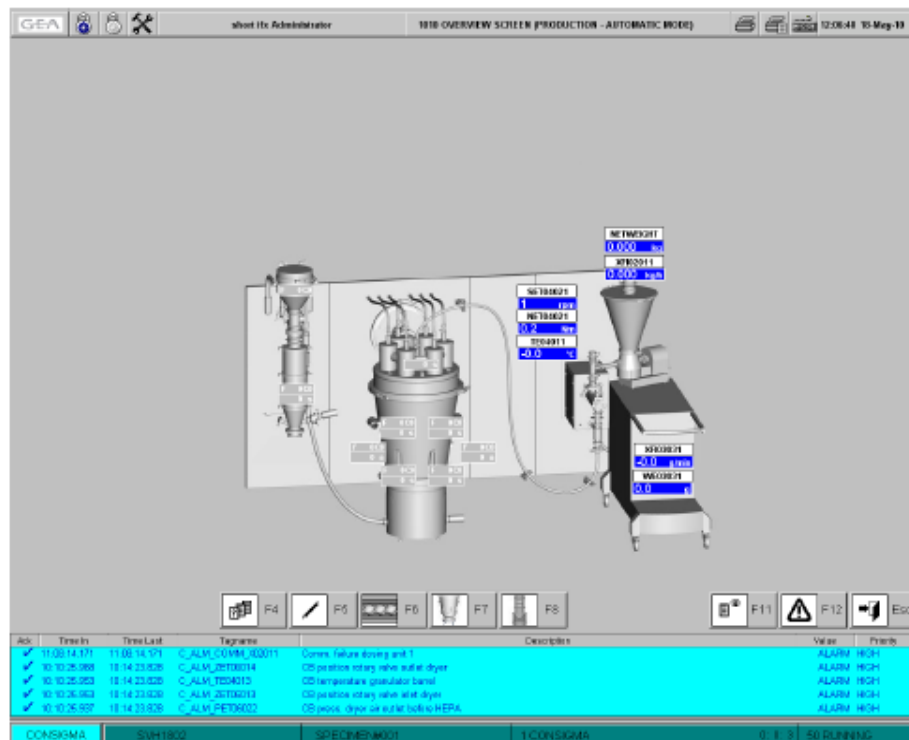


Figure 6 – [1010 OVERVIEW SCREEN (PRODUCTION – AUTOMATIC MODE)]

This overview screen displays a general graphical overview of the machine's installation. Different parts of this graphical overview can be selected to access the specific unit's detailed screen.

Screen numbers and titles:

- [1010 OVERVIEW SCREEN (PRODUCTION – AUTOMATIC MODE)] for Automatic Production Mode.
- [1006 OVERVIEW SCREEN (PRODUCTION – MANUAL MODE)] for Manual Production Mode.

The Overview Screen is the start screen and has no further functionality, except from navigating to the other Unit screens. To give a better overview of the active campaign process more detailed Unit screens have been created. On these screens, the phases and items of the machine have been grouped together, relevant to a certain unit of the machine.

The following actual tagged value measurement displays are also shown:

Measurement	Depicted where
Actual value torque granulator drive (Nm)	Undemeath TAG NET04021
Actual value speed granulator drive (rpm)	Undemeath TAG SET04021
Actual value temperature granulator barrel (°C)	Undemeath TAG TE04011
Actual value weight granulation liquid tank (g)	Undemeath TAG WE03031
Actual value calculated mass flow powder dosing 1 (kg/h)	Undemeath TAG XFI02011
Actual value calculated mass flow granulation liquid (g/min)	Undemeath TAG XFI03031
Actual value net weight of product in dosing unit	Undemeath NETWEIGHT
Actual FILL and CELL identification and tracking	Readouts all-over Dryer Unit graphic and Product Evaluation graphic

OPERATING MANUAL

for Collette™ machine number: 07CG025002R



Document file name and revision:
OM07CG025002R00.docx

Customer: Universiteit Gent - Belgium
Machine type: ConsiGma™ 25
Project reference: V001001327

GEA Pharma Systems N.V.
Collette™

2.6.2.1.3. Detailed screen for Granulator Unit

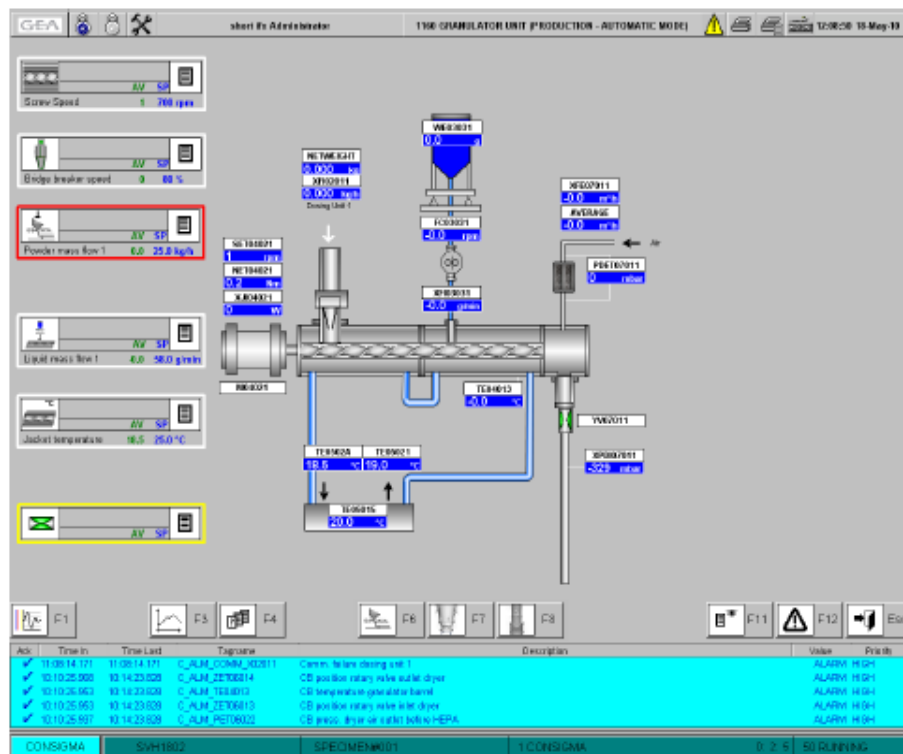


Figure 7 – [1160 GRANULATOR UNIT (PRODUCTION – AUTOMATIC MODE)]

The detailed screen for Granulator Unit displays phase related boxes, with actual values (AV) and setpoint values (SP), and items relevant to the Granulator Unit of the machine.


Screen numbers and titles:

[1160 GRANULATOR UNIT (PRODUCTION – AUTOMATIC MODE)] for Automatic Production Mode.

[1150 GRANULATOR UNIT (PRODUCTION – MANUAL MODE)] for Manual Production Mode.

The following actual tagged value measurement displays are also shown:

Measurement	Depicted where
Actual value liquid pumps speed (rpm)	Undemeath TAG FC03031
Actual value torque granulator drive (Nm)	Undemeath TAG NET04021
Actual value pressure difference air inlet wet granule transfer	Undemeath TAG PDET07011
Actual value speed granulator drive (rpm)	Undemeath TAG SET04021
Actual value temperature granulator barrel (°C)	Undemeath TAG TE04013
Actual value temperature TCU vessel (°C)	Undemeath TAG TE05015
Actual value temperature outlet granulator jacket (°C)	Undemeath TAG TE0502A
Actual value temperature inlet granulator jacket (°C)	Undemeath TAG TE05021
Actual value weight granulation liquid tank (g)	Undemeath TAG WE03031
Actual value pressure difference wet granule transfer	Undemeath TAG XDPI07011
Actual value air inlet wet granule transfer	Undemeath TAG XFE07011
Actual average value air inlet wet granule transfer	Undemeath (TAG XFE07011) AVERAGE
Actual value calculated mass flow powder dosing 1 (kg/h)	Undemeath TAG XFIO2011
Actual value calculated mass flow granulation liquid (g/min)	Undemeath TAG XFIO3031
Actual value power granulator drive (W)	Undemeath TAG XJIO4021

OPERATING MANUAL for Collette™ machine number: 07CG025002R		 GEA Pharma Systems N.V. Collette™
Document file name and revision: OM07CG025002R00.docx	Customer: Universiteit Gent - Belgium Machine type: ConsiGma™ 25 Project reference: V001001327	

Measurement	Depicted where
Actual value net weight of product in dosing unit	Undemeath NETWEIGHT

2.6.2.1.4. Detailed screen for Powder Feed Detail

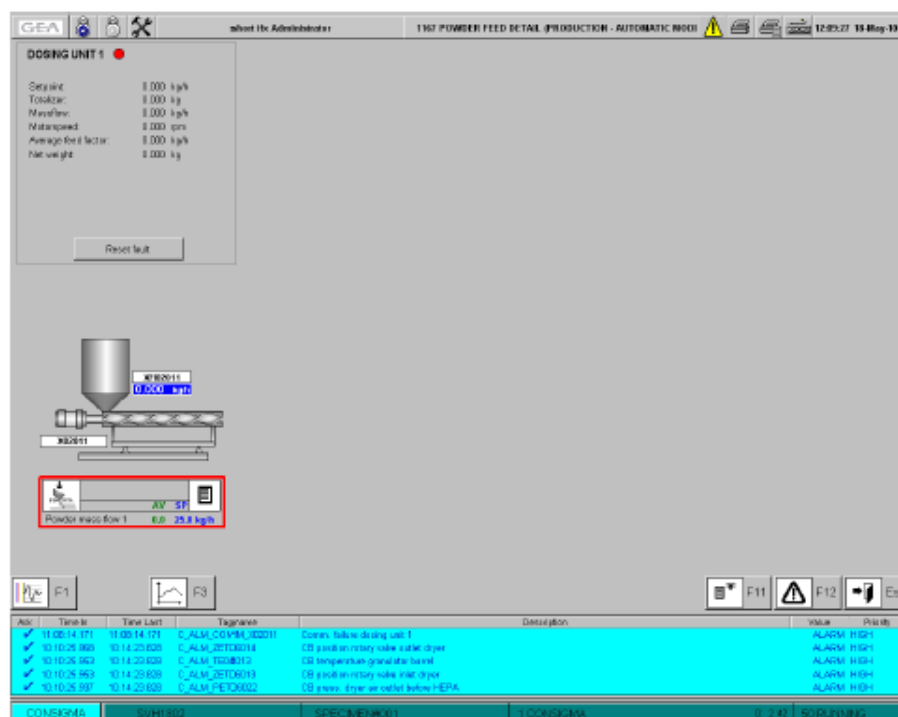


Figure 8 – [1167 POWDER FEED DETAIL (PRODUCTION – AUTOMATIC MODE)]

The detailed screen for Powder Feed Detail displays the phase related box, with actual values (AV) and setpoint values (SP), and items relevant to the Powder Dosing phase.

Screen numbers and titles:

[1167 POWDER FEED DETAIL (PRODUCTION – AUTOMATIC MODE)] for Automatic Production Mode.
 [1157 POWDER FEED DETAIL (PRODUCTION – MANUAL MODE)] for Manual Production Mode.

The following actual tagged value measurement displays are also shown:

Measurement	Depicted where
Actual value calculated mass flow powder dosing 1 (kg/h)	Undemeath TAG XF102011

For each powder dosing unit a specific box is displayed above the powder dosing graphics. It contains following information and functionality:

- The status of the profibus communication:
 - GREEN indicates a normal and active communication;
 - RED indicates a disnormal and non-active communication.
- Actual values of device specific parameters:
 - Setpoint (kg/h) = setting 'Powder mass flow'
 - Totalizer (kg) = total amount (counting up) of product
 - Massflow (kg/h) = actual value mass flow
 - Motorspeed (rpm) = actual value motorspeed

OPERATING MANUAL

for Collette™ machine number: 07CG025002R



Document file name and revision:
OM07CG025002R00.docx

Customer: Universiteit Gent - Belgium
Machine type: ConsiGma™ 25
Project reference: V001001327

- Average feed factor (kg/h) = actual value average feed factor
- Net weight (kg) = actual value net weight of product in dosing unit
- Buttons for manual control of dosing unit.
- Tare = taring of the powder dosing unit weight scale (Net weight = 0 kg)
- Feed Factor Calibration = self tuning of the powder dosing unit (phase active during fixed time)
- Reset fault = resets faults on the powder dosing unit

2.6.2.1.1. Detailed screen for Dryer Unit

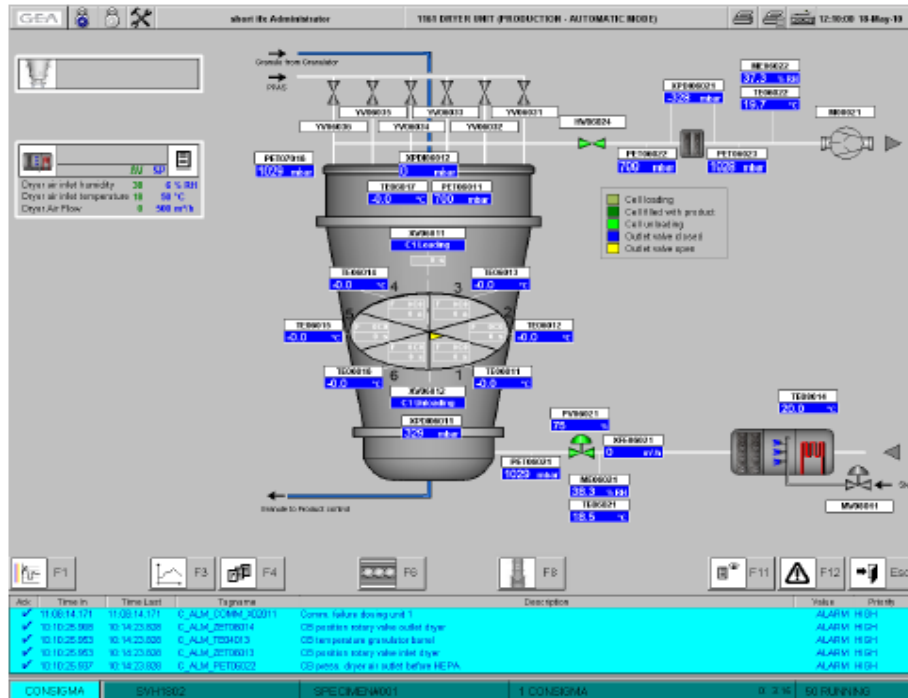


Figure 9 – [1161 DRYER (PRODUCTION – AUTOMATIC MODE)]

The detailed screen for Dryer Unit displays phase related boxes, with actual values (AV) and setpoint values (SP), and items relevant to the Dryer Unit of the machine.


Screen numbers and titles:

[1161 DRYER UNIT (PRODUCTION – AUTOMATIC MODE)] for Automatic Production Mode.

[1151 DRYER UNIT (PRODUCTION – MANUAL MODE)] for Manual Production Mode.

The following actual tagged value measurement displays are also shown:

Measurement	Depicted where
Actual value relative humidity dryer air inlet (% RH)	Undemeath TAG ME06021
Actual value relative humidity dryer air outlet (% RH)	Undemeath TAG ME06022
Actual value pressure dryer top (mbar)	Undemeath TAG PET06011
Actual value pressure dryer air inlet (mbar)	Undemeath TAG PET06021
Actual value pressure dryer air outlet after HEPA (mbar)	Undemeath TAG PET06023
Actual value pressure atmospheric pressure	Undemeath TAG PET07016
Actual status opening control valve pressure dryer air inlet (%)	Undemeath TAG PV06021
Actual value temperature dryer cell 1 (°C)	Undemeath TAG TE06011

OPERATING MANUAL for Collette™ machine number: 07CG025002R		 GEA Pharma Systems N.V. Collette™
Document file name and revision: OM07CG025002R00.docx	Customer: Universiteit Gent - Belgium Machine type: ConsiGma™ 25 Project reference: V001001327	

Measurement	Depicted where
Actual value temperature dryer cell 2 (°C)	Underneath TAG TE06012
Actual value temperature dryer cell 3 (°C)	Underneath TAG TE06013
Actual value temperature dryer cell 4 (°C)	Underneath TAG TE06014
Actual value temperature dryer cell 5 (°C)	Underneath TAG TE06015
Actual value temperature dryer cell 6 (°C)	Underneath TAG TE06016
Actual value temperature dryer top (°C)	Underneath TAG TE06017
Actual value temperature dryer air inlet (°C)	Underneath TAG TE06021
Actual value temperature dryer air outlet (°C)	Underneath TAG TE06022
Actual value temperature filter dryer air handling unit (°C)	Underneath TAG TE06014
Actual value pressure difference dryer hole plate & bed (mbar)	Underneath TAG XDPI06011
Actual value pressure difference filters dryer cells (mbar)	Underneath TAG XDPI06012
Actual value pressure difference filter dryer air outlet (mbar)	Underneath TAG XDPI06021
Actual value flow dryer air inlet (m³/h)	Underneath TAG XFE06021
Actual status rotary valve inlet dryer	Underneath TAG XV06011
Actual status rotary valve outlet dryer	Underneath TAG XV06012
Actual FILL and CELL identification and tracking	Readouts all-over Dryer Unit graphic

2.6.2.1.2. Detailed screen for Product Evaluation Unit

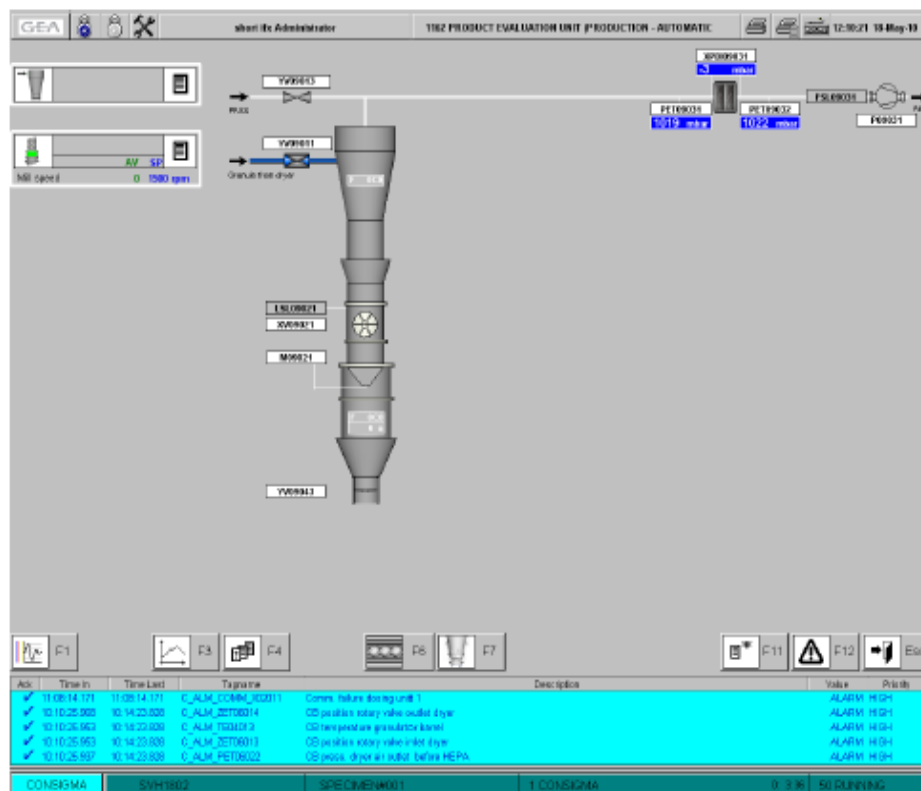


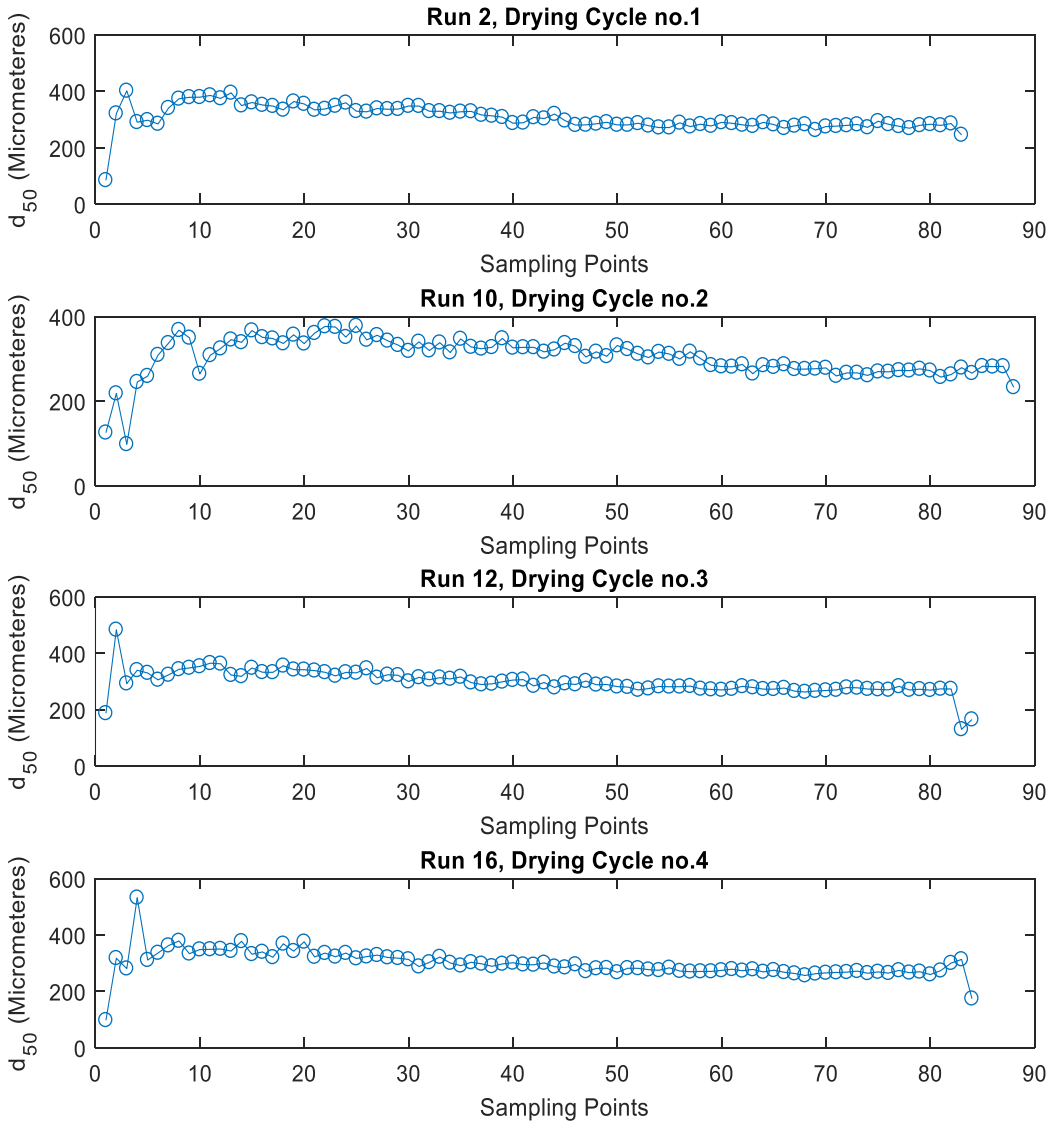
Figure 10 – [1162 PRODUCT EVALUATION UNIT (PRODUCTION – AUTOMATIC MODE)]

The detailed screen for Product Evaluation Unit displays phase related boxes, with actual values (AV) and setpoint values (SP), and items relevant to the product evaluation unit of the machine.

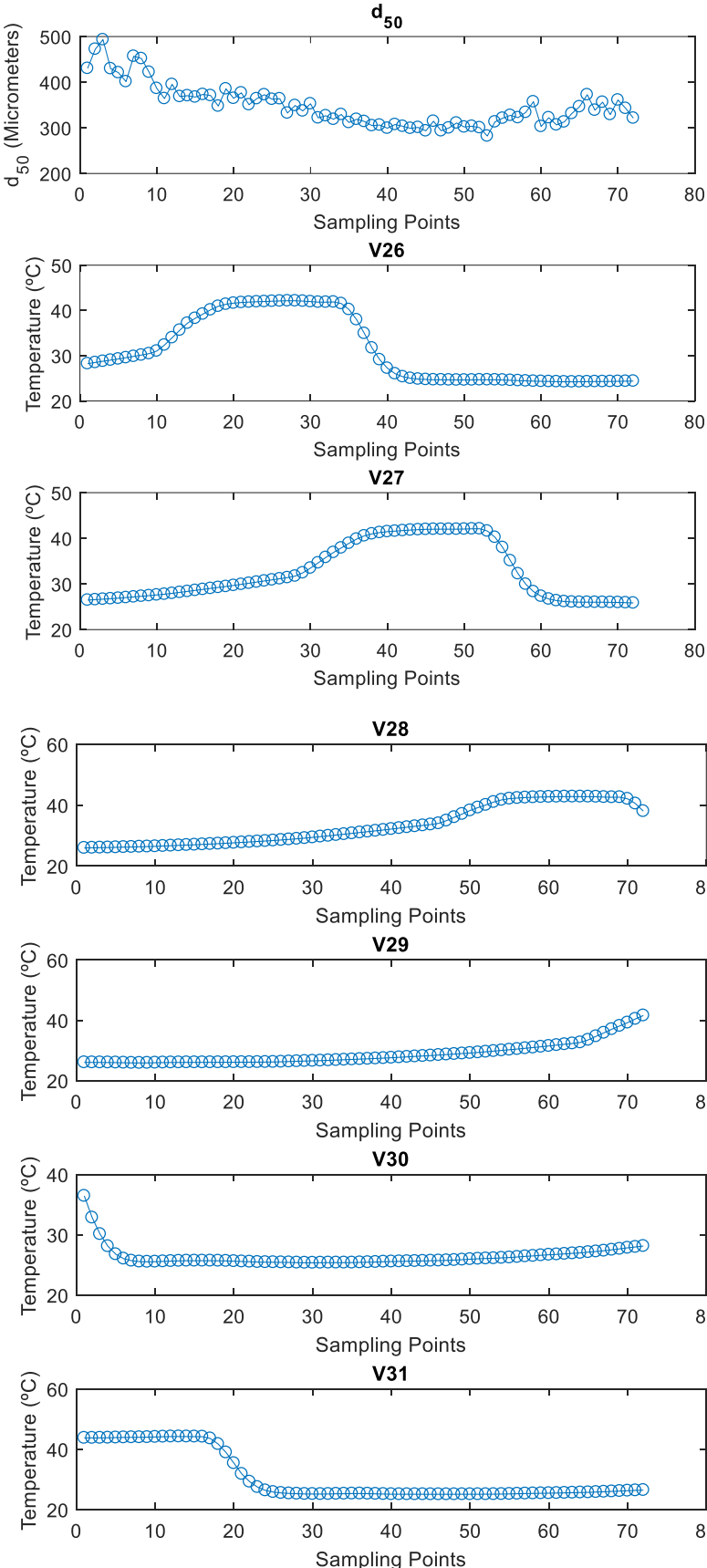
Annex 3: Details regarding the training of the neural networks.

Architecture	Multilayer feedforward neural network (recurrent)
Topology	Three layers
Initialization	Weights and Bias randomly initialized
Inputs scaling	Unit variance
Transfer functions	Input layer: None
	Hidden layer: Hyperbolic tangent
	Output layer: Linear
Training procedure	Back propagation
Training scheme	Batch
Training algorithm	Levenberg-Marquardt (second-order)
Training criterium	Minimize validation error

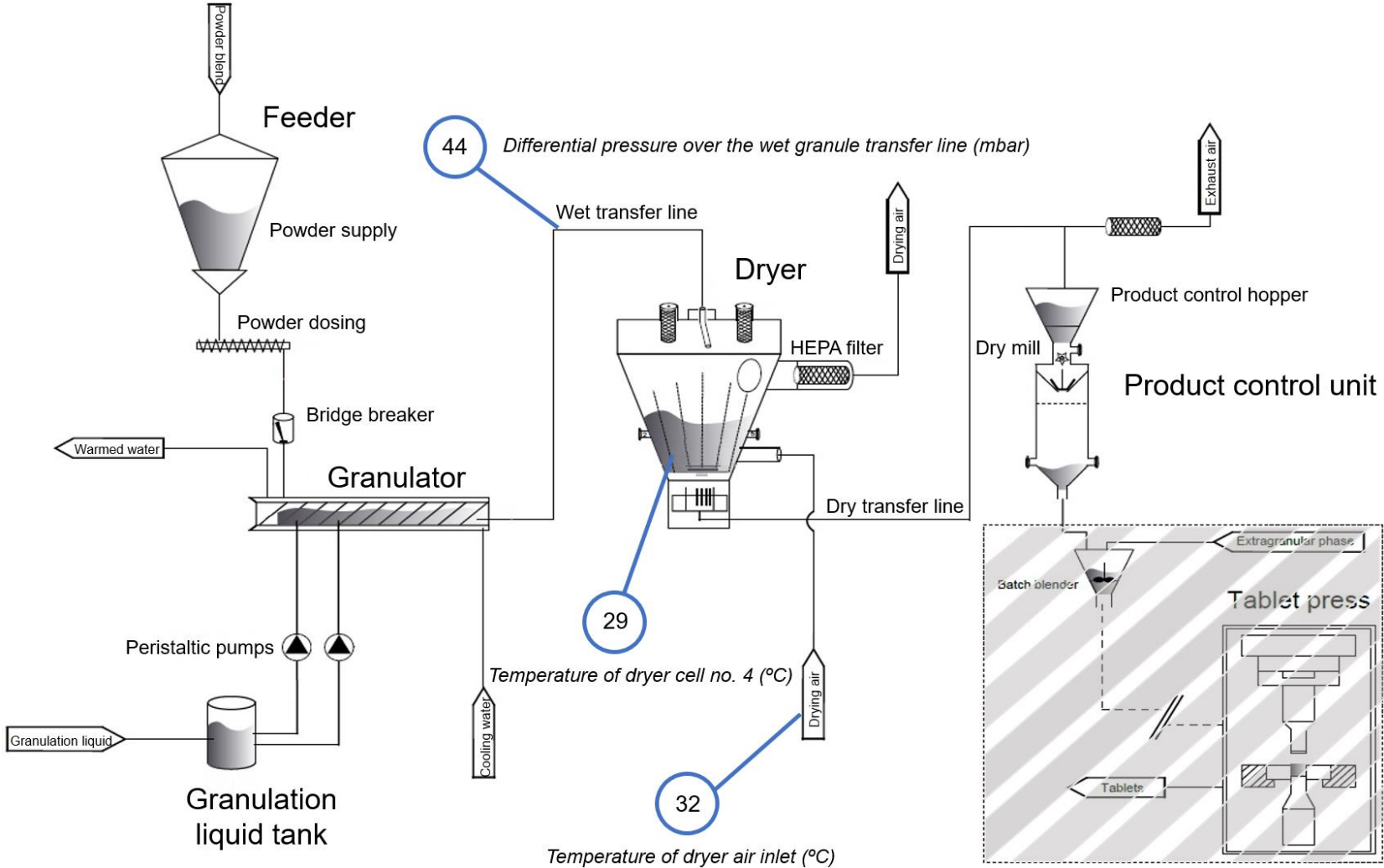
Annex 4: Close-up of the drying cycles no. 1, 2, 3 and 4 of Runs 2, 10, 12 and 16, respectively.



Annex 5: Comparison between the d50 profile and the temperature of dryer cells no. 1, 2, 3, 4, 5 and 6 of the first drying cycle of Run 8.



Annex 6: Location at which V29, V32 and V44 were monitored within the ConsiGma™-25 continuous line.



Annex 7: Predictions of the d50 value for drying cycles no. 3, 4, 5 and 6 of run 5 and drying cycles no. 4, 5 and 8 of run 6.

